

# dDNP as a method to assess altered cellular metabolism in vitro

**Malinowski, Ronja Maja**

*Publication date:*
2018

*Document Version*
Publisher's PDF, also known as Version of record

# dDNP as a method to assess altered cellular metabolism *in vitro*

PhD thesis · October 2018 · Ronja Maja Malinowski

DTU Electrical Engineering
Department of Electrical Engineering

# Preface

This thesis is the product of three and a half years of research as a Ph.D. student at Center for Hyperpolarization of Magnetic Resonance (HYPERMAG), Technical University of Denmark. The research was carried out under supervision of Prof. Jan Henrik Ardenkjær-Larsen, Assoc. Prof. Pernille Rose Jensen and Prof. Jens Øllgaard Duus with financing from Danish National Research Foundation, grant no. [DNRF124] and Innovation Fund Denmark, grant no. [1308-00028B].

First and foremost, I would like to thank Jan for giving me the opportunity to work with dDNP and being a part of HYPERMAG. I am grateful for the excellent guidance and support during the years. It has been a pleasure being a part of your group while it transformed into a state-of-art research center with many new employees. I also want to thank Pernille for excellent guidance and support. Also, thanks to Jens for always being available for scientific discussions and giving excellent suggestions.

Next, I would like to thank Dr. Murali Cherukuri for allowing me to visit his group for five months at National Institutes of Health, Maryland, US. I want to thank the whole group for making my stay enjoyable. It was truly a great scientific experience to work in your lab at NIH. I want to thank Otto Mønsted Fonden for financial support for my external stay.

Thanks to Prof. Thomas Mandrup-Poulsen and Dr. Seyed Mojtaba Ghiasi from Copenhagen University for a fruitful collaboration.

I owe a big thank to everyone at HYPERMAG for being fantastic colleagues. Special thanks to Ditte Juhl Mogensen and Jan Kilund for technical assistance during this project – your help was much appreciated - also special thanks to Signe Holm for your help and support during the years.

Furthermore, I would like to thank my friends and family for support and being patient and understanding throughout the years. Thanks to Christian and Daniel for numerous entertaining, scientific discussions in and outside the lab - thanks to Didde for always being there to remind me of the life outside lab and visiting me in the US during my external stay. I could not have done this without all your support.

# Abstract

Lifestyle diseases are expanding global health problems that are contributing to the global burden of chronic diseases. To link diet to metabolic outcome, it is necessary to understand the metabolic fate and interaction of the nutritional components in living organisms. The link between metabolic perturbations and human diseases has led to growing interest in metabolic research. The objective of this project is to study perturbed metabolism using dissolution Dynamic Nuclear Polarization (dDNP) in several disease models *in vitro*. By overcoming the sensitivity issues related to traditional magnetic resonance, dDNP offers the advantage of non-invasive metabolic visualization *in vitro* and *in vivo*.

In the first part of the thesis, dDNP is used to probe slow biochemical reactions in combination with Stable Isotope-Resolved Metabolomics (SIRM). By application of this method, the timeframe of the experiment can be extended from minutes to hours or longer. The dDNP-SIRM approach is applied to investigate early handling of excess fuel in insulin producing β-cells before they reach a glucotoxic state which is a pathogenic factor in type 2 diabetes. Glucose-derived pyruvate is found to correlate with a high fuel burden for the cells and is hypothesized to be a potential biomarker in the development of insulin impairment. In conclusion, this study shows that β-cells actively use different metabolic pathways to reduce excess metabolites formed due to uncontrolled glycolysis. Glycerol- and fatty acid metabolism is the most likely candidate for this deviation pathway. Further studies are needed to elucidate this fundamentally important and relatively overlooked defense mechanism important for protecting the β-cell against glucotoxicity.

In the second part of the thesis, dDNP is applied to study real time kinetics using hyperpolarized [1-$^{13}$C]pyruvate to visualize metabolism in cancer cells. The biological model represents pancreatic cancer, demonstrated by different cell lines representing various stages of the cancer. For this purpose, a bioreactor with a home-built flow cell was constructed and tested. It was demonstrated that the cells grown on microcarriers showed pyruvate to lactate conversion in the flow cell. Furthermore, the bioreactor was found suitable for longitudinal cell studies over several hours, but also revealed that flow stress is an important limitation for many cell systems on microcarriers.

The third part of the thesis concerns three different bioprobes for novel applications, *in vivo* and *in vitro*. The sample formulation and solid-state DNP polarization were optimized for each bioprobe. Biological applications are discussed for each probe, and initial studies were performed to assess potential for hyperpolarization studies.

In summary, this thesis shows the versatility of dDNP for metabolic research and potential diagnostic applications demonstrated by the polarization of $^{13}C$ labeled substrates *in vitro*.

# Resumé

Livstilssygdomme er et stigende globalt sundhedsproblem, som bidrager til den globale byrde af kroniske sygdomme. For at linke diæt til metaboliske sygdomme, er det nødvendigt at forstå den metaboliske konsekvens og interaktion af næringsstoffer i levende organismer. Linket mellem metaboliske forstyrrelser og menneskesygdomme har medført en stigende interesse i metabolisk forskning. Formålet med dette projekt er at studere perturberet metabolisme ved brug af dissolution Dynamic Nuclear Polarization (dDNP) i adskillige sygdomsmodeller *in vitro*. Ved at overkomme sensitivitetsproblemerne forbundet med traditionel magnetisk resonans, er det med dDNP muligt at visualisere metabolisme non-invasivt både *in vitro* og *in vivo*.

I første del af afhandlingen bliver dDNP anvendt til at undersøge langsomme biokemiske reaktioner i kombination med stable isotope-resolved metabolomics (SIRM). Ved at anvende denne metode kan tidshorisonten for forsøget øges fra minutter til timer eller længere. dDNP-SIRM metoden anvendes til at undersøge tidlig håndtering af overskudsnæringsstoffer i insulinproducerende β-celler inden de når et glukotoksisk stadium, som er en patogen faktor i type 2 diabetes. Mængden af glukose-deriveret pyruvat korrelerer med en høj næringsstofsbyrde, og derfor er hypotesen at pyruvat er en potentiel biomarkør i udviklingen af insulin dysfunktion. Opsummeret viser studiet at β-celler aktivt bruger forskellige metaboliske ruter for at formindske overskudsmetabolitter, som formes som følge af ukontrolleret glykolyse. Glycerol- og fedtsyremetabolismen er den mest sandsynlige kandidat for denne afledende rute. Yderligere studier skal udføres for at udlede denne fundementalt vigtige og relativt oversete forsvarsmekanisme, som er vigtig for at beskytte β-cellen mod glukotoksicitet.

I anden del af afhandlingen er dDNP anvendt til at undersøge metabolisme i realtid ved brug af hyperpolariseret [1-$^{13}$C]pyruvate til at studere metabolismen i kræftceller. Den biologiske model repræsenterer kræftceller fra bugspytkirtel, demonstreret ved forskellige cellelinjer der repræsenterer forskellige stadier af kræft. Til formålet blev en bioreaktor med en hjemmebygget flowcelle konstrueret og testet. Det blev vist at celler groet på microcarriers gav pyruvat til laktat omdannelse i flowcellen. Ydermere viste bioreaktoren sig at være anvendelig til longitudinelle studier over adskillige timer, men viste også at flowstress er en vigtig begrænsning for mange cellesystemer på microcarriers.

Tredje del af afhandlingen vedrører tre forskellige bioprober for nye anvendelser, *in vivo* og *in vitro*. Formuleringen og fastfase DNP polarisering for hver bioprobe blev optimeret. Biologiske

anvendelser diskuteres for hver probe, og initielle studier blev udført for at vurdere deres potentiale ved brug i hyperpolariseringstudier.

Opsummeret viser denne afhandling mangfoldigheden af dDNP for metabolisk forskning og potentielle diagnostiske anvendelser demonstreret ved polarisering af $^{13}C$ mærkede substrater *in vitro*.

# List of abbreviations

| | |
|---|---|
| 2HG | 2-hydroxyglutarate |
| 3PG | 3-phosphoglycerate |
| αKG | alpha ketoglutarate |
| Acetyl-CoA | acetyl coenzyme A |
| ALA | alanine |
| ATP | adenosine triphosphate |
| ALT | alanine transaminase |
| AML | acute myeloid leukemia |
| BBB | blood-brain barrier |
| BDPA | 1,3-bisdiphenylene-2-phenylallyl |
| C | Celcius |
| CA | carbonic acid |
| CE | cross effect |
| CSF | cerebrospinal fluid |
| DHAP | dihydroxyacetone phosphate |
| dDNP | dissolution Dynamic Nuclear Polarization |
| DMSO | dimethyl sulfoxide |
| EDTA | ethylenediaminetetraacetic acid |
| EPR | electron paramagnetic resonance |
| FT-IR | Fourier-transform infrared spectroscopy |
| GC | gas chromatography |
| GCS | γ-glutamylcysteine synthetase |
| Gd | gadolinium |
| GGT | γ-Glutamyl Transpeptidase |
| GHz | gigahertz |
| GSH | glutathione |
| HAP | hypoxia-activated prodrug |
| Hz | hertz |
| HP | hyperpolarized |
| I.D. | inner diameter |
| IDHs | isocitrate dehydrogenases |
| K | Kelvin |
| Lac | lactate |
| LDH | lactate dehydrogenase |
| µL | microliter |
| MCTs | monocarboxylate transporters |
| min | minute |
| mg | milligram |
| mm | millimeter |
| mM | millimolar |
| MR | magnetic resonance |
| MRI | magnetic resonance imaging |
| MRSI | magnetic resonance spectroscopy imaging |
| MS | mass spectrometry |
| MTT | 3-(4,5-dimethylthiazol-2-yl)-2,5-diphenyltetrazolium bromide |
| NAC | N-acetylcysteine |
| NAPB | N-acetyl-p-benzoquinoneimine |
| NMR | nuclear magnetic resonance |
| O.D. | outer diameter |
| OX063 | (tris[8-carboxyl-2,2,6,6-benzo(1,2-d:4,5-d)-bis(1,3)dithiole-4-yl] methyl sodium salt |
| PBS | phosphate-buffered saline |
| PC | pyruvate carboxylase |

| | |
|---|---|
| PCA | perchloric acid |
| PCL | polycaprolacetone |
| PDAC | pancreatic ductal adenocarcinomas |
| PEEK | polyether ether ketone |
| PEP | phosphoenolpyruvate |
| PET | positron emission tomography |
| PHIP | parahydrogen induced polarization |
| PKM | Pyruvate kinase isoenzyme |
| PDH | pyruvate dehydrogenase |
| ppm | part per million |
| PTFE | polytetrafluoroethylene |
| Pyr | pyruvate |
| QC | quality control |
| ROS | reactive oxygen species |
| s | second |
| SE | solid effect |
| SIRM | stable isotope resolved metabolomics |
| SLC | signal loss coefficient |
| SNR | signal-to-noise ratio |
| SPECT | single-photon emission computed tomography |
| T | temperature |
| TCA | tricarboxylic acid cycle |
| TEMPO | (2,2,6,6,-tetramethylpiperidin-1-yl)oxyl |
| TM | thermal mixing |

# List of publications

## Paper I

Lerche, M.H.; Yigit, D.; Frahm. A.B.; Ardenkjær-Larsen, J.H.; **Malinowski, R.M**.; Jensen, P.R. Stable Isotope-Resolved Analysis with Quantitative Dissolution Dynamic Nuclear Polarization, *Anal. Chem.*, **2018**, 90, 674-678.

## Paper II

**Malinowski, R.M**.; Ghiasi, S.M.; Mandrup-Poulsen, T.; Lerche M.H.; Ardenkjær-Larsen, J.H.; Jensen, P.R. Pancreatic β-cells respond with early metabolic switch to fuel pressure, *submitted to Journal of Biological Chemistry*

## Paper III

**Malinowski, R.M**.; Lipsø, K.W.; Lerche, M.H.; Ardenkjær-Larsen, J.H. Dissolution Dynamic Nuclear Polarization capability study with fluid path, *J. Magn. Reson.*, **2016**, 272, 141-146.

All papers are included in the thesis.

# Contents

# 1. Introduction

Lifestyle diseases such as obesity [1], diabetes [2], specific cancers [3] [4] [5] and cardiovascular conditions [6] are expanding global health problems. The consumption of foods high in fat and sugar is increasing throughout in the developing world, contributing to the global burden of chronic diseases [7]. The result of this development is increased health expenses, reduced life quality and early death. In order to link diet to metabolic outcome, it is necessary to understand the metabolic fate of the nutritional components in living organisms. The connection between perturbed metabolism and human disease has led to a growing interest in metabolic research [8]. An example of pathogenic metabolism is the Warburg effect in cancerous cells [9], and by using analytical methods to quantify metabolites from cancerous tissues, the severity of cancer can be assessed.

In this thesis, a novel magnetic resonance (MR) based method, dissolution dynamic nuclear polarization (dDNP), is used to examine metabolism non-invasively in biological systems. The inherently low signal in traditional MR based methods is overcome by *ex situ* polarization of isotope labeled molecules, enhancing their signal dramatically. There are several ways in which dDNP can be used to investigate metabolism *in vitro* among which are real time kinetics (non-invasively) and endpoint metabolomics (extracts). In the real time kinetic experiment, a biologically relevant substrate (bioprobe) is polarized and then injected into the cell system. The result of this is conversion of the bioprobe in real time, revealing uptake and enzymatic activity. The non-invasiveness of this approach makes it suitable for *in vivo* imaging [10] and the diagnostic properties of the method is being employed in clinical trials [11]. dDNP can also be used for endpoint metabolomics. In this type of experiment, the cell system is initially incubated with the isotope labeled substrate following an extraction procedure and hyperpolarization of the final sample. This approach makes it possible to extend the time frame of the dDNP experiment from minutes to hours or longer.

This thesis demonstrates the use of dDNP for both types of metabolic studies on two different *in vitro* disease models: metabolism in insulin producing β-cell as a function of time and glucose stimulation, and real time kinetics in pancreatic cancer cells by exposure to hyperpolarized [1-$^{13}$C]pyruvate. Furthermore, the potential of three novel bio-probes are investigated and discussed in last part of this thesis:

**Part I** Endpoint metabolomics by dDNP of cell extracts:

Early, transient changes of metabolites in the β-cell as a function of time and glucose concentration by dDNP of cell extracts and development of dDNP-SIRM method.

**Part II** Real time metabolism in living cells:

Using a dDNP/NMR compatible bioreactor for longitudinal studies in living pancreatic cancer cells to study metabolism in real time.

**Part III** Investigation of novel bioprobes:

Optimizing the polarization of $^{13}C$-labeled bioprobes for *in vivo* studies.

# 2. Metabolomics

## 2.1 Metabolism

Metabolism is the chemical engine responsible for driving the living process. Single and multicellular organisms support their existence through utilization of a massive repertoire of enzymatic reactions and transport processes. This allows the organism to process and convert thousands of organic compounds into essential biomolecules through an extensive map of pathways [12]. Metabolism can conveniently be divided into three types of functions; catabolism, the breakdown of molecules to produce energy and building blocks, anabolism, the synthesis of essential compounds for the cell e.g. proteins, DNA and cell structure, and waste disposal responsible for eliminating toxic compounds [13] [8]. Therefore, metabolism is closely linked to nutrition and the availability of nutrients, which are mainly gained through dietary carbohydrates, lipids and proteins [14]. The metabolic pathways are closely controlled by enzymes, which allows the reactions to proceed quickly and efficiently. The enzymes regulate the metabolic pathways in response to changes in the cells environment or signal from other cells, and this plasticity is useful for e.g. excessive or lack of nutrition, or other environmental changes in order to maintain normal cell function.

## 2.2 Perturbed metabolism

When biochemical pathways malfunction, either because of genetic or environmental reasons, it can lead to metabolic disturbances and disease, because the cells can no longer maintain normal function. As example, glucotoxicity is an established pathogenic process in the β-cell, that may lead to type 2 diabetes [15]. β-cells, which are responsible for sensing glucose levels and respond with suitable amount of insulin, can lose or reduce their capability of insulin response after being exposed to excess fuels for longer duration. Excessive fuels require faster metabolism or metabolism through additional pathways, leading to formation of harmful products such as reactive oxygen species (ROS), which is harmful for cells, especially the β-cell, since it contains less anti-oxidant compared to other cell types [16]. The cell damage depends on exposure time and concentration of excessive fuels and the damage can be reversible to a certain extent in some conditions [17].

The prime example of a common human disease with pathological metabolic perturbation is cancer. Altered cellular metabolism is the hallmark of cancer. The “Warburg effect”, named after the discoverer Otto Warburg [18], is the metabolic shift in cancer tissue in which the cells consume more glucose and secrete more lactate than normal tissue, even though they have access to sufficient $O_2$ to

metabolize glucose completely to $CO_2$, Figure 1. The glycolysis is decoupled from pyruvate oxidation, such that carbohydrates are not used for maximum adenosine triphosphate (ATP) generation in the mitochondria [9]. Even though cancers are hugely diverse in type and etiology, they share this particular metabolic abnormality; a wasteful alteration of glycolysis.

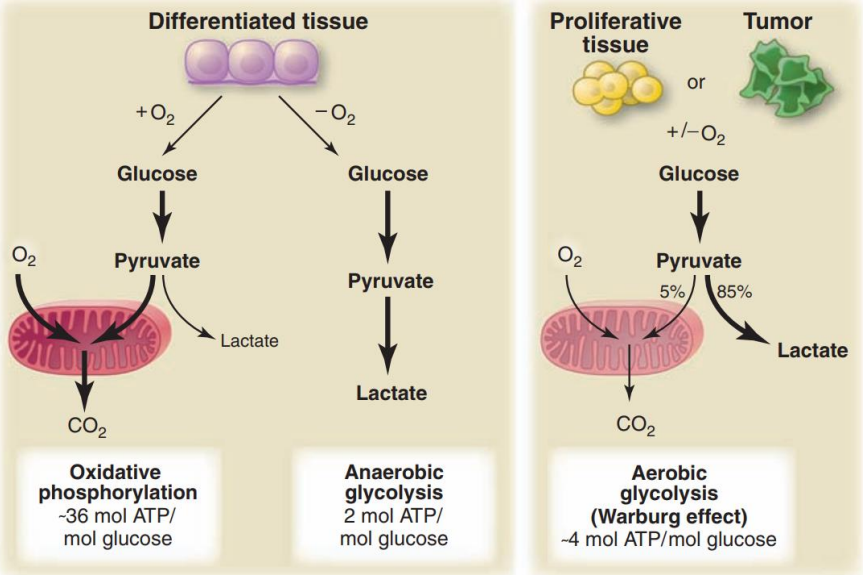


*Figure 1 – Left: Two pathways for ATP production in healthy cells. If oxygen is available, the cells metabolize glucose to pyruvate, which is then oxidized to $CO_2$ in the mitochondria, the most energy efficient pathway (aerobic pathway). If the oxygen levels are low, the cells can use the generated pyruvate for producing lactate (anaerobic pathway), a much less energy efficient pathway. Right: the Warburg effect. The cells convert most of the glucose to lactate regardless of oxygen levels. From [9]. Reprinted with permission from AAAS.*

Downstream the glycolysis the aerobic ATP generation takes place in the mitochondria through a series of chemical processes referred to as the tricarboxylic acid (TCA) cycle. TCA cycle and oxidative phosphorylation are central to metabolic energy production. In normal cells, a substantial energy source for the TCA cycle is glucose-derived pyruvate from glycolysis [19]. Studies have revealed that perturbation in the TCA cycle is connected to many disease states [20] [21] [22]. In cancers, oncogenes impair some of the enzymes responsible for driving the TCA cycle [23]. Evidence suggest, that the TCA cycle is altered in many neurodegenerative diseases, such as Alzheimer's, Parkinson's, Huntington's disease and amyotrophic lateral sclerosis [20].

The breakdown of ATP is the only immediate source of energy for the heart contraction, maintenance and other vital functions. Cardiac ATP is in very close interplay with the TCA cycle activity. Many pathological states in the heart creates a mismatch between the anaerobic and oxidative metabolism via the TCA cycle [24]. Some of these processes are connected to e.g. myocardial ischemia, where oxidative metabolism is suppressed even though glycolytic rate is maintained [25]. These metabolic differences between disease and normal tissue motivates the field of metabolic research in order to gain better understanding of developing metabolic disorders, diagnosis and potential treatment.

The central process in the TCA cycle is the energy metabolism, in which acetyl coenzyme A (acetyl-CoA) derived from carbohydrates, fats and proteins is oxidized to $CO_2$. For the constant function of the cycle, intermediates are replenished (anaplerosis) or removed (cataplerosis) [26], Figure 2.

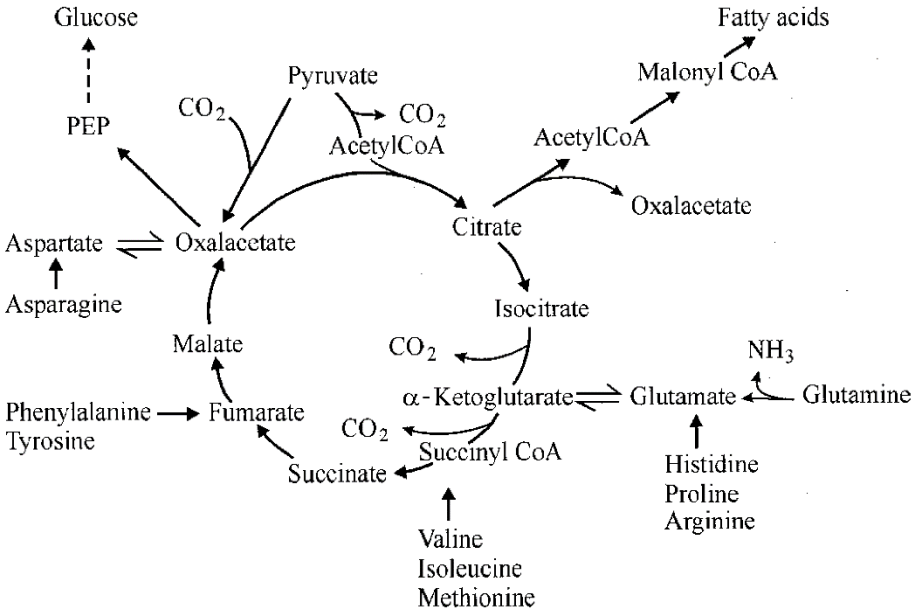


*Figure 2 – The TCA cycle and the interplay between anaplerosis and cataplerosis. Being the end product of glycolysis, pyruvate enters the TCA cycle and contributes to producing components for ATP production - one of the key processes in the energy production. From [26]. Reprinted with permission from ASBMB.*

## 2.3 Metabolomics reveal altered metabolism

The link between metabolic perturbations and human disease has led to growing interest in metabolic research [8]. By studying the unique, chemical fingerprints that specific cellular processes leave behind, a metabolic profile can be deduced. The profile represents a set of metabolites, which are products of cellular processes in the given cell model. A metabolic profile can give a snapshot of the cells physiological state and potentially lead to the discovery of clinically relevant biomarkers [27] such as the Warburg effect or TCA cycle impairment, as mention in previous section.

### 2.3.1 Methods

No single analytical technique covers the entire spectrum of the human metabolome [28]. Existing platforms for metabolomics studies commonly involve mass spectrometry (MS) and chromatography for separation of compounds [29], Fourier-transform infrared spectroscopy (FT-IR) [30] and nuclear magnetic resonance (NMR). Once optimized, these methods may produce quantitative or semi-quantitative data on many metabolites simultaneously. MS can analyze hundreds of small molecular weight metabolites according to their molecular mass with a higher detection sensitivity than NMR. However, due to variations in ionization properties of instrument and molecules, neither absolute nor relative concentrations can be accurately determined [29]. NMR is a non-destructive method, which is capable of interrogating all molecules simultaneously in the sample if they contain NMR active nuclei. NMR can be quantitative, and is capable of producing high-resolution spectra of biological samples, such as biological fluids, cells and intact tissues. A unique feature of NMR is its ability to determine stable isotope labeling at specific atomic position within the molecule (molecular/isotopomer analysis) [31]. The non-invasiveness of NMR combined with the molecular analysis makes it a desirable method of *in vitro* or *in vivo* metabolic studies.

The term “molecular imaging” has been used to describe the methods that directly or indirectly monitor the spatiotemporal distribution of molecular or cellular processes for biological, biochemical, diagnostic or therapeutic applications. A variety of techniques fits this category: positron emission tomography (PET), single-photon emission computed tomography (SPECT), optical imaging and Raman spectroscopy [32]. Magnetic resonance spectroscopic imaging (MRSI) originating from magnetic resonance imaging (MRI) and NMR has been applied for clinical use since the 80s [30]. A limitation of MR based methods is the sensitivity. The inherently low sensitivity of NMR makes it

impossible to track important metabolic intermediates at their physiological concentrations. This problem has been addressed by recent advancement in hyperpolarization, which allows spin polarization of the nucleus to be enhanced beyond the thermal equilibrium. This creates a dramatic, yet short-lived, increase of signal from the substrate molecule, making it possible to interrogate metabolism in real time. Among several hyperpolarization techniques, two have been used for *in vivo* work using $^{13}C$-containing organic molecules: para-hydrogen-induced hyperpolarization (PHIP) [33] and dissolution dynamic nuclear polarization (dDNP) [34]. PHIP requires simpler equipment than dDNP, but can only be used for polarization of $^{13}C$ in a limited number of molecules, whereas dDNP is more versatile, and can be applied to many molecules and other nuclei as well ($^{1}H$, $^{13}C$, $^{15}N$, etc.).

## 2.4 Overcoming low sensitivity: dDNP

### 2.4.1 Enhancement of SNR by hyperpolarization of nuclear spins

In magnetic resonance the signal-to-noise ratio (SNR) is correlated to the gyromagnetic ratio of the given nuclei (γ), the polarization (P) and concentration of spins (c), equation (1) [35]:

$$SNR \propto \gamma P c \qquad (1)$$

The polarization can be defined as the difference in population between the two possible energy states, where the nuclei are either parallel or anti-parallel to the external magnetic field based on Boltzmann's law. Nuclei with spin quantum number I = ½ (e.g. $^{1}H$, $^{3}He$, $^{13}C$, $^{129}Xe$) have two eigenstates in a magnetic field. The polarization can then be defined by equation (2) [36]:

$$P = \frac{N^+ - N^-}{N^+ + N^-} = tanh\left(\frac{\gamma \hbar B_0}{2k_B T}\right) \qquad (2)$$

Besides $k_B$ being the Boltzmann constant and $\hbar$ the reduced Planck constant, contributing parameters are the gyromagnetic ratio γ of the given nucleus, applied magnetic field $B_0$ and temperature T. At room temperature the equation can be reduced to equation (3):

$$P = \left(\frac{\gamma \hbar B_0}{2k_B T}\right) \qquad (3)$$

From this expression it is evident, that the polarization of protons in a 1.5 T MR scanner is ~$5.0 \cdot 10^{-6}$ – meaning that 5 out of 1000000 nuclear spins contribute to the net signal in a traditional NMR experiment. For carbon this number is even less because of the low gyromagnetic ratio, ~$1.3 \cdot 10^{-6}$. This effect is the major cause for the low sensitivity of MR, generally defined as SNR per square root unit of measurement time. For this reason, accumulation of scans in order to achieve useful SNR can become very time-consuming. If the polarization reaches unity, this means a 200.000 times improvement of proton polarization and 800.000 times for carbon. By hyperpolarization it is possible to force this population difference much further from thermal equilibrium, resulting in a dramatically increase in SNR.

### 2.4.2 Principles behind dDNP

The underlying mechanism of DNP is transferring the high electron spin polarization to the nuclear spin via microwaves, thereby creating larger differences in spin population. The microwave-driven polarization transfer process occurs at temperatures of few Kelvin and magnetic fields of several Tesla [37]. Under these conditions, the electrons are almost fully polarized, and a nuclear polarization of unity can in principle be reached. By irradiating the sample with microwaves close to the resonance frequency of the electron spin, it is possible to transfer the spin to the nuclei. DNP can occur through several fundamental mechanisms which are active under different experimental conditions: the solid effect (SE) involving hyperfine interactions between nucleus and electron pairs, the cross effect (CE) relying on a three-spin electron-electron-nucleus interaction and thermal mixing (TM), a multi spin effect [38]. As effect, the bulk nuclei gain polarization from the electrons, Figure 3 (left). Hence, the polarization efficiency depends both on parameters characterizing the various spin systems but also on technical factors such as microwave frequency and power [39].

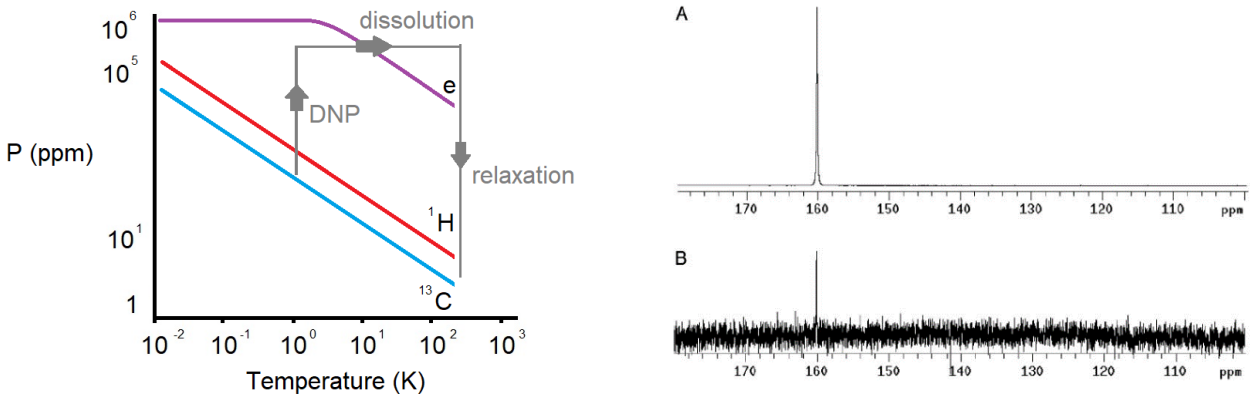


*Figure 3 – Left: principle of dDNP. At room temperature at e.g. 3T, the $^{13}$C nuclei are very weekly polarized. By lowering the temperature to around 1K, polarization increases, but the electron spin has a 2700 times stronger magnetic moment, hence it is easily polarized and will reach almost 100% polarization under these conditions. Microwaves can then induce electron-nuclear transitions, and the nuclear spin polarization will be increased. The hyperpolarized molecule is obtained after a quick dissolution in super-heated buffer, after which the relaxation starts with a time constant $T_1$ of typically 40-80 s for carboxylic acids. Right: A) Naturally abundant hyperpolarized urea $^{13}$C spectrum (20% polarization) vs B) Thermal equilibrium of same sample after average of 232128 scans, 65 h. at 9.4 T spectrometer. From [40]. Copyright 2003 by National Academy of Science, reprinted with permission.*

For the hyperpolarized molecule to be useful for living systems, it has to be dissolved in a buffer after the solid-state polarization has reached its maximum. This process ensures physiological temperature, desired concentration of substrate and pH correction if the hyperpolarized (HP) agent is either acidic or basic. Unlike in traditional NMR spectroscopy, where non-equilibrium polarizations can be regenerated by repeating the microwave irradiation and NMR acquisition, the hyperpolarized signal will decay irreversibly after dissolution until it reaches the thermal equilibrium, Figure 3 (right): A) hyperpolarized sample vs B) relaxed sample. The relaxation happens with a speed determined by the $T_1$ of the molecule, hence it is desirable that the dissolution process and transfer to NMR spectrometer happens as fast as possible, where highest possible spin polarization is retained.

### 2.4.3 Instrumentation for dDNP

The process of irradiating a sample with microwaves while keeping a temperature of 1 K, and then being able to dissolve it to reach a physiological temperature within seconds requires specialized equipment. The method was initially described by Ardenkjær-Larsen in 2003 [40]. Most solid-state DNP is performed at magnetic field between 0.35 – 16.5 T and at temperatures from below 1K to room temperature [41] [42]. The essential components for dDNP experiment are: a superconducting magnet, mechanical pumps to achieve a temperature around 1 K, a microwave source and a dissolution stick to bring the sample to physiological temperature. Two commercially available systems are Hypersense and GE SpinLab. The HyperSense is mostly suitable for small samples but can be modified to successfully polarize samples of up to 1000 mg, with specially made sample cups [43]. GE SpinLab requires sample loading by use of a fluid path, where sample and dissolution media are both placed, and the whole fluid path is placed in the polarizer [44]. This system can accommodate large samples for human patients, and can be sealed in a sterile way, which makes it possible for translation to clinical applications. Furthermore, it is equipped with a quality control (QC) module, which can check the parameters of the hyperpolarized solution (temperature, pH, concentration of electron paramagnetic agent, concentration of substrate), to ensure safe injection. The analyses are preformed instantly upon dissolution not to lose valuable seconds for highest possible polarization, when the solution reaches the subject, Figure 4.


*Figure 4 – Left: GE SPINlab polarizer, operating at 5 T and 0.9 K. The polarizer is equipped with four independent channels able to accommodate four samples (fluid paths) simultaneously. The cylindrical black unit is the quality control (QC) module, capable of measuring relevant parameters for the product (post dissolution), before the sample is released and injected into the subject. Right: Fluid path. The sample is sealed in a vial and the dissolution media is placed separately in a dissolution syringe, which is loaded into the SPINlab polarizer. Adapted from Malinowski et al. (Paper III).*

### 2.4.4 Sample preparation

The components of a dDNP sample include the MR-active molecular probe of interest, an organic free radical and a solvent that creates an amorphous solid at cryogenic temperatures, which ensures a homogeneous distribution of the radical. For polarization of $^{13}C$ nuclei, radicals with narrow electron paramagnetic resonance (EPR) line width such as trityls usually lead to best polarization (OX063, BDPA), whereas radicals with broad EPR line width such as TEMPO are suitable for both $^{1}H$ and $^{13}C$, but results in a lower polarization of carbon than a trityl radical [45]. Bringing the solid sample into solution from 1K requires dissolution in super-heated buffer, resulting in physiological temperature. For biological samples, an aqueous buffer is used. A chelating agent, usually ethylenedinitrotetraacetic acid (EDTA), is added to the buffer to bind paramagnetic ions that might increase relaxation. Furthermore, acid or base can be added to the dissolution media to ensure neutral pH in the final sample. The major consideration when choosing a molecular probe for dDNP is how its $T_1$ relates to the speed of the biological reaction it is intended to undergo. The time frame in which

it is possible to capture metabolic reactions is less than three times $T_1$ of probes developed today (30-180 s) [46], which makes small molecules desirable because of long $T_1$. Furthermore, *in vivo* applications of HP molecules require 10-150 mM sample concentration, so the components of the samples should be biologically tolerable.

### 2.4.5 Molecular probes for dDNP

HP $^{13}C$ agents, which are endogenous molecules modified only by $^{13}C$ or $^{2}H$ enrichment are used to follow basic biochemistry, and have many potential applications in oncologic imaging [32]. The information from these agents, or bioprobes, are fluxes through metabolic pathways to help understanding disease and improve treatment. Most $^{13}C$ dDNP bioprobes are carbonyls, including carboxylic acids, ketones, esters and amides. Especially carboxylic acids are useful since they are abundant in endogenous molecules. They are typically water-soluble, often amenable to $^{13}C$ enrichment, have relatively long $T_1$'s and are usually involved in or located near sites of biochemical modifications. This is critical, because a change in chemical shift is the method to observe reactions *in vivo* and *in vitro*. The most widely used bioprobe is pyruvate because of its interesting biochemistry and advantageously long $T_1$. Choosing the position of the $^{13}C$ labeling depends on the biochemistry the probe is intended to investigate, Figure 5 [32].

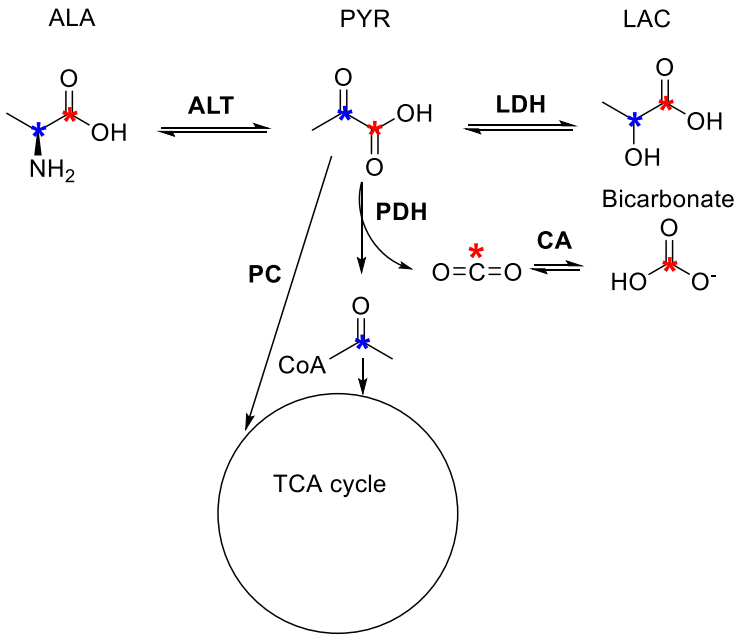


*Figure 5 – Scheme representing labeling resulting from HP pyruvate. Red star indicates carbon in the [1-$^{13}C$] position, while blue star is the [2-$^{13}C$] position. ALA: alanine PYR: pyruvate LAC: lactate, LDH: lactate dehydrogenase ALT: alanine transaminase CA: carbonic anhydrase PC: pyruvate carboxylate PDH: pyruvate dehydrogenase complex CoA: coenzyme A.*

Pyruvate with [1-$^{13}$C] labeled position is particularly useful for probing the flux through lactate dehydrogenase (LDH) to lactate, to probe e.g. Warburg effect in cancerous tissue. On the other hand, if the target is to measure TCA cycle intermediate, the [2-$^{13}$C] position is more suited. Other studies have probed pyruvate production by using [1-$^{13}$C]lactate or [1-$^{13}$C]alanine to probe the backward reaction [47] [48] [49].

### 2.4.5 Clinical translation

The standard approach to diagnosing cancer is tissue biopsy and subsequent histopathology. Once the diagnosis is established, therapeutic decisions usually rely on a combination of clinical evaluation and radiologic imaging. Invasive sampling methods are inconvenient for longitudinal monitoring and screening programs. For these reasons there is an interest in minimally invasive techniques [10]. The non-invasiveness of dDNP makes it an attractive technique for molecular imaging in human patients because of the potential of assessing prognosis in disease development. Currently, there is no widely accepted modality that provides information about aggressiveness and response to therapy in prostate cancer [50]. The first-in-human study of hyperpolarized [1-$^{13}$C]pyruvate was carried out in 2013, demonstrating safety and feasibility of the method [11]. The study involved 31 patients with untreated, biopsy-proven localized prostate cancer. The MRSI data showed higher [1-$^{13}$C]lactate signal in slices including the tumor, which was low or undetectable in slices from regions of the prostate that did not include tumor. Interestingly, in one patient the study showed an additional tumor that was not detected by conventional anatomic imaging methods. An MR guided biopsy performed subsequent to the study confirmed this finding, fueling the motivation for hyperpolarized [1-$^{13}$C]pyruvate being useful for assessing cancer development in slow growing cancers, where active surveillance is performed prior to potential surgical removal.

In 2016, the first experiment visualizing cardiac metabolism using [1-$^{13}$C]pyruvate was performed in four healthy individuals [51]. This study showed the first $^{13}$C images of the human heart, where the main products of [1-$^{13}$C]pyruvate are $^{13}$C bicarbonate and [1-$^{13}$C]lactate. As altered cardiac metabolism plays a role in the progression towards heart failure, potential bio-markers of such can be monitored longitudinally, representing another clinically relevant use of hyperpolarization for molecular imaging.

# 3. Part I – Stable isotope-resolved analysis of metabolites by dDNP

*Paper I - "Stable Isotope-Resolved Analysis with Quantitative Dissolution Dynamic Nuclear Polarization" was carried out at Center for Hyperpolarization in Magnetic Resonance (HYPERMAG) at Technical University of Denmark, and concerns the technical development of metabolite extract assay.*

*Paper II "Pancreatic β-cells respond with early metabolic switch to fuel pressure" is a result of a collaboration with Thomas Mandrup-Poulsen and Seyed M. Ghiasi from the Dept. of Biomedical Sciences, University of Copenhagen, and concerns the metabolic profile of the β-cells exposed to supra physiological glucose concentrations using the developed dDNP assay.*

## 3.1 Stable Isotope-Resolved Analysis with Quantitative Dissolution Dynamic Nuclear Polarization (Paper I)

The classical dDNP experiment offers detection of real time conversion of the hyperpolarized substrate in a cell suspension with subsecond resolution [52]. Since the hyperpolarized signal is short lived (~1 min.) it requires high uptake and turnover rates. Changing the order of events gives the possibility of expanding the timeframe of such experiments. Cells can be incubated for hours with isotope labeled substrates followed by an extraction of metabolites, and the metabolite extract can then undergo dDNP and NMR detection to allow quantification. Such an approach has previously been described for drug therapy monitoring by excreted metabolites in blood and urine [53], for investigating physical parameters of metabolites such as redox state [54] and for metabolomics approach in analysis of breast cancer and plant cells [55]. In this study, two cancer cell lines, MCF7 and PC3, are used to show the labeling pattern obtained by dDNP of extracts, when cells are incubated with uniformly labeled glucose at different time points. A robust protocol is demonstrated for obtaining cancer type specific metabolic pathways by metabolite analysis.

### 3.1.1 Sample preparation and optimization of polarization time

Human prostate adenocarcinoma cells (PC3) and human mammary adenocarcinoma cells (MCF7) were used as model systems for this study. At 90% confluence the cells were harvested and placed in Eppendorf tubes at a concentration of $10 \cdot 10^6$ cells in 500 µL. 100 µL of 120 mM [U-$^{13}$C,U-$D_7$]glucose was added to the Eppendorf tubes, and the cells were incubated in a shaking thermostat at 37º C for 0, 1, 3, 10 or 30 min. respectively. The entire cell suspension was then quenched by addition of 400 µL 2.2 M perchloric acid (PCA), and the metabolites were neutralized with KOH and

placed on ice for 10 min. After centrifugation, the supernatant was freeze-dried to yield the final lyophilized sample. The lyophilized samples were dissolved in 150 µL polarization medium (70 mg OX063, 1227 mg glycerol, 944 mg Milli-Q water, 28.8 mg Gadoteridol (100 µmol/g)), and 5 µL 50 mM HP001 (250 nmol) was added as an internal standard. The sample was polarized in a HyperSense polarizer at 3.35 K and 1.4 K with microwave frequency of 94 GHz. Upon dissolution, the samples were dissolved in 5 mL phosphate buffer (40 mM, pH 7.4) and quickly transferred to a 9.4 T Varian NMR spectrometer into a 5 mm NMR tube. The transfer time was approximately 12 s. 1D $^{13}C$ spectra of the metabolites were recorded with a 70º pulse.

To find the optimal time for dissolution, test samples were polarized for 30, 90 and 240 min. The test samples contained 60 µmol [U-$^{13}C$,D] glucose in polarization medium with HP001 as internal standard, Figure 6.

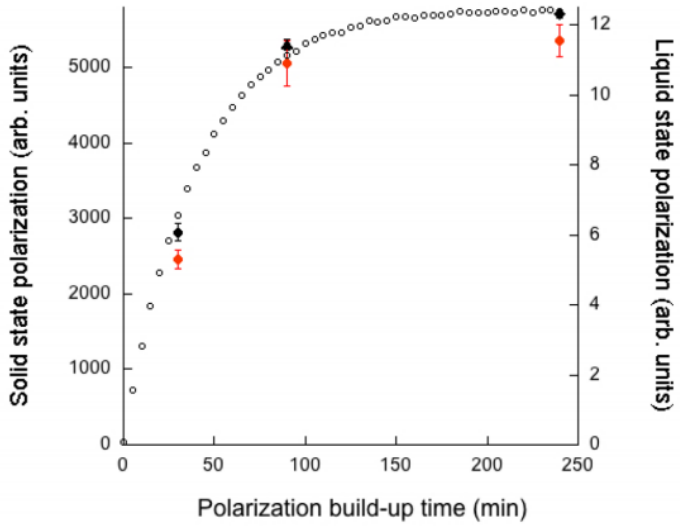


*Figure 6 – Solid-state buildup of samples containing [U-$^{13}C$,D]glucose in polarization medium with HP001 as internal standard, n=3 for 30 and 90 min., n=2 for 240 min. Red symbols show liquid state polarization of HP001. From paper I [156].*

After 90 min. 93% of the maximal achievable polarization is reached and therefore chosen as optimal dissolution time as a tradeoff between maximum SNR and throughput. It has been assumed that all metabolites polarize with approximately the same time constant, but this may not be the case in practice.

### 3.1.2 Correlation between relative quantification and absolute concentration of metabolites

In order to quantify the metabolites in a sample, the integrals of the peaks are measured with respect to the HP001 peak which is conveniently placed up-field and does not interfere with the carbonyl carbon chemical shift range. This leads to a relative concentration of metabolites. Since the integrals are affected by relaxation which depends on factors such as $T_1$, an uncontrolled magnetic environment during transfer from polarizer to spectrometer, temperature, transfer time, some signal loss, individual for each molecule is expected. For the method to be able to quantify the metabolite concentration, this loss should be known. Hence, a sample with four commonly occurring metabolites, acetate, lactate, alanine and pyruvate, was polarized and compared with thermal spectra of an aliquot of the same sample achieved after 4096 scans (repetition time 2 s) on a Bruker 800 MHz spectrometer. Since thermal NMR signal does not suffer from signal relaxation loss, the signal loss coefficient (SLC) is calculated as ratio between DNP signal and thermal signal, Figure 7.

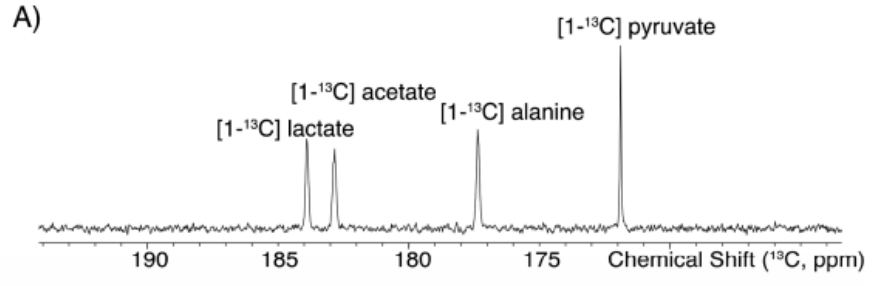


| compound (Com) | DNP ratio (Com/ HP001) | NMR ratio (Com/ HP001) | SLC (%) |
|---|---|---|---|
| lactate, C1 | 0.55 ± 0.03 | 0.67 ± 0.07 | 82 ± 8 |
| acetate, C1 | 0.58 ± 0.04 | 0.61 ± 0.04 | 95 ± 6 |
| alanine, C1 | 0.60 ± 0.04 | 1.08 ± 0.01 | 55 ± 4 |
| pyruvate, C1 | 0.57 ± 0.09 | 0.53 ± 0.01 | 108 ± 9 |

*Figure 7 – Top: liquid spectrum of the four metabolites after 90 min. polarization. The carbonyl carbons are detected because of their advantageously long $T_1$. Bottom: table with metabolite ratios relative to HP001 from the DNP experiment calibrated to values obtained with thermal NMR. From paper I [156].*

The SLC varies from 55-108 %, depending on the molecules specific relaxation behavior, and this suggests that SLC should be determined for each metabolite in order to calculate absolute concentrations.

### 3.1.3 Applying the method *in vitro*

The lyophilized samples from PC3 and MCF7 cells at time points 0, 3, 10, and 30 min (n=3), were polarized to yield spectra with a specific metabolic profile for each time point. As seen in figure Figure 8, five different metabolites were identified based on chemical shift referenced to HP001 at 23.7 ppm, namely pyruvate, lactate, alanine, 3-phosphoglycerate (3PG), phosphoenolpyruvate (PEP), and dihydroxyacetone phosphate (DHAP), furthermore 3PG was identified based on pH dependent chemical shift [56]. Lactate is the far most abundant metabolite, which is expected for cancerous cells due to the Warburg effect. The metabolic pattern becomes clearer over time (from 1 min. to 30 min.), and it is evident that after 30 min. the two cells lines show a distinct cell type dependent metabolic pattern. By measuring the SLC of the relevant metabolites, it is possible to quantify the absolute amount of metabolites.

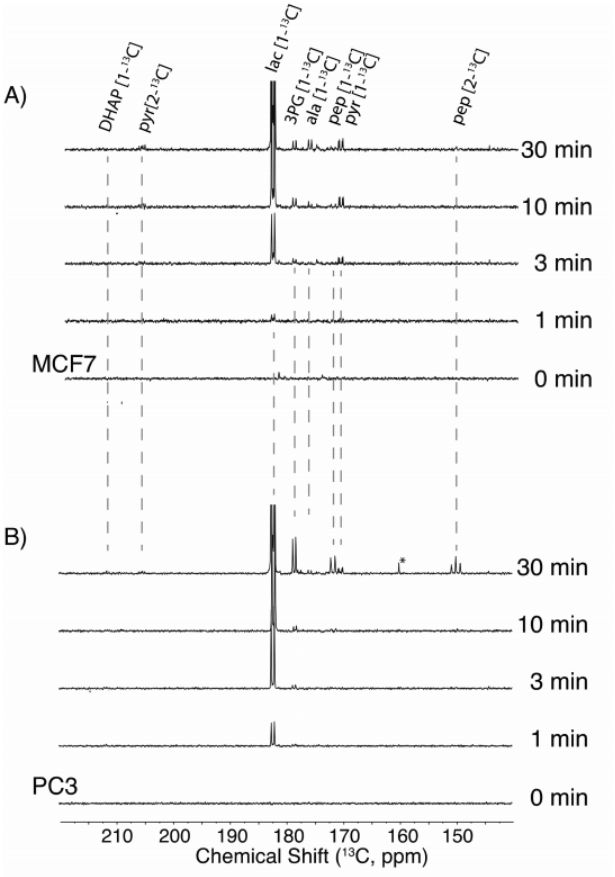


*Figure 8 – dDNP-NMR spectra from incubations with [U-$^{13}$C,D]glucose in the two cell lines, A) MCF7 and B) PC3. The cells were incubated for 0, 1, 3, 10 and 30 min. From paper I [156].*

In Figure 9 the absolute concentration is shown for the two cancer cell lines, PC3 and MCF7. MCF7 mainly produces pyruvate and its downstream metabolites, alanine and lactate, whereas PC3 accumulates PEP and DHAP. Both cell lines produce 3PG, but PC3 produced 6 times more 3PG than MCF7. Accumulation of glycolytic intermediates in the PC3 cell line could indicate an alternative use of glucose metabolism. These findings support the highly glycolytic nature of MCF7 cells, while the metabolism in PC3 is more complex. PEP and DHAP accumulate, which supports that the active isoform of pyruvate kinase (PKM2) in cancer is inhibited in aggressive prostate cancer cells [57].

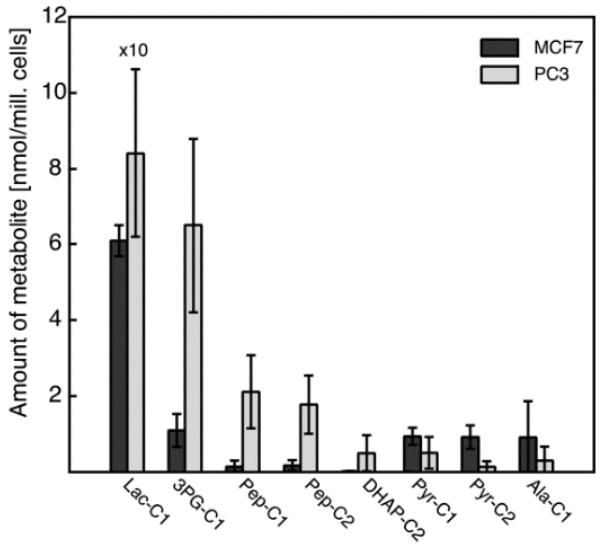


*Figure 9 – Metabolites quantified with respect to HP001 and corrected with SLC to result in an absolute concentration in the two cell lines PC3 and MCF7. From paper I [156].*

### 3.1.4 Discussion and conclusion of stable isotope-resolved analysis

The developed quantitative dDNP analysis for metabolic extracts allows for prolongation of the experiment time. Whereas the classical DNP experiment is limited by the $T_1$ of the bioprobe, this experiment is rather dependent of the biological model, pushing the time frame for experiment from minutes to hours. The analysis can be performed quantitatively, provided that internal standard is applied with laboratory dependent calibration (SLC). This loss is not universal, since it is affected by factors that may vary from set-up to set-up. As can be seen in this case, specific metabolic fingerprints supporting the two cancer cells behavior, can be seen after 30 min of incubation. Whereas certain cells are suitable for the classical dDNP experiment because of rapid turnover rate, other cell lines will have metabolites that will not yet have reached a sufficient isotope enriched concentration for detection within 1 min. At longer time frames (e.g. 30 min. of incubation) they may become visible.

HP001 is conveniently used as internal standard, since it is soluble in water, has a long $T_1$, and up-field chemical shift (23.7 ppm) that does not interfere with the region of interest, which is usually the carbonyl carbon region, and polarizes well with DNP. OX063 was used as electron paramagnetic source added in 15 mM concentration, since a relatively broad maximum around 15 mM OX063 has been reported in literature for polarization matrices [58]. A mixture of 50% water and 50% glycerol was used as glassing agent, and gadolinium-DOTA complex, to benefit from the gadolinium effect in order to get maximum polarization [59]. In this type of experiment only a single time point (single spectrum) is needed, and therefore maximum detection of signal is important without saturating the receiver. Hence, a 70º pulse was used to acquire the spectrum. Optimization of this system could include a faster transfer system, e.g. automated transfer as implemented in other laboratories [60] [61] to reduce signal loss on the way from polarizer to NMR spectrometer. Furthermore, the HyperSense is commonly used with 5 mL dissolution buffer. This leads to a dilution of metabolites. Since it is not possible to reduce the dissolution media buffer in order for the dissolution to work properly, a two-phase system could be applied containing total 5 mL mixture of apolar and aqueous dissolution medium, forcing the metabolites to remain in the aqueous fraction. Higher concentration would lead to more magnetic spin in same volume, and hence better SNR.

A unique feature of the NMR based metabolic approaches is the isotope coupling patterns in the up-field region. In some cases, this can be used to extract further information about which biochemical route the metabolite is the result of. Unfortunately, such carbons have very short $T_1$ since they have directly attached protons, making this approach difficult for hyperpolarization, unless the experimental process is optimized e.g. automated transfer to reduce transfer time.

## 3.2 Pancreatic β-cells respond with early metabolic switch to fuel pressure (Paper II)

Glucotoxicity is a well-understood pathogenic factor that leads to pancreatic β-cell failure in diabetes type 2, one of the most rapidly increasing disease of our time [62] [63] [15]. Glucotoxicity is developed when cells take potentially irreversible damage due to chronic exposure to elevated glucose levels. It is thus crucial to understand insulin release and lack thereof in the development of glucotoxicity and diabetes. Understanding early metabolic markers in β-cells under developing glucotoxicity could lead to earlier diagnosis. Substantial literature describe metabolomics in β-cells under established glucotoxicity, e.g. 16.7 mM glucose for 48 h [15] [64] or 25 mM for 20 h [65] since the development of glucotoxicity is dependent on time of exposure and glucose concentration. Short exposure times, 1-4 h, has been described as well [66] [67] [68] [69] [70]. The mechanism by which β-cells handle excess fuel to avoid glucotoxicity is however not fully understood [66].

β-cell metabolism is particular compared to other cell types. They sense glucose levels in a narrow concentration range and respond accordingly with insulin secretion. The uptake of glucose within these cells are not regulated, which results in a quick equilibration between intra and extracellular glucose [71]. The β-cell cannot block the glucose uptake and must rely on metabolic reactions to get rid of the glucose. In this study, the very early metabolic response to elevated glucose was investigated by dDNP combined with stable isotope resolved metabolomics (SIRM). Exposing β-cells to high concentrations for short timepoints (2-8 h) allowed for insight into the biochemistry of the glucose-diverting function of the β-cell, before any impairment of insulin secretion was observed.

### 3.2.1 Glucose-stimulated insulin secretion in the β-cell

Insulin release as response to elevated glucose levels is the most remarkable feature of the β-cell and has hence been widely studies. The initial mechanism of glucose-stimulated insulin secretion is well-known, Figure 10; pyruvate is generated from glycolysis and enters the TCA cycle. This results in a rise in ATP:ADP ratio, causing the ATP-regulated $K^+$ channels ($K_{ATP}$) to close, depolarization of the plasma membrane, activation of the $Ca^{2+}$ channels which opens the $Ca^{2+}$ influx, resulting in exocytosis of stored insulin [72] [73]. However, the second and sustained phase of insulin secretion in which new insulin vesicles are recruited, are not known in detail [74]. A body of work supports a pathway that is independent of the $K_{ATP}$ channels [75]. It has been proposed that pyruvate, which is taken up by the anaplerotic enzyme pyruvate carboxylase (PC) into the TCA cycle, creates an efflux of intermediates from the mitochondria. These intermediates are the used to synthesize important

coupling factors for stimulation of insulin release [76] [77]. The pathways, in which pyruvate is recycled, has been suggested: pyruvate-malate cycle [76] [78], pyruvate-citrate cycle [79] and pyruvate-isocitrate cycle [80]. They all have the same by-product in common: NADPH, and this has been suggested to serve as signal for insulin release. This is supported by the fact that pyruvate cycling is directly correlated with GSIS in a panel of INS-1 type cell-lines and NADPH/$NADP^+$ ratio increases proportionally with glucose concentration and GSIS in rodent islets [81] [69] [82].

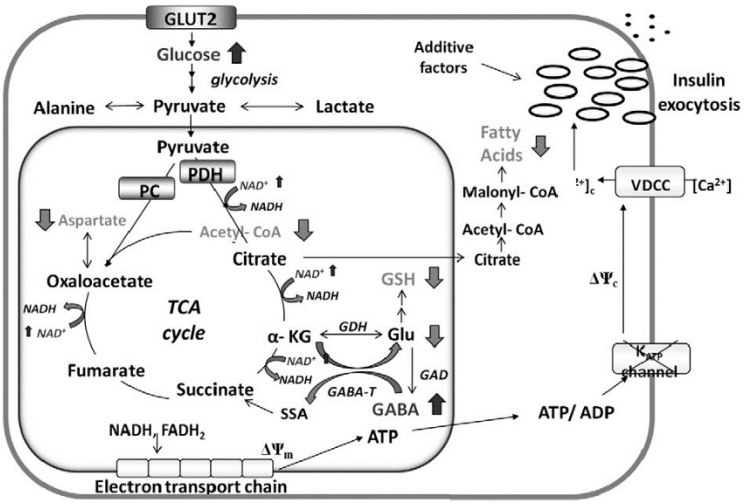


*Figure 10 – β-cell upon exposure to high glucose concentration. Glucose is transported into the cell and metabolized into pyruvate. A fraction of pyruvate is then channeled into the TCA cycle, where it creates signals leading to insulin exocytosis. From [65] Copyright 2013 by Elsevier, reprinted with permission.*

### 3.2.2 Glucotoxicity

When β-cells are incapable of releasing sufficient insulin to elevated glucose levels, glucotoxicity has been established [15]. The initial stage of glucotoxicity involves a defected insulin gene expression. If cells are exposed to elevated glucose for longer periods of time they might be irreversibly damaged and undergo apoptosis [16]. This can be detected by insulin ELISA, in which cells are exposed to basal glucose levels (2 mM) and the high glucose levels (16.7 mM), and their insulin response or lack thereof can tell whether the cells are damaged. For *in vitro* studies glucotoxicity is commonly achieved after 48 h at 16.7 mM glucose after which GSIS is reduced compared to cells cultured at lower glucose concentrations [15] [83]. At concentrations of 30 mM glucotoxicity is reported to occur hours into exposure [84]. Evidently, it is both concentration and exposure time that plays a role in development of glucotoxicity, making it a complex task to pinpoint the exact point in which the cells undergo irreversible damage.

### 3.2.3 Sample preparation

Immortalized insulin producing β-cells derived from rat (INS1) were used as a model system for this study. At 90% confluence, the cells were harvested and placed in Eppendorf tubes at a concentration of $10 \cdot 10^6$ cells in 333 µL phosphate buffer (40 mM). 167 µL [U-$^{13}$C,D]glucose (7, 11.7, 17 or 35 mM, final concentration) was added and the cells were incubated in a shaking thermostat at 37º C for respectively 2, 4 and 8 h. The entire cell suspension was then quenched with PCA, and the metabolites were neutralized, extracted and finally freeze-dried. The lyophilized samples were dissolved in 50 µL Milli-Q water and mixed with 92.5 mg glycerol containing 15 mM OX063, Omniscan and 5 µL HP001 (50 mM) as an internal standard. The sample was polarized in a HyperSense polarizer at 3.35 K and 1.4 K. Upon dissolution, the samples were dissolved in 5 mL phosphate buffer (40 mM, pH 7.4) and quickly transferred to a 9.4 T Varian NMR spectrometer into a 5 mm NMR tube. The transfer time was approximately 12 s. 1D $^{13}$C spectra of the metabolites were recorded with a 70º pulse.

### 3.2.4 Hyperpolarized SIRM of β-cells

Initially, the concentration ranges of glucose were defined based on a literature survey. Three different concentrations were chosen: 3 mM representing basal glucose levels also termed "low concentration", 11.7 mM termed "normal concentration" with respect to glucose concentration in growth medium, and 17 mM termed "high concentration", since this concentration is able to induce glucotoxicity in β-cells [15]. Initially, 4 h incubations were performed on cells with 11.7 mM glucose to investigate their metabolic profile. Four metabolites were identified based on their chemical shift derived from uniformly labeled glucose, namely pyruvate, alanine, glutamate and lactate. Their distinct chemical shifts were identified as followed: 2-$^{13}$C-pyruvate (Pyr, 205.8 ppm), 1-$^{13}$C-lactate (Lac, 183.4 ppm), 5-$^{13}$C-glutamate (Glu-C5, 182.2 ppm), 1-$^{13}$C-alanine (Ala, 176.8 ppm), 1-$^{13}$C-glutamate (Glu-C1, 175.6 ppm) and 1-$^{13}$C-pyruvate (Pyr, 171.2 ppm). The metabolites were quantified with respect to HP001, Figure 11.

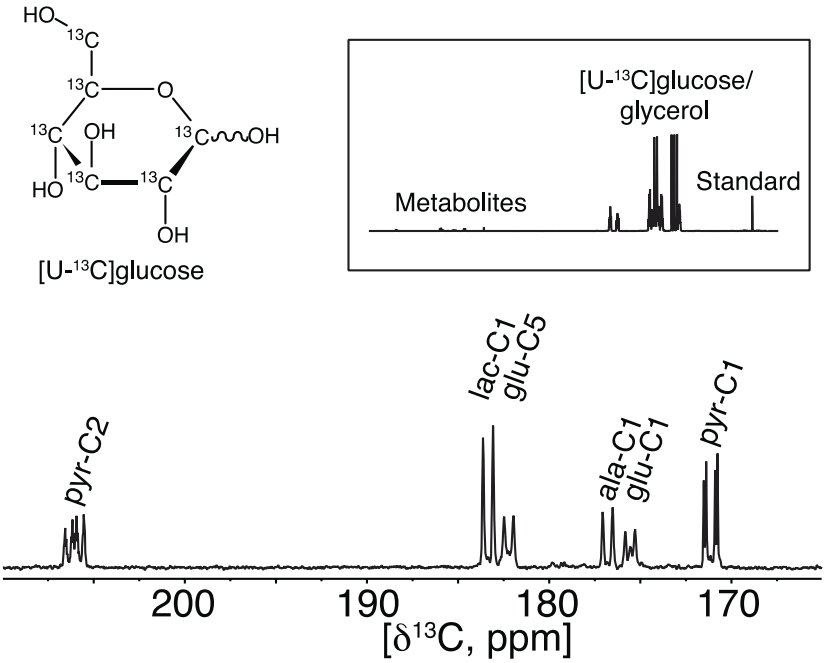


*Figure 11 – $^{13}C$ 1D spectrum of hyperpolarized metabolites after 4 h of incubation with 11.7 mM [$^{13}C_6$-$d_7$]glucose. Four metabolites were observed with distinct carbonyl shifts, namely pyruvate, lactate, alanine, glutamate. The full spectrum can be seen in the insert. Other components in the sample are residual labeled glucose, glycerol to mediate the hyperpolarization and an internal standard for quantification. From Paper II [157].*

Using the PCA extraction method, it should be noted that only the polar metabolites are visualized. Furthermore, since the whole cell suspension is used for these extracts, the sample shows the sum of both intra- and extra cellular metabolites and does not take the separate pools into account.

### 3.2.5 Concentration dependent development of metabolic profile

Extending the concentration range while keeping the incubation time constant allowed for the investigation of concentration effect on the metabolic fingerprint. Incubations at 3, 11.7 and 17 mM glucose after 4 h can be seen in Figure 12, A. It is clear by a mere comparison of the spectra, that the measured metabolites increase with increasing glucose concentration. The insulin release and content from the supernatant and cell pellet respectively for the corresponding incubation can be seen in Figure 12, B. The insulin release is increasing with increasing glucose concentration whereas insulin content decreases, which is in accordance with literature [72].

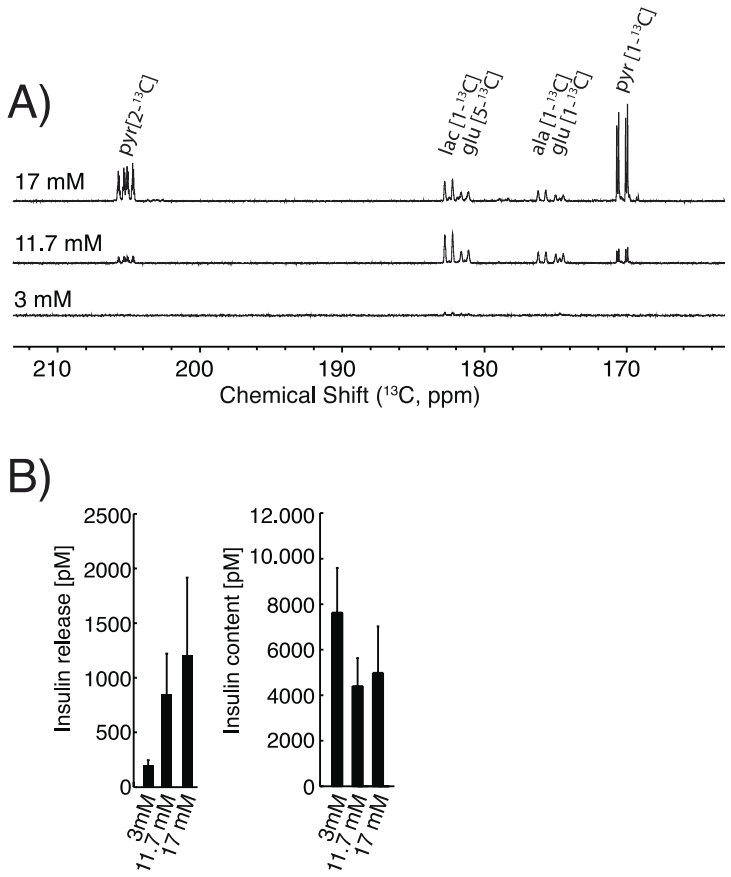


*Figure 12 – A) Metabolic fingerprint developing across concentrations (3, 11.7, and 17 mM) after 4 h incubation with fully labeled glucose. The four metabolites appear in varying concentration. B) Corresponding insulin release and content based on insulin ELISA on the extracts used for dDNP SIRM. From Paper II [157].*

Motivated by the changes in metabolite concentrations as response to glucose concentration, the extracts ranging from concentrations of 3 – 35 mM, representing basal to very high glucose concentration, were performed on 4 h incubations. The dose response of A) sum of metabolites and B) glucose consumption, correlated with glucose concentration can be seen in Figure 13.

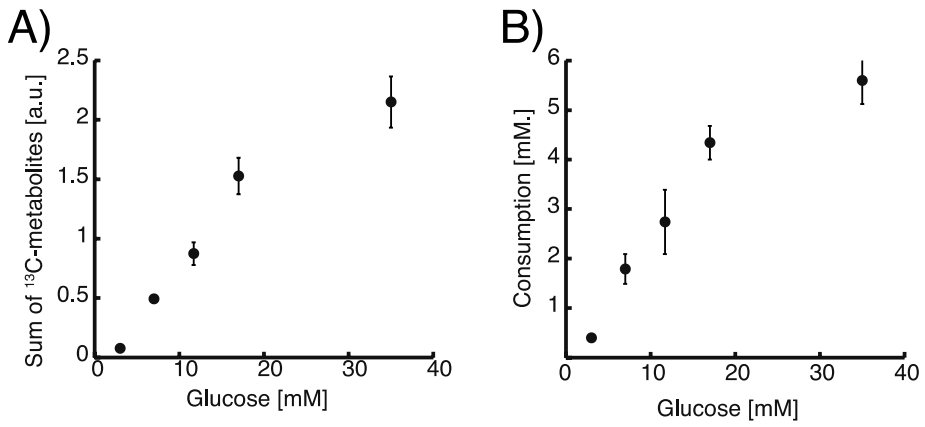


*Figure 13 – A) The sum of metabolites quantified on spectra based on 4 h incubations from 3 – 35 mM labeled glucose B) Corresponding glucose consumption in mM measured by glucose assay. From Paper II [157].*

Two interesting features should be noted; the sum of metabolites increases linearly from 3-17 mM, after which a stagnation is observed, and the trend seen in the metabolite sum is directly reflected in the glucose consumption. This points towards increase in glycolytic flux with increasing glucose concentration, which is in accordance with literature [85]. However, the shift in metabolic conversion after 17 mM points towards the possibility of shift in in metabolism.

### 3.2.6 Time dependent development of metabolic profile

To explore the effect of exposure time, the concentration was held constant and the incubation time was varied at 2, 4 and 8 h. Two concentrations were chosen, 11.7 and 17 mM glucose, representing normal and high glucose concentrations. The change in metabolite concentration can be seen in Figure 14, A) and the corresponding insulin release and content B).

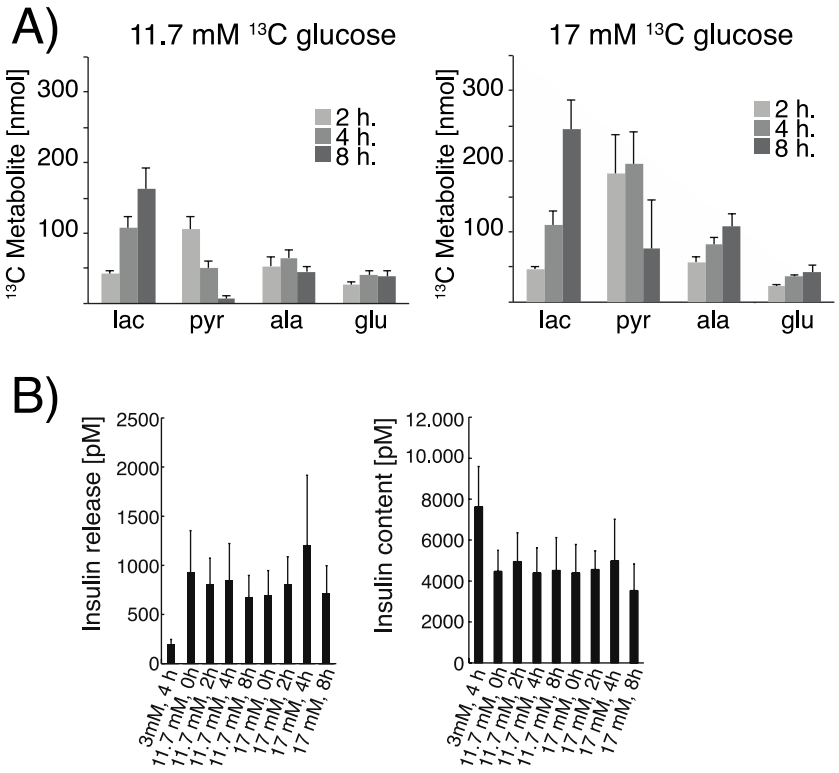


*Figure 14 – A) Change in the four metabolites over time at 11.7 mM and 17 mM glucose concentration for 2, 4 and 8 h incubations, quantified with regard to internal standard B) corresponding insulin release and content. From Paper II [157].*

Lactate accumulated over time in both cases, but more prominent in the case of 17 mM Glc. Being the end product of glycolysis, lactate is formed and exported out of the cell leading to an accumulation which is more pronounced when glycolysis is faster. Pyruvate on the other hand, seems to decrease over time. Alanine is stable in the 11.7 mM case but increasing in the 17 mM case. This could be explained by the exchange between pyruvate and alanine by alanine transaminase (ALT), so when the pyruvate pool is increased, the alanine pool will increase as well. The last observed metabolite is glutamate, which seems to be stable in 11.7 mM but increasing in 17 mM case. Glutamate is a direct readout of the TCA cycle and the flux through the TCA cycle is increasing with increased glycolysis, which is reflected in the accumulation of glutamate in the 17 mM incubation.

Intrigued by the significant changes in lactate and pyruvate, three conditions were investigated further; 11.7 mM, 17 mM and 35 mM glucose concentrations, and the metabolites were depicted individually and as a sum, Figure 15.

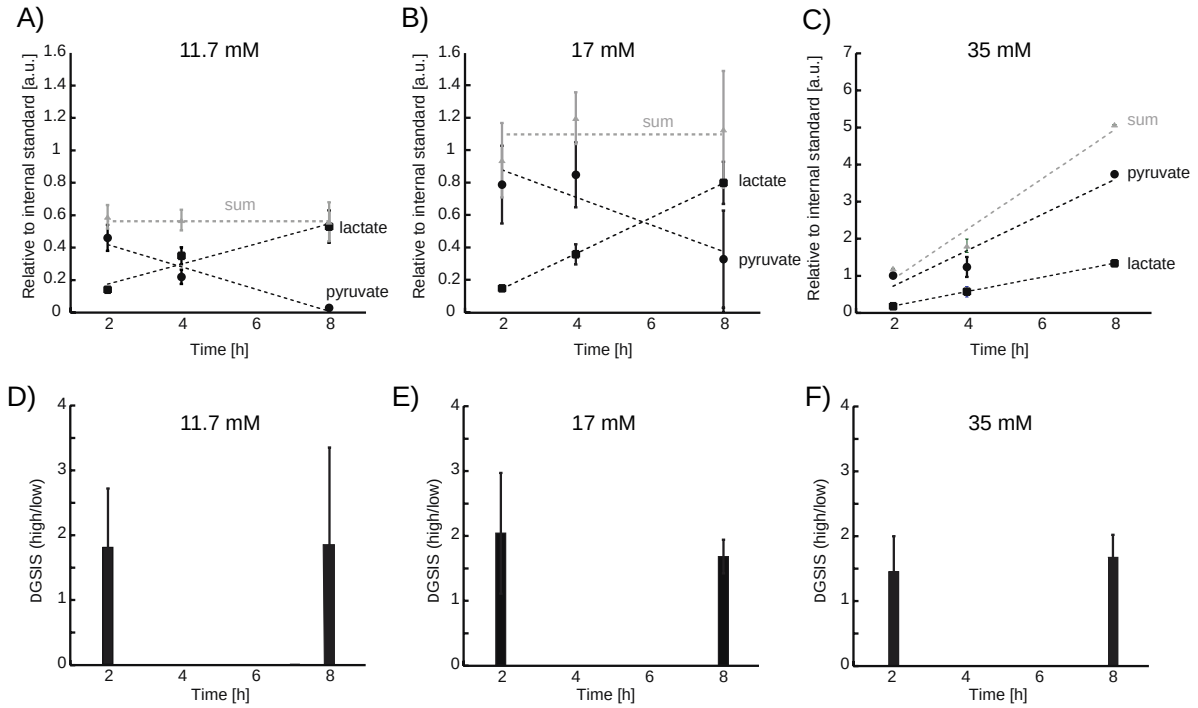


*Figure 15 – A-C) sum of metabolites (AU) as function of time during incubation with three different concentrations of glucose (11.7, 17 and 35 mM respectively) D-F) Insulin release based on ELISA assay ratio between low/high glucose. From Paper II [157].*

The total sum of pyruvate and lactate is constant in the case of 11.7 mM and 17 mM across all the time points. Individually, pyruvate and lactate change over time. The intersection of these, or the point when the pyruvate/lactate ratio is 1, seems to depend on glucose concentration. This becomes apparent in the case of 35 mM glucose incubation. Here, the total sum is increasing, and so is both pyruvate and lactate throughout the time course of 8 h with no intersection. This metabolic profile is different from the two other cases. However, the insulin secretion does not seem to be affected in any of the three cases, Figure 15 D) – F). This is the ratio between low and high Glc exposure during GSIS on cells (ΔGSIS), that have undergone incubation with 11.7 – 35 mM Glc for 2 and 8 h compared. This points toward the fact that the metabolism is perturbed before the insulin secretion is affected at these time-points and concentrations. Viability did not change dramatically throughout the experiment, Table 1.

Table 1 – Viability of INS1 cells under various conditions (n=2).

| Viability, 40 mM phosphate buffer | 2 h. | 4 h. | 8 h. |
|---|---|---|---|
| 11.7 mM | 94% | 94% | 90% |
| 17 mM | 94% | 94% | 92% |
| 35 mM | 93% | 94% | 94% |

In summary, this data indicate that the β-cells cannot control the uptake of glucose. Pyruvate seems to be accumulated until a certain threshold, after which the cells start to respond with a metabolic switch to reduce the pyruvate pool and by this way, adjusting the glycolytic flux. This ability is lost at very high glucose concentrations (35 mM). Since the ΔGSIS was not affected, these metabolic perturbations appear before insulin impairment, and must be the early response of the normal funtioning β-cell to excessive glucose concentration.

### 3.2.5 Discussion of metabolic switch in β-cell

This study investigated the energy metabolism of β-cells exposed to glucose concentrations ranging from 3-35 mM over the time course of 2-8 h with the aim of investigating early metabolic events of excess fuel handling and observed a significant pyruvate accumulation over a large span of glucose concentrations from 3 to 35 mM. An increase of the pyruvate metabolite has been described in literature at various glucose concentrations (2.8 mM – 16.7 mM) at short exposure times, 1 h [66] and long exposure times [15]. However, this switch observed with $^{13}C$ flux revealed by the change in pyruvate metabolism has not been described previously.

On its own, pyruvate is not increasing GSIS and can therefore not be considered a direct coupling factor for GSIS. A by-product of pyruvate cycling reaction is NADPH, which is proposed to be a coupling factor [86] [87] [88]. Mugabo et al. [66] has suggested that metabolic ways of handling excess fuel before insulin impairment could involve glycerol production and lipid synthesis. Here, pyruvate was observed to increase after 17 mM glucose, and could potentially qualify as an important biomarker for early excess fuel handling. Metabolism of pyruvate can occur through glucose oxidation via TCA, anaplerosis via pyruvate cycling and glycerol/fatty acid cycling [89]. Since no pronounced changes in TCA activity is observed in terms of glutamate concentration in this study,

and GSIS is also constant, we suggest that glycerolipid/fatty acid cycling is the pathway coupled to pyruvate change.

The consumption of the accumulated pyruvate at hour timescale points to an upregulation of a diverging pathway, which we hypothesize is the glycerol/fatty acid cycle.

An important observation of this study is that no changes in GSIS was observed. Hence, the metabolic changes occur before insulin impairment, and can be considered early events prior to β-cell failure. On very high glucose concentrations (35 mM) this diverging pathway is lost, and pyruvate is accumulated over the timeframe of 8 h. We suggest that when exposed to excess fuels, the β-cell initially protects itself by modulating the pyruvate pool while upregulating the divergence pathway – a process that occurs before insulin secretion is impaired. In conclusion this study shows that the β-cells use different metabolic pathways to reduce excess metabolites formed from uncontrolled glycolysis. Glycerol/fatty acid metabolism is the most likely candidate responsible for this deviation pathway. Further studies are needed to deduce this fundamentally important and not yet well-described defense mechanism against glucotoxicity.

## 3.3 Discussion and conclusion of part I

In part I, a stable isotope-resolved quantitative dDNP assay was developed to enable the use of dDNP for end point metabolomics. Initially, the method was developed by polarization of samples "mimicking" common metabolites, lactate, pyruvate, alanine and acetate. After polarizing these, it was evident that the $T_1$ decay in the hyperpolarized samples were slightly different then the $T_1$ measured by thermal NMR on the same molecules. This $T_1$ disagreement was attributed to the relaxation mechanisms, which affects the molecule during transfer from polarizer to spectrometer. To correct for this, a signal loss coefficient (SLC) was introduced, based on the difference between thermal and polarized $T_1$. The SLC was necessary for converting the integrals to concentrations, based on a known amount of internal standard, HP001. The method was then demonstrated on PC3 and MCF7 cells, and showed cell line specific metabolic patterns after up to 30 min. incubation with fully labeled glucose.

The method was then applied on a different cell system, INS1, an insulin responsive cell line. The cells were treated with 3-35 mM fully labeled glucose, and the end point metabolomics scan were acquired after 2, 4 and 8 h to get insight into the very early metabolic events in the β-cells when exposed to excessive glucose. From the spectra it was possible to see, that glucose-derived pyruvate accumulated initially but was consumed within the timeframe of the experiment (8 h) at 11.7 and 17 mM glucose concentrations, but at 35 mM glucose, pyruvate accumulated throughout the duration of the experiment. The pyruvate pool was hypothesized to be a potential biomarker for excessive fuel handling, and the consumption of pyruvate was thought to occur through glycerol/fatty acid cycle. However, at very high glucose concentrations (35 mM) this divergence pathway was diminished, which resulted in constant accumulation of pyruvate. Importantly, these metabolic changes occurred before insulin impairment and are therefore hypothesized to be early metabolic events before established glucotoxicity.

There is an interesting continuation of the β-cell study; since the INS1 cells are an immortalized cell line, it can be expected to show some cancer-like features. For instance, it is known for β-cells that they contain very little LDH [85] [90], still a stable lactate production was observed. This could be explained by the Warburg-effect in the immortalized cells. To be able to generalize these observations it should be shown in primary β-cells. For insulin studies, it is common to extract primary islet tissues from mice. It was investigated that in order to make a sample with sufficient SNR for metabolite quantification, no less than $10 \cdot 10^6$ cells should be used per sample, at least with current set-up in

our lab. $10 \cdot 10^6$ cells will correspond to sacrificing a substantial number of mice, and since islet extraction is a delicate procedure requiring experience and time, this would not be a sustainable solution for a vast number of experiments. Therefore, the attention should be turned to the set up to improve SNR such that even smaller samples could be investigated. E.g. the dissolution occurs in 5 mL buffer, of which only 600 µL is used in the NMR tube, rest is discarded. This dissolution media could be reduced, e.g. by a two-phase system as previously mentioned. Also, the transfer could be optimized, e.g. by automated transfer or magnetic shielding.

Furthermore, since the cells were incubated in Eppendorph tubes, hypoxia could have played a role. It is therefore not known if hypoxia could have affected the cell system. Viability and glucose intake were stable throughout the 8 h of experiment, which indicates the cells are viable at the given scan times.

Potentially, it is an interesting discovery, since glucotoxicity can be reversible. It can be shown *in vitro*, that cells, if they are removed from high glucose media and allowed to recover in basal glucose media, can fully restore their function [91]. But since glucotoxicity developing across a parameter span between glucose concentration and time of exposure, the exact stage on when cells start to suffer from permanent damage could be useful information.

The unique feature of stable isotope method compared to other analytical tools is the additional information that can be extracted from coupling patterns arising from the tracer molecule. In this project, only fully labeled glucose was used, resulting in all other carbons derived from glucose being labeled, which involves upper glycolysis and TCA cycle. For further information about specific biochemical pathways, specifically labeled glucose could be applied.

# 4. Part II – Bioreactor for visualization of real time metabolism in pancreatic cancer cells

*The study was carried out partially at Center for Hyperpolarization in Magnetic Resonance (HYPERMAG) at Technical University of Denmark and partially at National Institutes of Health, Bethesda, Maryland U.S., National Cancer Institute, Radiation Biology Branch in the laboratory of Dr. Murali Cherukuri. In vitro data by bioreactor was generated at HYPERMAG using a home-built flow cell and a bioreactor purchased from Medorex, Germany.*

## 4.1 Living cell metabolism by dDNP

The easiest and most common approach to study live cell metabolism by dDNP is by suspending living cells in medium directly in the NMR tube and then add the HP substrate [92] [93] [94]. The metabolic conversion of the HP substrate can then be monitored dynamically by NMR. The simplicity of this set up makes it practical and easy to mix the cell suspension with the HP substrate. However, in contrast to *in vivo* experiments, where the same animal can be used several times for multiple metabolic measurements (repeated injections of HP bioprobe), *in vitro* experiments require new cells for each measurement [95]. Growing new cells or extracting primary cells from tissues can be a tedious process. Furthermore, the time between preparation of experiment (placing cells in NMR tube and setting up NMR experiment) and conduction of experiment is typically minutes, during which time the cell suspension may become hypoxic and metabolism may be altered.

To address these issues, cell perfusion, or "bioreactors" have been developed during the last three decades [95]. Such systems have been used to monitor steady state metabolites and their changes as a factor of time [96]. dDNP offers the signal enhancement necessary to gain temporal resolution to monitor fast kinetic reactions in real time. Therefore, dDNP compatible bioreactors have started emerging:

Various bioreactor designs can be found in the literature that are specifically designed for dDNP experiments:

- Keshari et al. (2010) [95] and Sriram et al. (2015) [97] have developed a system in which the cells are placed in the NMR tube in the spectrometer, while the medium is circulated by a peristaltic pump from a vessel. A gas exchanging module is regulating the atmosphere to 95% air and 5% $CO_2$, and all medium containing tubes are heated by water in surrounding tubes.

The cells are fixed in the NMR tube by electrostatic encapsulation in alginate [97]. The inlet tube is placed in the suspension with the cell containing alginate beads, creating an upward flow while a restrictive baffle is keeping the cells in the active volume of the tube, Figure 16.

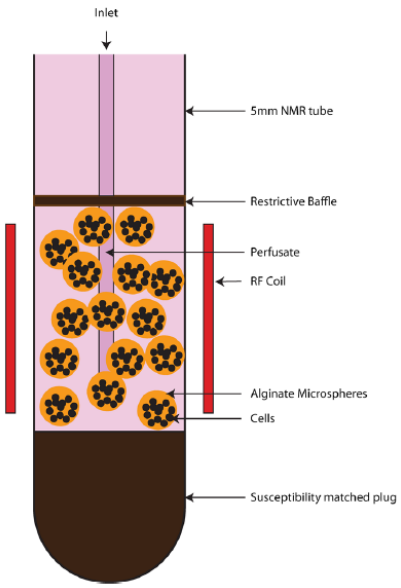


*Figure 16 – Graphical representation of the 5 mm MR compatible bioreactor flow cell with alginate encapsulated cells. The flow cell is equipped with a susceptibility matched plug and restrictive baffle, to keep the encapsulated cells within the active volume during perfusion. From [97]. Copyright 2015 by John Wiley and Sons. Reprinted with permission.*

- Lauritsen et al. (2015) [98] describe a perfusion system, where cells are grown on 3D printed scaffolds from polycaprolacetone (PCL) plastic. The scaffolds are placed in a bioreactor cell, which is subsequently perfused. There is no circulation within the bioreactor itself, since the medium passes through and exits the other end of the chamber.

- Breukels et al. (2015) [99] describe a flow cell for a non-perfused system with resolution, sufficient to differentiate between intra- and extra cellular lactate on two million cells. This flow cell consists of a 5 mm Shigemi NMR tube with a modified plunger for injection of HP substrate. A polytetrafluoroethylene (PTFE) capillary (O.D. 0.7 mm, I.D. 0.5 mm) is placed through the plunger and placed just above the active volume.

## 4.2 Objective of the study and experimental design

Within most solid tumors, significant areas of hypoxia exist containing cancer cells that are resistant to traditional chemotherapy and radiation treatment. Thus, therapeutics which are specifically targeting these areas may provide clinical benefits [100]. TH-302 is a hypoxia-activated prodrug (HAP) known to activate selectively under the hypoxic conditions. Currently, the drug is undergoing clinical trials, including Pancreatic Ductal Adenocarcinomas (PDAC) trials. Studies have demonstrated varying sensitivity towards the TH-302 drug in several human PDAC cell lines in xenograft models (Hs766t>MiaPaCa-2>Su.86.86) involving metabolic response *in vivo* and *in vitro* [101] using HP pyruvate and $^{13}C$ MRI. In this study, the cell lines Hs766t and MiaPaCa-2 are used for *in vitro* study with HP-$^{13}C$ pyruvate to show early metabolic changes as response to the TH-302 treatment. The longitudinal studies will be carried out using a bioreactor set up, which is NMR compatible and able to carry out experiments under hypoxic atmosphere to potentiate the TH-302 drug effect. The two pancreatic cancer cell lines (Hs776t and MiaPaCa-2) of varying glycolytic activity were chosen as a model system of PDACs. The two cell lines represent pancreatic cancers from two different metastatic sites: MiaPaCa-2 from primary site and Hs766t from lymph node metastatic site [102].

TH-302 is activated in severely hypoxic regions, $< 0.5\%$ $O_2$. In the presence of oxygen, the radical anion prodrug reacts rapidly with oxygen to generate the original prodrug. Therefore, TH-302 is relatively inert under normal oxygen conditions. When exposed to hypoxic conditions similar to those found in tumors, the radical undergoes irreversible fragmentation releasing the active drug Br-IPM, an azole derivative. This is a cytotoxin, capable of alkylating DNA, Figure 17 [103].

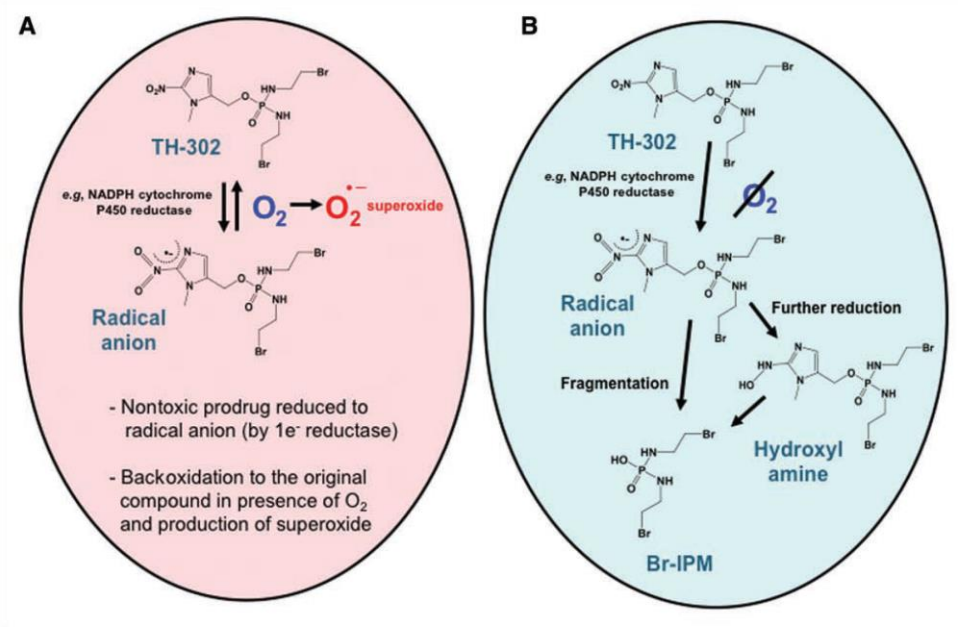


*Figure 17 – TH-302 is activated by a 1-electron reduction mediated by cellular reductases e.g. NADPH cytochrome or P450 reductase. A) Under normoxic conditions, the formed radical quickly reverts back to the original prodrug while generating superoxide. B) under hypoxia, the radical is either directly fragmenting or endures further reduction before eventually fragment into the active drug, Br-IPM. From [103]. Copyright 2011 by American Association for Cancer Research. Reprinted with permission.*

In this project, cancer cells are exposed to TH-302 for 2 h, after which, early metabolic changes can be monitored non-invasively by HP pyruvate. These early metabolic changes are thought to occur before cell viability starts decreasing after days [101]. For this *in vitro* study the experiment is designed as seen on Figure 18. Two hours of treatment has been described in literature [104].

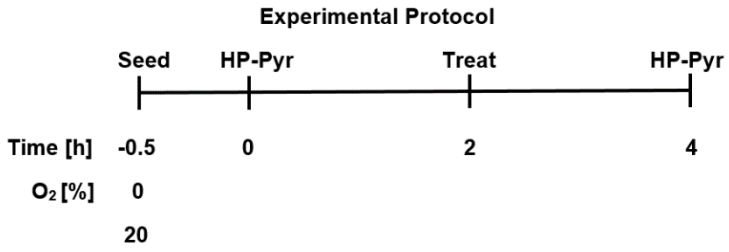


*Figure 18 – Experimental design for early drug treatment response in vitro. Initially, cells are placed in the bioreactor under perfusion under either normoxic or hypoxic atmosphere. A baseline spectrum is recorded with HP $^{13}$C-Pyruvate after 30 min. After 2 h of equilibration, treatment with TH-302 is initiated for 2 h after which point HP $^{13}$C-Pyruvate is injected and the metabolism is compared to the baseline spectrum. Furthermore, viability is measured at start and after 4 h of experiment.*

This study requires the combination of several components:

- Construction of dDNP-NMR compatible bioreactor and flow cell, capable of creating and maintaining a hypoxic atmosphere, section 4.3 – 4.4.
- Strategy for cell adherence onto surface for longitudinal studies, section 4.5.
- A reliable method for cell quantification in flow cell, section 4.6.
- Treatment with TH-302, $IC_{50}$ and the potentiation under hypoxia, section 4.7.
- Good SNR from cells in flow cell, which entails quick injection and sufficient mixing of HP substrate, section 4.8.
- Perfusion behavior of cell and viability in bioreactor, section 4.9.

## 4.3 Construction of dDNP-NMR compatible bioreactor

The goal of the desired perfusion system is to be able to perform longitudinal studies on cell cultures. Additionally, it is desired to construct a system that is capable of controlling the atmosphere to e.g. prevent or induce hypoxia for the duration of the experiment, since cell metabolism is known to be affected by hypoxic conditions [9]. To achieve this, a closed, circulating perfusion system with atmosphere control was designed, Figure 19. In this section, the vessel controlling the media parameters (A) is referred to as "bioreactor" and the NMR tube (B) in which the cells are fixed is referred to as "flow cell".

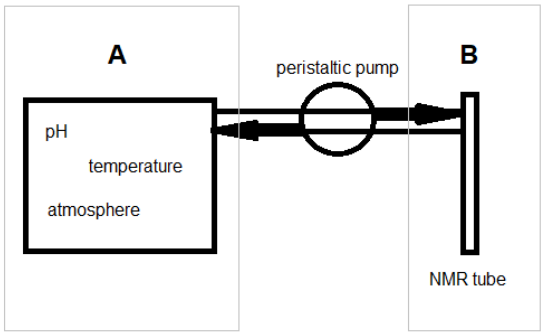


*Figure 19 – Simple schematic of the perfusion system. Part A) is the bioreactor chamber, a vessel, which is responsible for conditioning the medium by controlling temperature, atmosphere and pH. The medium is then circulated from the vessel A) to the flow cell B) by a peristaltic pump. The flow cell is an NMR tube, which can be placed directly in the spectrometer with the living cell at 37°C.*

### 4.3.1 Part A (bioreactor)

A Vario 500 bioreactor was purchased from Medorex, Germany. The main vessel consisted of an outer vessel (500 mL) and a conical inner vessel, which could accommodate 50-125 mL of liquid. The vessel lid was equipped with 10 ports for probes and stirred by an axial stirring system. The bioreactor compatible probes were temperature probe (Pt1000), DO-sensor (Medorex), pH sensor (Medorex) and a heater. Furthermore, a gas inlet was submerged in the medium to create the desired atmosphere, which was either air or nitrogen for hypoxia experiments from separate bottles attached to flow meters. pH was controlled by automatic addition of either KOH or HCl (1 M), with a sensitivity in the range of pH 7 ± 0.1 through a separate inlet. The probes were connected to a control system, which could be controlled by a PC. The gas exchange module had to be controlled manually and could mix up to three gases by three different flow meters. The gas pass through a sterile filter,

before reaching the medium to avoid contamination. The software used for controlling the bioreactor allowed for monitoring of all the above-mentioned parameters, and could be automated, Figure 20.

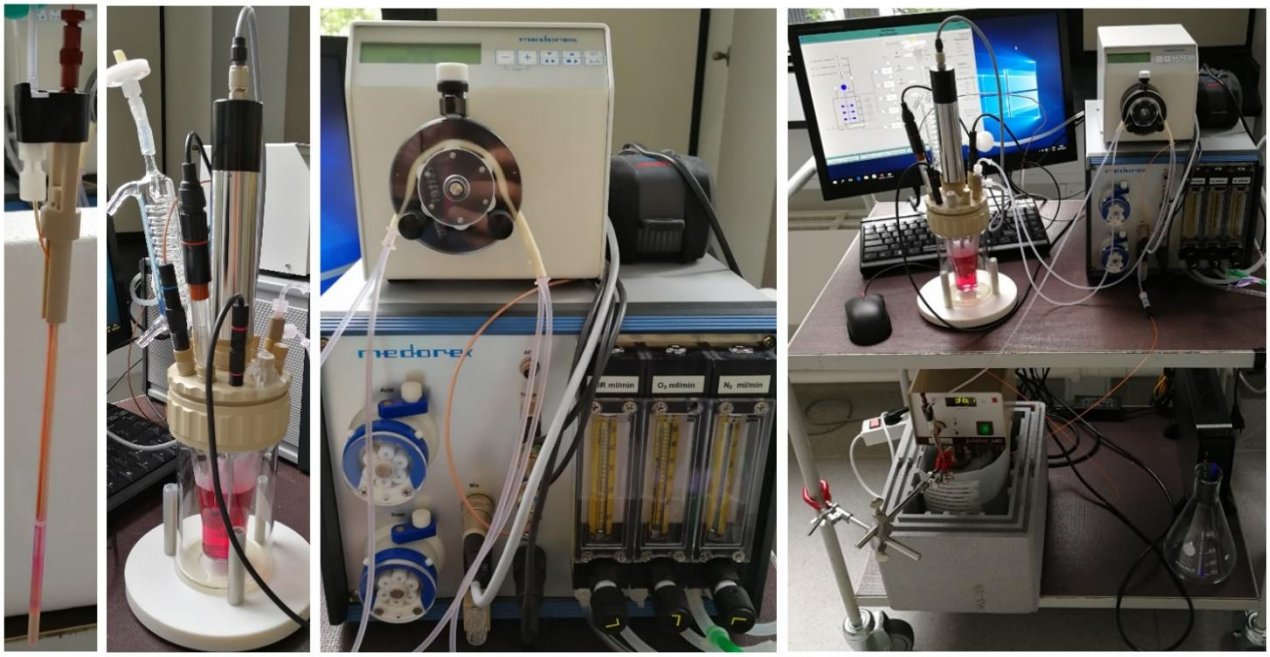


*Figure 20 - Medorex bioreactor, set up to perfuse living cells. From left to right: 1) flow cell with living cells, here demonstrated with a 5 mm NMR tube. The inlet tube perfuses the cells while an exit tube removes excess medium from the top of the NMR tube. 2) Bioreactor with probes, stirrer and inlet tubes. Here, medium is provided with the right parameters such as temperature, pH and atmosphere. 3) The peristaltic pump with two channels, responsible for creating the flow to and from the flow cell placed on the control unit. All probes are plugged into the control unit which is also responsible for mixing the gases through the flow meters. 4) Full set-up. The NMR tube is submerged into a water bath at 37º C.*

### 4.3.2 Part B (flow cell)

The flow cell consisted of an NMR tube, either 5 or 10 mm. The flow cell top consisted of polyether ether ketone (PEEK) material, modified to accommodate both 5 and 10 mm tubes, Figure 21. A gas chromatography (GC) tube was centered and placed such that the inlet created a bottom up flow, as seen in literature [97]. A filter was placed above the active volume to avoid cells escaping the active volume. Just above the filter, an exit tube was placed to keep the volume in the NMR tube constant. The cells were kept at 37 ºC in a water bath during the experiment.


*Figure 21 Flow cell with A) PEEK top with adaptors for tubes B) GC-tube centered in the NMR tube C) the top can be placed on a 5 or 10 mm tube D) a 10 mm tube with a PEEK plug to reduce the dead volume of the tube and ensure homogeneous flow through cells.*

## 4.4 Putting the bioreactor to test

To test the bioreactor reliability, cell viability test was run for up to 30 h. Hs766t cells ($20 \cdot 10^6$) were harvested and placed in the NMR tube in suspension. The bioreactor was switched on, and the flow was regulated to 100 µL/min which ensured a steady low flow to avoid cells being evacuated from the flow cell through the exit tube. Three conditions were tested: 1) flow with normoxia 2) flow with hypoxia 3) no perfusion. At given time points, 10 µL medium with cells was removed, dyed with trypan blue, and viability was based on viable cells in conjunction with total cell number, Figure 22.

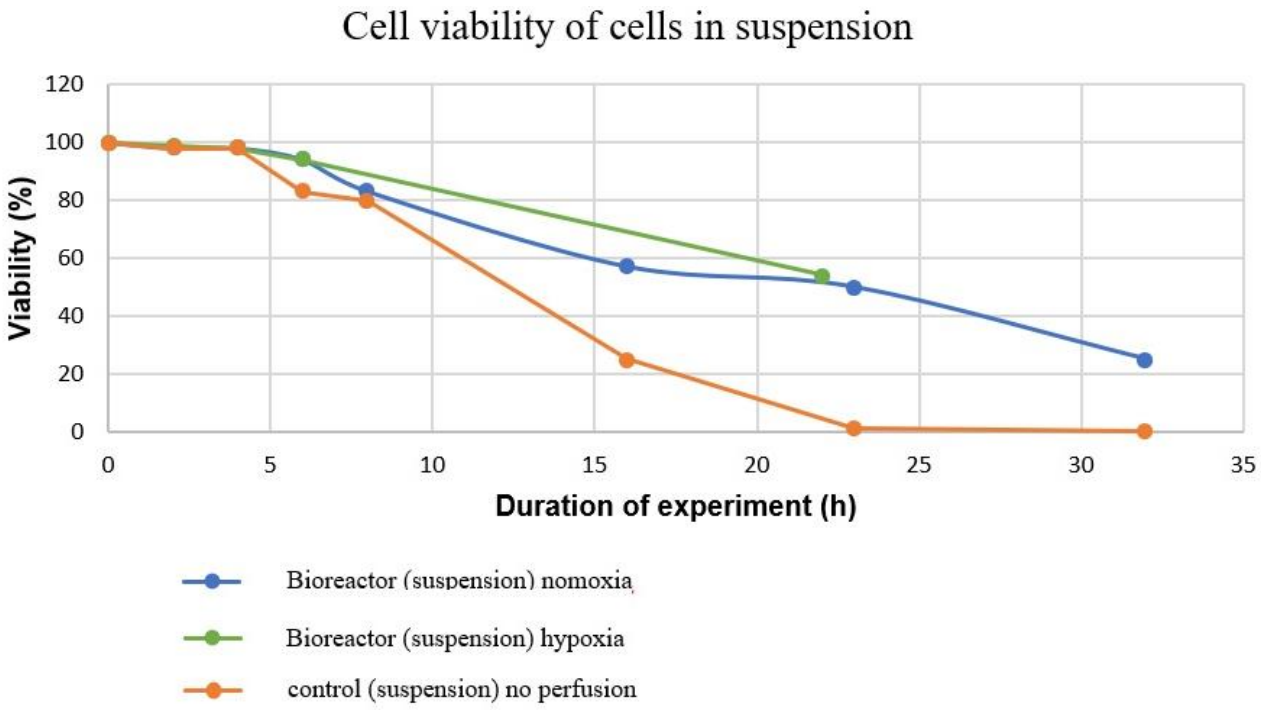


*Figure 22 – Viability of Hs766t cells in suspension under three different conditions. After 4 h, a drastic decrease in viability can be seen as consequence of anoikis.*

Evidently, after 4 h the cells start losing viability drastically in all the conditions. When adherent cell lines, such as cells from epithelial origin cannot adhere, they will undergo anoikis – a particular type of apoptosis [105]. Therefore, for longitudinal experiments cells need to adhere to a surface.

## 4.5 Strategies for cell adherence

2D cell cultures, involving monolayers adhered to a plastic surface, is the most easy and convenient to set up with good cell viability. A way to use this approach for bioreactors has been developed decades ago, involving growing cells on microcarriers [106]. A further development of this method could involve scaffolds modified to fit into the given flow cell [98]. Innovative approaches describe 3D methods which entails spheroid formation, either by encapsulating cells in a viscous matrix such as alginate [97] or by growing the cells into larger aggregates [107].

Initial strategy involved growing the cell line MiaPaCa-2 on microcarriers and test the SNR achievable for HP experiment in a 5 and 10 mm tube. 500 mg microcarriers (Cytodex III) were placed in a 15 mL falcon tube. The tube was filled with ethanol (70%), shaken well and left for at least 24 h. The ethanol was aspirated carefully. The tube was filled with the respective medium, shaken well,

and the microcarriers were allowed to sediment. The medium was removed carefully. This was repeated twice, at which point the ethanol was considered to be washed out. Medium was added until 10 mL, such that 1 mL medium contained 50 mg microcarriers. A confluent flask of MiaPaCa-2 was harvested. $5 \cdot 10^6$ cells in 1 mL were placed in a petri dish with 8 mL medium and 1 mL microcarriers. The petri dish was incubated for 48 h, at which point the cells covered the microcarriers, Figure 23.

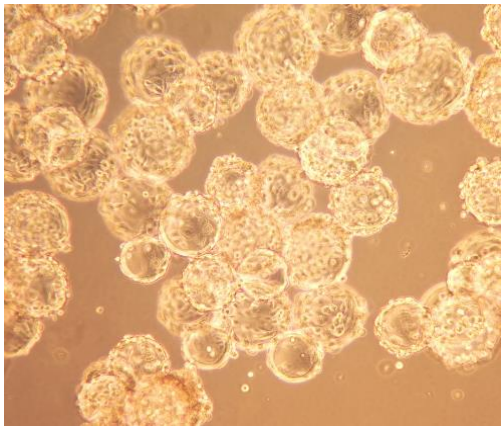

*Figure 23 – Microcarriers covered with MiaPaCa-2 cells after 48 h of incubation. The confluence of the microcarriers after 48 h depends on the cells doubling time.*

## 4.6 Quantification of cells on microcarriers

To quantify cells on microcarriers, a method based on 3-(4,5-dimethylthiazol-2-yl)-2,5-diphenyltetrazolium bromide (MTT) assay was developed. Since trypsinization of cells from microcarriers showed to be non-reproducible because of the difficulties of separating microcarriers from cells, MTT offered a less invasive quantification based on cell number and viability directly on the microcarriers with cells. MTT is a yellow tetrazole, which is reduced to a purple formazan in living cells by mitochondrial reductases [108]. The formed formazan is insoluble in the medium. The reaction is quenched by addition of dimethyl sulfoxide, which stops the reaction and dissolves the formazan. This yields a purple solution with a maximum absorbance at the wavelength of 540 nm, and the absorbance corresponds directly to the amount of viable cells. A standard curve was prepared on a known number of cells such that the absorbance measured on microcarriers could be correlated to the cell number, Figure 24.

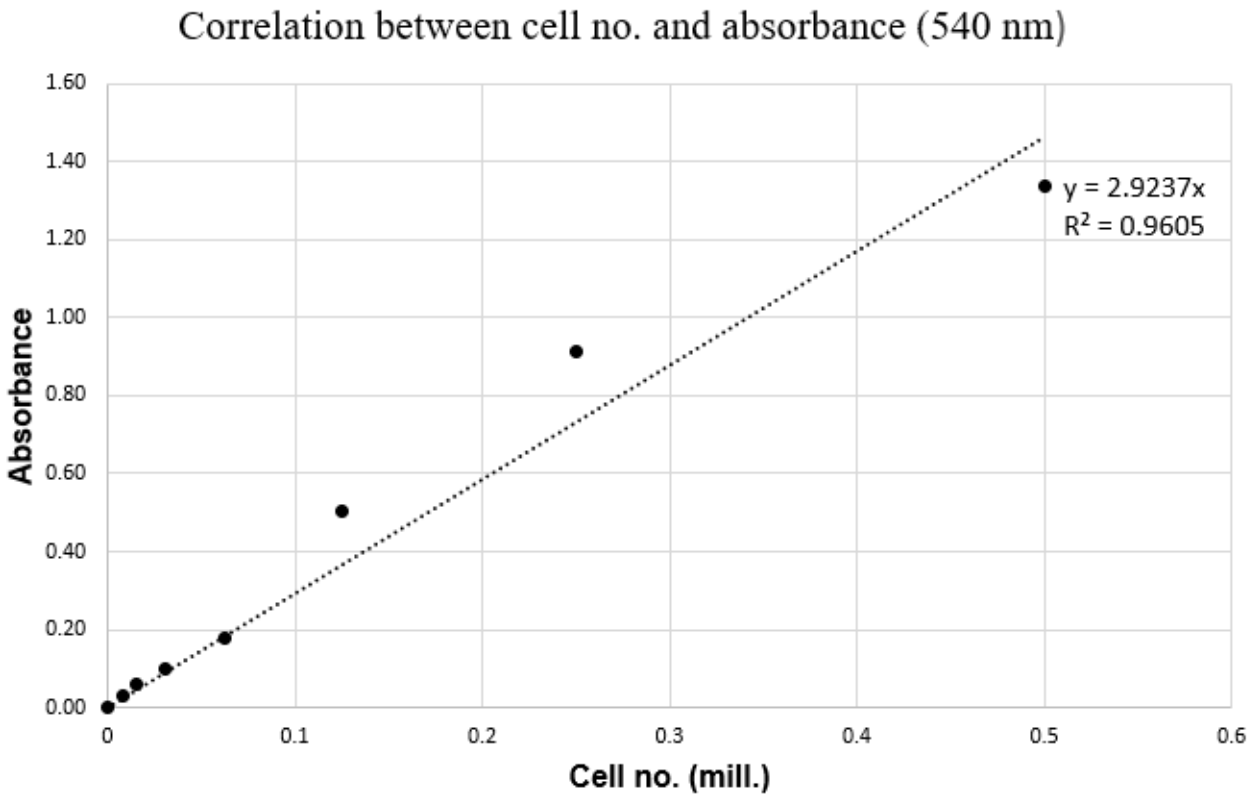


*Figure 24 – Standard curve correlating absorbance and cell number in the MTT assay. The linear range was designed for cell numbers up to $6 \cdot 10^5$ after 3 h of incubation following 20 min incubation with DMSO. The absorbance was measured at 540 nm.*

The experiment was based on a known number of MiaPaCa-2 cells in 24-well plate after adherence (1.5 h). Cells on microcarriers were subjected to MTT assay directly, since they were already adhered. The wells were incubated in 500 µL MTT medium (0.5 mg/mL MTT in minimal medium) for 3 h after which 300 µL medium from each well was discarded and 500 µL DMSO was added following 20 min of incubation. 100 µL from each well was used in a 96-well plate and the absorbance was measured at 540 nm on a BioTek EPOCH 2 microplate reader (Holm & Halby, Brøndby, Denmark). The procedure was adapted from [109].

Other approaches involving separating trypsinized cells from microcarriers by sedimentation speed and protein determination did not show reproducibility and were abandoned.

## 4.7 TH-302 treatment study

TH-302 was acquired from MedChemExpress. It has been shown that the $IC_{50}$ for MiaPaCa-2 cells was 2.1±0.7 µmol/L TH-302 under hypoxia and 210±49 µmol/L TH-302 under normoxia [104] after 2 h of treatment and followed by 3 days of incubation. This experiment was reproduced under normoxic conditions. Based on the doubling time, MiaPaCa-2 cells were seeded in a 24-well plate at a density of $7.5 \cdot 10^4$ cells. After 24 h the cells were treated with medium containing 210 µL TH-302 for 2 h after which the medium was discarded and the cells were incubated in full medium for 72 h (n=2). Conditions and results are summarized in Table 2.

*Table 2 – Conditions and results from TH-302 treatment study on MiaPaCa-2 cells in wells.*

| Condition | Cell line | Viability (%) | Seeding conc. | Experimental time (h) | Drug conc. (µM) |
|---|---|---|---|---|---|
| 24-well | Mia PaCa-2 | 51.9 | 75,000 | 72 | 210 |
| 24-well | Mia PaCa-2 | 54.2 | 75,000 | 72 | 210 |

The experiment resulted in an average viability of 53%, which is close to the $IC_{50}$ reported in the literature, which confirms the reported efficiency of the drug in MiaPaCa-2 cells. For Hs766t, the reported IC50 is 60±7.5 µmol/L TH302 under hypoxia and 1400 µmol/L TH-302 under normoxia, which we were not able to reproduce, Table 3, and further experiments were not possible within the timeframe of this study.

*Table 3 – Conditions and results from TH-302 treatment study on Hs776t cells in wells.*

| Condition | Cell line | Viability (%) | Seeding conc. | Experimental time (h) | Drug conc. (µM) |
|---|---|---|---|---|---|
| 24-well | Hs776t | 96.4 | 100,000 | 72 | 1400 |

## 4.8 HP [1-$^{13}$C]Pyruvate to visualize metabolism in MiaPaCa-2 cells on microcarriers

The conversion in MiaPaCa-2 cells was investigated by HP-pyruvate. The conversion of pyruvate to lactate in a suspension experiment was compared to the conversion on microcarriers. $10{\cdot}10^6$ MiaPaCa cells (either suspension or microcarriers) were placed in 1000 µL in a 10 mm NMR tube, equipped with a PEEK plug to simulate a Shigemi set up. 1000 µL HP-pyruvate was added, yielding a final concentration of 2 mM, acquired with a flip angle of 10º and a repetition time of 2 s, Figure 25.

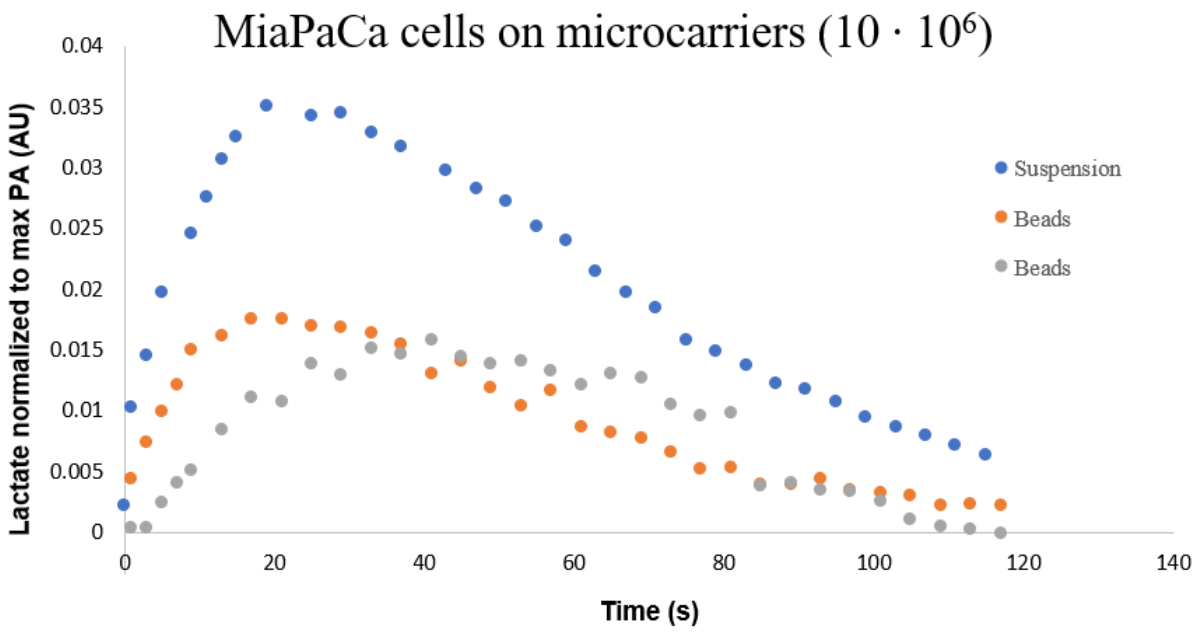


*Figure 25 – Suspension (n=1) vs. microcarriers (n=2). Microcarriers induced magnetic field inhomogeneity due to sedimentation during injection. Conversion ($Lac_{max}/Pyr_{LacMax}$) ~ 5%. $10{\cdot}10^6$ MiaPaCa cells were placed in 1000 µL in a 10 mm NMR tube, equipped with a PEEK plug. 1000 µL HP-PA was added, yielding a final concentration of 2 mM, acquired with a flip angle of 10º and a repetition time of 2 s.*

An important consideration in this experiment was good mixing of HP-pyruvate in the flow cell. The experiment was performed in a 5 mm NMR tube several times, but achieving conversion of 5% required $50{\cdot}10^6$ cells in suspension. This number of cells was not achievable within the active volume when adhered to microcarriers, leading to too poor SNR for further studies in the 5 mm NMR tube (<1% conversion). Furthermore, the microcarriers packed very tightly in the 5 mm tube, preventing homogeneous distribution of HP-pyruvate throughout the cells. For these reasons, the 10 mm flow-cell was selected for further studies.

## 4.9 Viability in bioreactor

Viability of cells on microcarriers was examined to ensure no loss in viability occurred during sole perfusion with no treatment. Since the measurement of viability was based on the MTT assay directly on microcarriers it would mean that cells detached from the microcarrier would not contribute to the viability measurement. Therefore, it was examined whether mechanical stress would result in cell detachment, and hence lower viability during perfusion. All data from the perfusion study can be found in Table 4.

Cells were grown on microcarriers in petri dishes. For each dish, a fraction of microcarriers was placed in the flow cell; remaining microcarriers were used for determination of cell number and viability, referred to as *control*. Viability and cell number for each experiment was determined as percentage of absorbance after experiment compared to control. Initially, a validation of this procedure was required: microcarriers were placed in the flow cell and removed without perfusion to validate that perfusion (t = 0) is equal to control. Table 4 demonstrates that a 10 mm flow cell yields better recovery and Hs766t cells yields better recovery.

*Table 4 – Results from perfusion study. Results are collected from study with both MiaPaca-2 and Hs766t cells in flow cells of varying diameter with or without perfusion. Viability is calculated as MTT absorbance after experiment compared to start absorbance (control).*

| Cell line | Sample size | Flow cell (mm) | Flow (mL/min) | Time (h) | Viability (%) |
|---|---|---|---|---|---|
| MiaPaCa-2 | 2 | 5 | - | - | 40.5 |
| MiaPaCa-2 | 1 | 5 | 0.5 | 1 | 39 |
| MiaPaCa-2 | 6 | 10 | - | - | 101.2 |
| MiaPaCa-2 | 1 | 10 | 0.5 | 1 | 60 |
| MiaPaCa-2 | 3 | 10 | 1 | 2 | 72.7 |
| | | | | | |
| Hs766t | 2 | 5 | - | - | 91.5 |
| Hs766t | 2 | 5 | 0.5 | 1 | 99 |
| Hs766t | 2 | 5 | 0.5 | 4 | 88.5 |
| Hs766t | 1 | 5 | 0.5 | 20 | 57 |
| Hs766t | 2 | 10 | - | - | 102.5 |
| Hs766t | 2 | 10 | 1 | 2 | 101.5 |
| Hs766t | 1 | 10 | 1 | 4 | 85 |

This observation could be explained by the potential cell loss during recovery in a 10 mm flow cell which was a lesser fraction of the total volume compared to cell loss in a 5 mm flow cell. Furthermore, it was observed that MiaPaCa-2 cells were less adherent than Hs766t cells, which could also be observed during trypsinization. Hs766t cells required longer exposure to trypsin than MiaPaCa-2 cells. Few more perfusion studies were carried out with the 5 mm flow cell, yielding better results with the Hs766t cell line, but after HP experiments showed much better mixing in the 10 mm flow cell, the 5 mm flow cell was abandoned, and systematic studies with 10 mm flow cell were carried out. At t = 0, a recovery of MiaPaCa-2 cells were found to be 101±20% and Hs766t cells 103±4%. Upon perfusion, MiaPaCa-2 cells showed poor recovery after 2 h, which was attributed to their poor adherence to the microcarriers. Hs766t cells stayed within a recovery range of 15% after 4 h and was thought to be more resistant to mechanical stress.

The originally designed experiments of 4 h would only be able to be carried out on the Hs766t cells and not MiaPaCa-2 cells because of adherence issues. Unfortunately, the slow doubling time of Hs766t cells did not allow time for more experiment within the time frame of the study.

## 4.9 Discussion and conclusion of part II

In this study, a circulating bioreactor with atmosphere, pH and nutrition control and an NMR compatible flow cell was assembled and tested. Results combining the TH-302 study and longitudinal bioreactor experiments could not be accomplished within the time frame of the PhD study, and will be future work. However, the separate components have been tested:

The bioreactor has shown to be reliable within the time frames of up to 30 h, controlling pH, atmosphere and temperature in the vessel. With correct tubing, the peristaltic pump performed reliably, ensuring constant flow in and out of the vessel and NMR flow cell. The flow cell was compatible with both a 5 and 10 mm NMR tube. Cell detachment was observed as response to mechanical stress when cells were perfused in certain conditions, and flow rate should be regulated as a tradeoff between mechanical stress and hypoxia, since hypoxia was created within minutes without perfusion.

To avoid cells being detached from microcarriers, a different approach could be used for cell adherence, such as spheroids. These methods might require specialized equipment but may offer several advantages. Potentially eliminating the issue with mechanical stress, 3D methods such as spheroids may allow higher cell density in the active volume, since there are no microcarriers / scaffolds to take up the space which is convenient from an SNR point of view. Hs766t cells were more adherent to the microcarriers, which would make it possible to carry out the initially planned 4 h experiment. This would however not be possible with MiaPaCa-2 cells, which detached after only 1 h of perfusion. There is a wide span of parameters that could be responsible for cell adherence and lack thereof such as cell specific genes responsible for adherence in the different cell lines, protein in circulating medium, mechanical stress due to flow etc. making the monolayer approach challenging in a bioreactor set up.

For this specific approach, a 10 mm flow cell showed the most promising results compared to a 5 mm flow cell: sufficient mixing of HP pyruvate to monitor lactate conversion in living cells on microcarriers, and better cell recovery for quantification. Further continuation of this project would involve injection of HP pyruvate after 4 h of circulation to validate that cell metabolism does not change as a response to the perfusion with and without hypoxia. Finally, treatment with TH-302 could be integrated, and a hyperpolarized 13C-pyruvate spectrum before and after treatment should reveal metabolic response to treatment.

With further development, a bioreactor with control of medium offers a sophisticated platform for drug treatment testing without the need for animal models. The hypoxic regions in tumors can be simulated by introducing hypoxia *in vitro*, and the possibility for longitudinal studies makes it more attractive to use valuable cells for experiments. With the correct cell adherence protocol, such perfusion system could be able to maintain viable cells for days allowing for numerous screenings with HP probes in the same cell system. However, extending the time frame to days would introduce new parameters such as cell growth, posing new challenges to cell quantification and confluence of cells on microcarriers.

In conclusion, part II showed potential application of bioreactors for longitudinal studies, but also revealed that flow stress is an important limitation for many cell systems on microcarriers.

# 5. Part III – Development of new bioprobes for *in vivo* imaging

*Part III was carried out at National Institutes of Health, Bethesda, Maryland U.S., National Cancer Institute, Radiation Biology Branch in the group of Dr. Murali Cherukuri. The data will be included in several publications currently in preparation.*

## 5.1 Requirements to bioprobes for hyperpolarized metabolic MR

For a bioprobe to be successful for hyperpolarization, a vast number of parameters need to be balanced. The ultimate goal is to achieve the highest possible level of polarization ($P_{hp}$) and the longest possible spin-lattice relaxation time ($T_1$) [46]. Maximum $P_{hp}$ and $T_1$ depend on chemical and physical factors of the bioprobe and the sample formulation: solubility of the bioprobe, molecular weight, deuteration, glassing agent, radical etc. Furthermore, using a bioprobe on biological systems requires high uptake, conversion rate and biological tolerance towards the sample. Pyruvate is an example of an excellent bioprobe; it has an advantageous long $T_1$, capable of achieving high polarization levels and since it is the end product of glycolysis, it is key intersection of several metabolic pathways. An important biological feature of pyruvate is the abundance of the transmembrane transporters - monocarboxylate transporters (MCTs) - that facilitate the cellular uptake of pyruvate and efflux of lactate [110] [111]. This ensures a fast conversion of pyruvate suitable for HP experiments. It is especially the conversion of pyruvate into lactate that has been the selling point for DNP-MR, since abnormal lactate production correlates with the Warburg effect and can be used as a metabolic readout for cancer in tissues [112].

The use of pyruvate as a bioprobe is not limited to cancer research. [1-$^{13}$C]pyruvate has been used for studying differences between a healthy heart and heart diseases [113] [114] [115] as well as other organs under healthy and pathological conditions [116] [117] [118]. Variations in HP lactate, alanine and bicarbonate have been linked to activity of LDH, ALT and PDH [119].

Besides pyruvate, other bioprobes are applied to probe various biological pathways. HP [1,4-$^{13}C_2$]fumarate has been used to probe cell necrosis [120], fully or specifically labeled glucose has been used for carbohydrate metabolism [121] and Saccharomyces cerevisiae yeast [122], and many other bioprobes for a variety of biological models exist.

With only a decade of research, dDNP hyperpolarization of compounds for metabolic studies is still in its infancy, and further bioprobes and applications are likely to emerge [46]. When designing new bioprobes for HP experiments, several important parameters should be considered for potential biological application, Table 5.

*Table 5 – Considerations for bioprobe design*

| Biological considerations | Chemical considerations |
|---|---|
| Uptake rate and transporters | Molecular weight |
| Biological tolerance | Labeling pattern |
| Biodistribution | Relaxation time $T_1$ and deuteration |
| Enzymatic activity | Solubility |
| | Stability |

Biological considerations include:

**Uptake rate and transporters** are important parameters, since HP experiments are limited by a time frame relating to $T_1$ of the bioprobe, which usually limits the experiment time to minutes. To achieve fast uptake, dedicated transporters for fast transport from the extracellular space to the cytoplasm are essential, e.g. MCTs for [1-$^{13}$C]pyruvate. Slow reactions are not suited for this experiment and other approaches could be considered (see Part I for dDNP-SIRM method).

**Biological tolerance** needs to be considered, since a dose of HP substrate for *in vivo* imaging requires a concentration in the range of 10-150 mM. In comparison, PET only requires few nanomoles or less of the radioactive tracer [46]. Toxicity should therefore be excluded under the development of a new bioprobes and sample formulation.

**Molecular weight** favors small molecules to be most useful for hyperpolarization, primarily because $T_1$ decreases with increasing molecular weight, but also ease of synthesis and solubility favors relatively low molecular weight [123].

**Biodistribution** is an important consideration because the bioprobe requires a fast transport to the organ of interest. This is not a problem *in vitro* in cell systems or *in vivo* in highly perfused organs

such as kidneys [124], but becomes challenging in poorly perfused organs or penetration of brain-blood-barrier (BBB) for delivery to brain [125]. Whereas the HP sample reaches the cells immediately during injection *in vitro*, *in vivo* experiments depend on the blood circulation, and in a human body the transport time from the intravenous injection site to the area of interest is 2-4 s for lungs, 4-6 s for heart and 15-30 s for most major organs [34].

**Enzymatic activity** for a fast conversion of the bioprobe to its product is necessary because of the short time frame of the experiment. Furthermore, enzyme activity is used to reveal whether the tissue metabolism deviates from the healthy tissue metabolism e.g. LDH in various cancer models or ALT and PDH in heart disease models and other pathological conditions [116] [118].

Chemical considerations include:

**Molecular weight.** Small molecules have an advantageously long $T_1$ since $T_1$ decreases with increasing molecular weight. Furthermore, ease of synthesis and solubility can also favor relatively low molecular weight [32].

**Labeling pattern** can be positioned as desired by selective synthesis. The choice of the position is mainly driven by the effort to maximize $T_1$ and the chemical shift difference between substrate and product. The most common relaxation process affecting $T_1$ is dipolar couplings. For $^{13}C$ probes, dipolar couplings originate mainly from $^{1}H$ nuclei coupled to the $^{13}C$ nuclei and as a consequence, $^{13}C$ nuclei directly attached to $^{1}H$ are poor probes because of short $T_1$. The isotope label should therefore be placed in a chemical group free of direct proton bond, e.g. at a carbonyl position. Such probes include carboxylic acids, ketones, and amides [32]. Carbonyl compounds are abundant in cellular metabolism, making them a good choice as HP bioprobes.

**Deuteration** contributes to prolonging $T_1$ on HP probes by exchanging the protons with the low magnetic moment deuteron $^{2}H$, reducing the dipolar relaxation [126] [127]. Care should be taken since exchanging protons with deuterons can impact metabolism and enzyme function because of the kinetic isotope effect [121].

## 5.2 Requirements to sample formulation of bioprobes

A successful polarization of a given bioprobe requires a proper sample formulation. This involves achieving highest possible $P_{HP}$ and longest possible $T_1$ after dissolution while performing a quick adjustment of sample parameters (if needed) to ensure physiological pH, temperature, potential removal of radical, adjustment of bioprobe concentration etc.

Formulation of sample requires a free electron source to facilitate hyperpolarization by DNP. The selection of radical is determined by the electron paramagnetic resonance (EPR) line width (and other spectral properties), solubility and stability. Among commonly applied and efficient radicals are trityl compounds, e.g. OX063 (tris[8-carboxyl-2,2,6,6-benzo(1,2-d:4,5-d)-bis(1,3)dithiole-4-yl] methyl sodium salt [128], BDPA (1,3-bisdiphenylene-2-phenylallyl) [129], nitroxides e.g. TEMPO (2,2,6,6-tetramethylpiperidin- 1-oxyl) [130], and galvinoxyl (2,6-di-tert-butyl-α-(3,5-di-tert-butyl-4-oxo-2,5-cyclohexadien-1-ylidene)- p-tolyloxy) [131] although many other radicals exist. Trityls and BDPA have narrow EPR linewidth [132], which allows for higher polarization of $^{13}C$ nuclei [133] [134]. Solubility should be optimized to achieve a homogenous mixing of the bioprobe and radical. The most commonly used trityl radical, OX063, is soluble in water, which makes it suitable for aqueous bioprobes. As a rule of thumb, a concentration of 15-45 mM radical has proven sufficient for good DNP efficiency and relatively short build-up time [46]. It is not beneficial to increase the concentration of radical, since the paramagnetic effect can decrease $T_1$ of the $^{13}C$ in solution and toxicity of the radical can in some cases be an issue.

In order for the DNP process to work efficiently, the homogenous mixture of bioprobe and free radical has to form an amorphous glass at cryogenic temperatures. This is usually achieved by a solvent or a solvent mixture. An interesting exception is pyruvic acid, which is self-glassing and can be used neat, with the free radical directly dissolved in the pyruvic acid [135]. The concentrations of the $^{13}C$ nuclei are typically in the in the range of 1-15 M, resulting in post dissolution concentrations of 10-500 mM suitable for *in vivo* use [46]. Increasing the solubility of the bioprobe is often desired, and modulation of pH, temperature and solvent can improve solubility [136]. If the sample is not self-glassing, which can be assessed by freezing the sample in liquid nitrogen and observe if it crystallizes, a glassing agent should be added. The most commonly added glassing agent is glycerol.

Finally, polarization enhancing molecules can be added to the sample formulation. Addition of gadolinium based paramagnetic molecules has been shown to increase the polarization level of $^{13}C$ labeled compounds [128] [137]. The gadolinium effect is case specific, depending on sample formulation, but for pyruvate, studies have shown that a maximum polarization enhancement is observed at concentrations of 4-5 mM $Gd^{3+}$. $Gd^{3+}$ doping can lead to an increase of 300% polarization in preparations of pyruvate and OX063 [137].

Final step in the HP experiment is the dissolution, and a proper dissolution buffer should be designed. The pH and volume of the buffer should be adjusted such that the final HP solution is physiologically isotonic with a physiological pH for *in vivo* use [138].

In the next section, the probe development process is demonstrated on three new probes for *in vitro* and *in vivo* HP $^{13}C$ experiments. The formulation of the bioprobes were optimized, and initial experiments were performed. This study was a part of a collaborations with Dr. Cherukuri's group, and concerns following bioprobes:

**Case 1:** N-acetylcysteine (NAC)
**Case 2:** alpha-keto glutarate ($\alpha$KG)
**Case 3:** $\gamma$-Glu-[1-$^{13}C$]Gly

## 5.3 N-acetylcysteine (NAC)

N-acetylcysteine (NAC) is a precursor of L-cysteine, which is a building block of glutathione (GSH), an essential anti-oxidant found in human cells [139]. NAC is deacetylated by cytosolic esterases to provide cysteine and thereby support the synthesis of GSH. The synthesis of GSH occurs through γ-glutamylcysteine synthetase (GCS) and GSH synthetase enzymes [140] mainly produced in the liver, Figure 26.

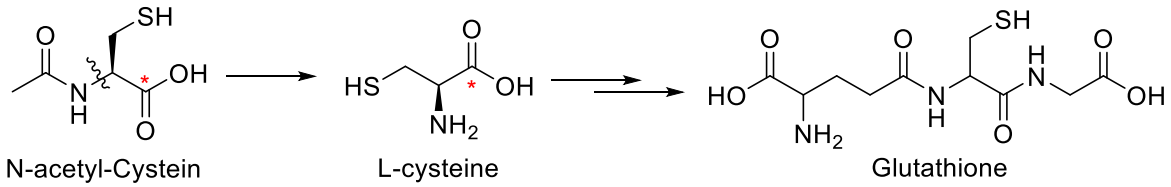


Figure 26 – Deacetylation of NAC to form L-cysteine, which is a building block for GSH, an essential anti-oxidant in human cells. The red star indicates the position in which NAC is labeled with $^{13}C$.

NAC is used as a medical drug for several purposes including paracetamol overdose. Following an excessive intake of paracetamol, the toxic metabolite N-acetyl-p-benzoquinoneimine (NAPB) is formed in the liver. This metabolite is detoxified by GSH, but if the NAPB is present in amounts that are much greater than GSH as a consequence of a very high paracetamol intake, this can result in hepatic toxicity [141]. NAC is administered as a source to assist production of GSH in such cases. Other uses of NAC involve application as mucolytic agent, for cancer chemotherapy, obstructive lung diseases and in psychiatry [142].

NAC was obtained as a pure white powder, specifically $^{13}C$-labeled on the cysteine residue. Naturally abundant NAC was used for formulation and glassing experiments, whereas $^{13}C$-labeled NAC was used for HP experiment, since the generation of labeled NAC required a specialized synthesis performed by the chemistry team at NIH.

*Formulation of NAC as a bioprobe for HP experiments*

The first step was to dissolve NAC in a suitable solvent. Dissolving NAC in DMSO resulted in a maximum concentration of 200 mg/ mL (1.2 M) with the ability of forming an amorphous glass. For

polarization, 17 mM Ox063 was added and 2.5 mM ProHance, as a source of gadolinium. The DNP buildup can be seen on Figure 27. All experiments were performed on HyperSense.

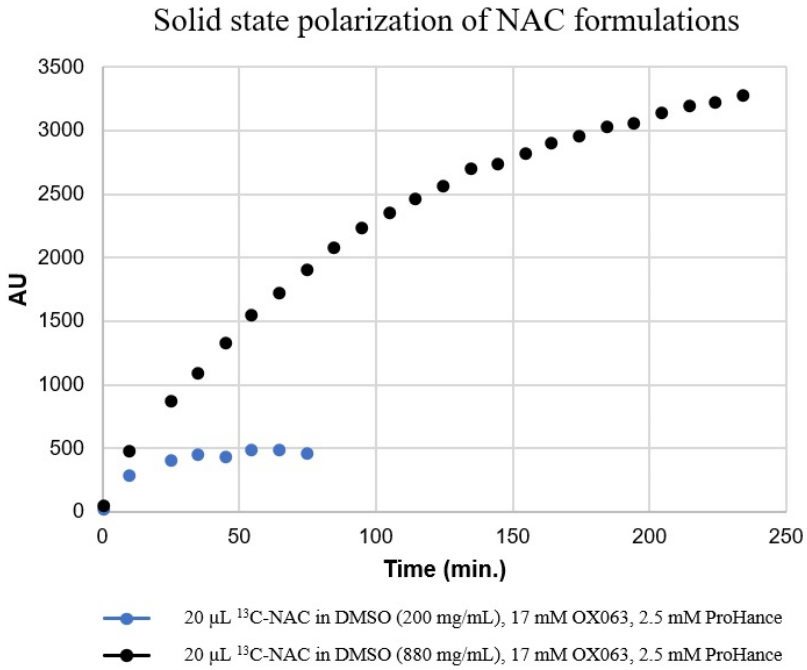


*Figure 27 – Two different sample formulations of NAC were tested. The first formulation was based on dissolving NAC in DMSO, resulting in a 1.2 M concentration. Increasing the concentration of NAC to 5.4 M by dissolution in 5 M NaOH resulted in a higher polarization. Both samples contained 17 mM OX063 as a source of EPA, and 2.5 mM ProHance as Gd-source.*

In order to achieve most efficient $P_{HP}$ for *in vivo* experiments, the sample formulation was optimized. Manipulating the pH can be an approach to increase the concentration [136]. Dissolving NAC in water yielded an acidic solution, but when NAC was dissolved in 5 M NaOH until neutral pH, the solubility was improved. A solubility of 880 mg/mL was achieved (5.4 M), and the formulation was self-glassing. The improvement of polarization compared to the formulation in DMSO can be seen in Figure 27. The dissolution was performed in 4 mL PBS buffer, yielding a final concentration of 27 mM. A $T_1$ of 16.5 s was recorded under these conditions, Figure 28.

A thermal spectrum was recorded to check the chemical stability of the compound. Liquid state spectra of hyperpolarized natural abundance NAC that had been formulated in 5 M NaOH can be seen in Figure 28.

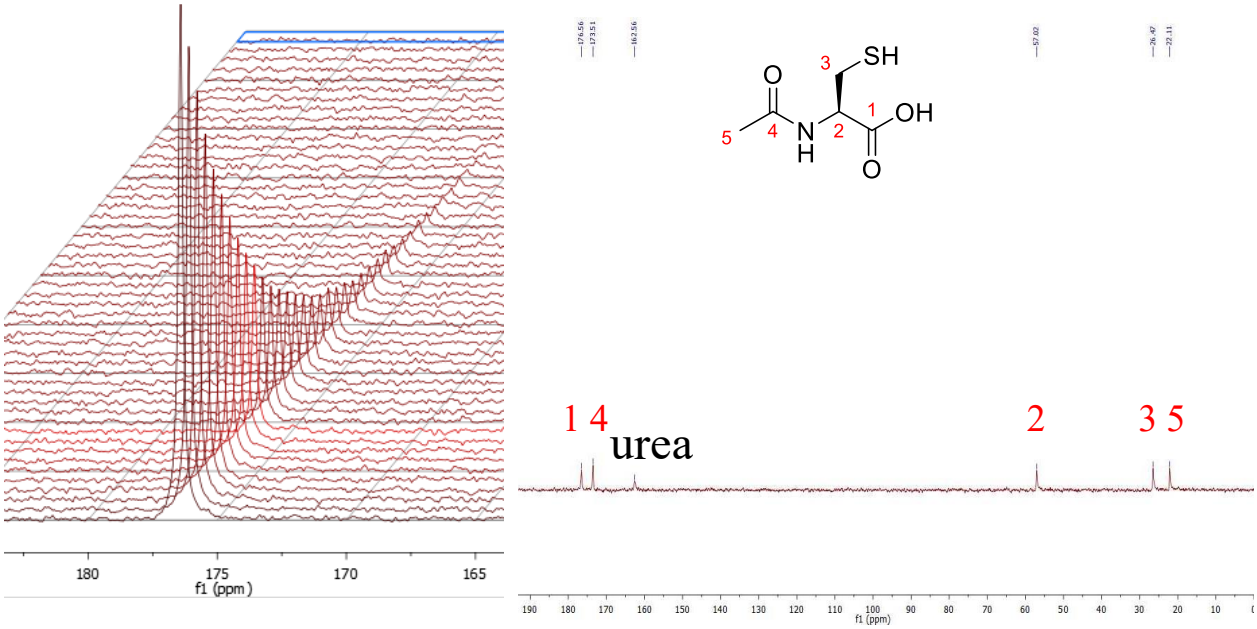


*Figure 28 – left: post dissolution $^{13}C$ NMR signal decay of the hyperpolarized signal from NAC in PBS buffer. This data was used for calculation of $T_1$. Right: thermal spectra of NAC (natural abundant) in 5 M NaOH dissolved in PBS buffer. No decomposition of NAC was observed during sample preparation in NaOH. The spectra were recorded using Magritek 1 T NMR spectrometer.*

### *Enzymatic deacetylation of NAC*

For a substrate to be useful as a bioprobe, it needs to be converted to its products within a reasonable timeframe relative to $T_1$. The initial reaction in which NAC is deacetylated to yield cysteine was therefore investigated enzymatically. Acylase I, which has been used to study deacetylation of various S-alkyl-N-acetyl-L-cysteines including NAC [143], was chosen.

40 µL NAC in 5 M NaOH, 17 mM Ox063 and 2.5 mM Gd was polarized in a SpinLab for 2.5 h. Meanwhile, 250 µL Acylase I solution (1 mg/mL enzyme corresponding to 120 U per 100 µL) was placed in a 5 mm NMR tube in the Magritek 1 T NMR spectrometer. HP-NAC was added 20 s post dissolution and the spectra recorded, Figure 29. As can be seen on the figure, the product peak changed chemical shift over time. This can be due to pH changes because of a very high concentration of enzyme.

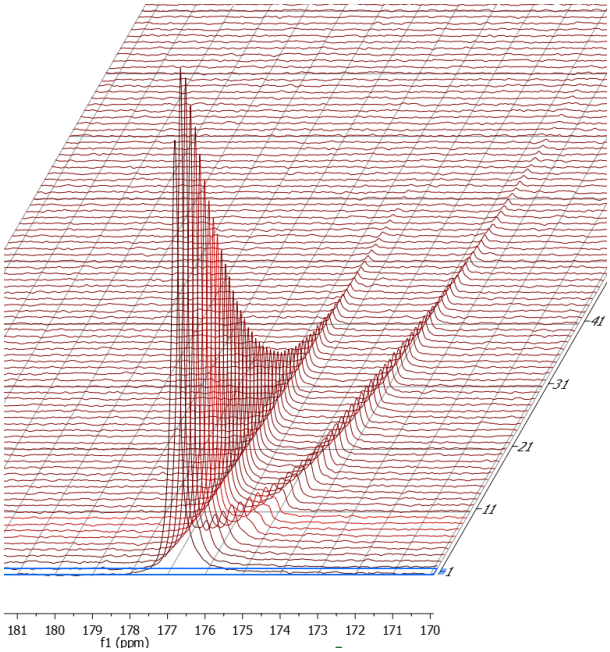


*Figure 29 – HP-NAC (176.5 ppm) converted into N-cysteine (approx 175 ppm) by acylase I. A change in pH affected the ppm of the product, resulting in a change of ppm over time.*

### *Pilot study in vivo – biodistribution*

To investigate the feasibility of using NAC *in vivo*, an experiment visualizing biodistribution was designed using a healthy mouse model. The sample was polarized in the SpinLab and transferred to a Phillips scanner, where it was injected into the mouse through the tail vein. The acquisition was started 20 s post injection. A volume head coil was applied for this set-up to monitor potential signal in the brain, Figure 30.

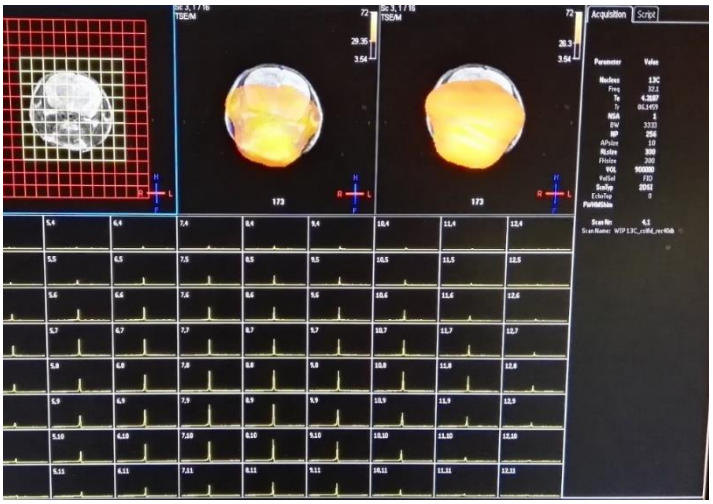

*Figure 30 – Signal originating from HP-NAC distributed within the brain of a healthy mouse. The sample was formulated as described previously and polarized in a fluid path by SpinLab. Spectra were recorded 20 s post dissolution.*

*Conclusion of study and future perspectives*

Further work with NAC as bioprobe for HP experiments would entail finding a suitable biological system, in which NAC could be applied for reporting the biological state. The use of NAC is primarily to treat conditions that require increase of the antioxidant GSH by providing NAC as a building block for this synthesis. However, this reaction is not suited for HP experiments, which requires fast biochemical reactions. Therefore, if NAC is to be used as a reporter molecule for a biological system, it needs to be converted fast, as seen during the deacetylation. NAC can serve as an anti-oxidant by itself directly to scavenge oxidant species, even though its far less potent than GSH [144]. Being a thiol, it can quickly react with $^{\bullet}OH$, $^{\bullet}NO_2$ and $^{\bullet}CO_3^-$ and thiyl radicals [145].

An interesting observation was that NAC seemed to cross the BBB in the *in vivo* pilot study in mouse. From literature, it is evident that there is controversy regarding whether NAC is able to cross the BBB, since studies have reported contradictory results: 1) small fraction NAC being able to cross the BBB [146] 2) NAC not being able to cross BBB [147] or 3) NAC being able to cross BBB very well [148]. NAC is converted into L-cysteine, which has been demonstrated to penetrate the BBB [145], so the signal could originate from L-cysteine, which has been formed through deacetylation in the blood stream. Further work would involve addition of reference molecule to establish which specie is able to cross BBB in the *in vivo* study.

## 5.4 α-ketoglutarate (αKG)

The catalysis of the oxidative decarboxylation of isocitrate to produce $CO_2$, NADPH and α-ketoglutarate (αKG), is mediated by a family of isocitrate dehydrogenases (IDHs), including the two isoforms IDH1 and IDH2 [149]. Studies show that mutations in IDH1 are present in more than 70% of grade II-III gliomas and secondary glioblastomas as well as in approximately 10-15% of patients suffering from acute myeloid leukemia (AML) [150]. This mutation results in dysfunction of the oxidative carboxylation of isocitrate, and results in production of the oncometabolite 2-hydroxygluterate (2HG), Figure 31. IDH1 mutation is an early genetic event in gliomagenesis and 2HG is believed to further promote tumorigenesis. Gliomas are rarely curable tumors with a low survival rate (34%) at 5 years [151].

The unique biology of 2HG makes this metabolite a very specific biomarker that can be used for diagnosis, prognosis and treatment response in the mutant IDH1 gliomas. 2HG can be detected non-invasively by *in vivo* magnetic resonance spectroscopy (MRS), which offers clear advantages compared to biopsies and 2HG in blood, urine and cerebrospinal fluid (CSF) samples have shown mixed results [151]. Using αKG as a bioprobe to visualize the IDH1 mutant activity could reveal glioma pathogenicity of a biological system by monitoring the αKG to 2HG conversion. The probe is available with $^{13}C$ labeling at the C-1 position, Figure 31:

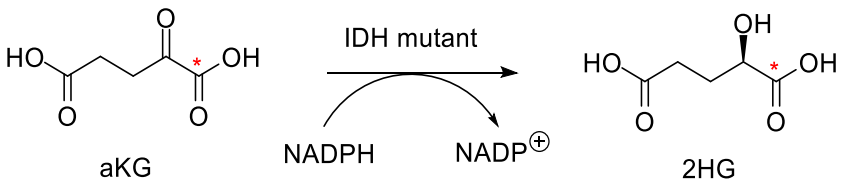


*Figure 31 – αKG transformed into the oncometabolite 2HG by IDH mutant, resulting in accumulation of 2HG. Using αKG as bioprobe would reveal the accumulation of 2HG related to development of glioma. Unfortunately, the chemical shift of the carbonyl in 2HG have similar chemical shift to [5-C] carbonyl on αKG resulting in an inaccurate quantification.*

However, after αKG is reduced to 2HG, the labeled position has a very similar chemical shift as the carbonyl at the C-5 position of αKG itself. This may pose a problem for the quantification, since naturally occurring carbon isotopes contain 1.1% $^{13}C$, and quantification of the product peak will be incorrect. Therefore, the chemistry team at NIH synthesized αKG, which was 100% $^{12}C$ at the C-5 position.

*Formulation of αKG as a bioprobe for HP experiments*

αKG was dissolved in water/glycerol 1:1 yielding a concentration of 5.9 M with 17 mM OX063 and 2.5 mM Gd. The DNP build-up curve is shown in Figure 32. The concentration was improved by dissolving αKG in 2 M NaOH until neutral pH, at which point the concentration was closer to 8 M, and the sample became self-glassing. The signal scales approximately with the increase in concentration, and ~ 30% higher signal was achieved.

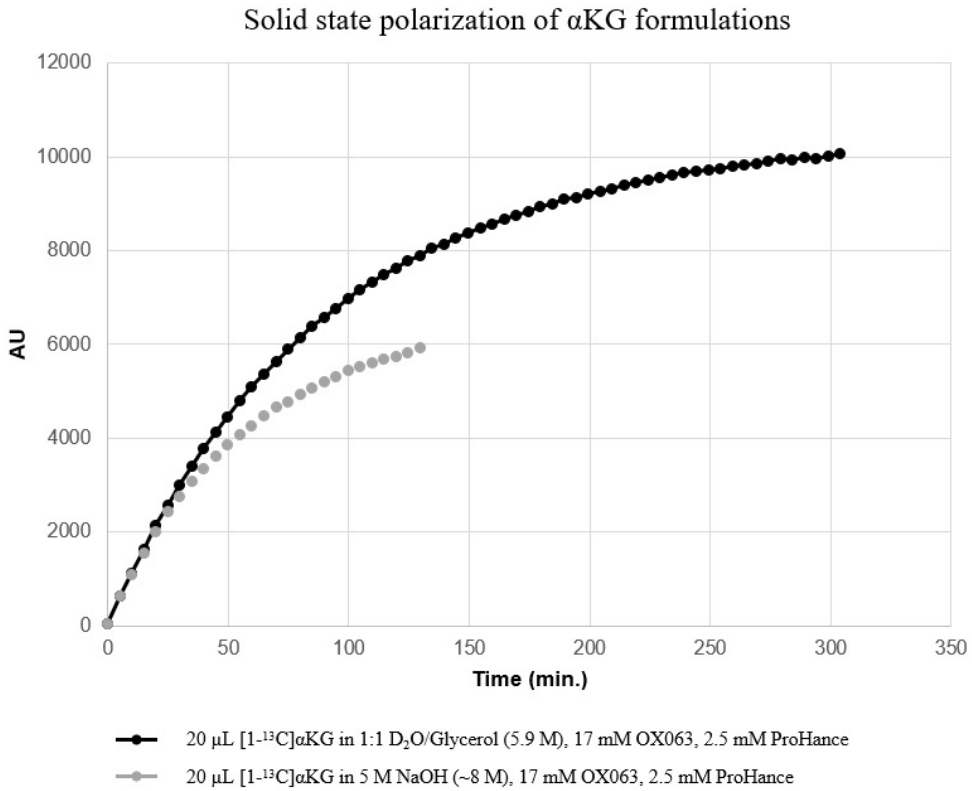


*Figure 32 – DNP build-up recorded for two different sample formulations of αKG, both with 17 mM Ox063 and 2.5 mM ProHance. The formulation based on NaOH reached a higher polarization proportionally with the increase in concentration of αKG.*

The αKG formulation polarized slowly which is problematic for throughput, but also if the experiment has to be carried out using a SpinLab, since typically the polarization time increases further with field strength [40]. Therefore, a further improvement of the polarization and time constant would involve increasing the radical concentration and optimizing the Gd concentration to find the best tradeoff between satisfactory polarization and acceptable polarization time. Within the time frame of the study αKG was not applied on a biological model, and this is left for future work.

## 5.5 γ-Glu-[1-$^{13}$C]Gly for γ-Glutamyl Transpeptidase (GGT)

The γ-Glutamyl Transpeptidase (GGT) enzyme is a surface enzyme which plays a role in the glutathione (GSH) homeostasis [152]. It is most abundant on the surface of epithelial-cell lining ducts, such as kidney and liver biliary ducts. The role of GGT is to catalyze the cleavage of γ-peptide bond between glutamyl and cysteinyl residues of GSH, Figure 33 (a) [153]. Elevated GGT levels are connected to diseases affecting the liver [154].

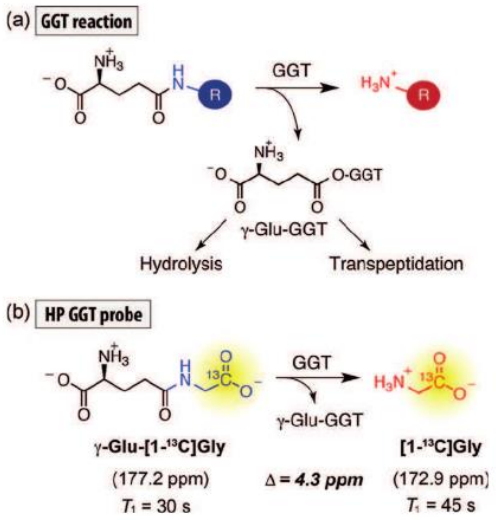


*Figure 33 – a) The GGT mediated cleavage of γ-peptide bond. b) The action of the GGT probe. After interaction with the GGT enzyme, the bioprobe is converted to glycine, resulting in chemical shift difference. From [153]. Copyright 2016 by John Wiley and Sons. Reprinted with permission.*

Furthermore, GGT has been implicated in the development and progression of malignant tumors. It is often overexpressed in cancerous tissues including tissues that do not normally express much GGT such as soft tissue sarcoma and ovarian adenocarcinoma [155]. This - together with the fact that GGT is a cell surface enzyme, and therefore easily accessible for a bioprobe - makes GGT an attractive enzyme for imaging applications. To achieve this, a GGT probe (γ-Glu-[1-$^{13}$C]Gly) was developed by Nishihara et al. [153], with a long $T_1$, chemical shift difference between substrate and product, and high biological tolerance for *in vivo* application. γ-Glu-[1-$^{13}$C]Gly will be a substrate for the GGT enzyme, and the substrate and product can be seen on Figure 33, (b).

*Formulation of γ-Glu-[1-$^{13}$C]Gly for HP experiments*

In the original formulation for HP experiments described in literature, γ-Glu-[1-$^{13}$C]Gly was dissolved in 85:15 $D_2O$/NaOH (1M) and glycerol-$d_8$ to yield a 1 M concentration [153]. The concentration was attempted optimized by dissolution of the probe in NaOH (5M) to a point where it became self-glassing, and glycerol was obsolete. Solid-state build-ups were recorded for several formulations of γ-Glu-[1-$^{13}$C]Gly on a HyperSense in order to find the optimal formulation of the sample. On Figure 34, five different formulations can be seen. The formulation resulting in highest $P_{HP}$ (b) was chosen for further experiments.

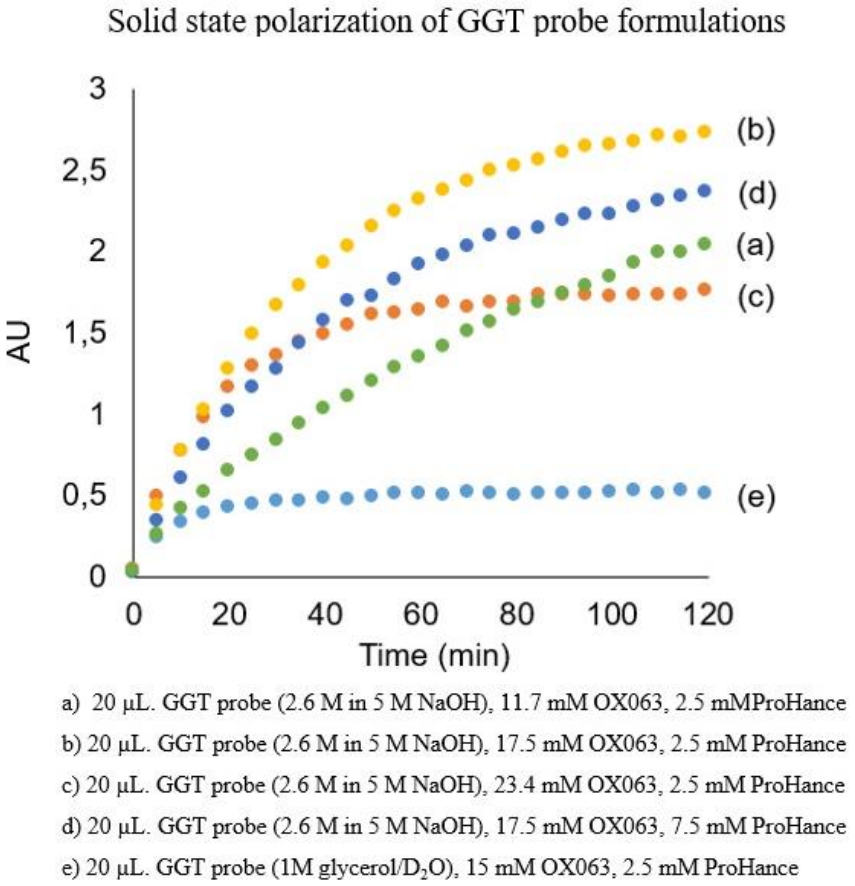


*Figure 34 – DNP enhancement for five different formulations of the GGT probe. The formulation was optimized in terms of concentration of probe, radical and gadolinium, and the optimal condition was found to be formulation (b).*

*In vivo experiment with γ-Glu-[1-$^{13}$C]Gly*

The formulation was tested *in vivo* to observe a potential conversion of γ-Glu-[1-$^{13}$C]Gly. 80 µL of the sample, corresponding to a final concentration of 52 mM, was dissolved in 40 mM TRIS buffer and 300 µL was injected through the tail vein of a mouse carrying a MiaPaCa-2 tumor xenograft on

the leg. GGT activity was detected in the tumor from the glycine signal, Figure 35. The experiment showed successful conversion *in vivo* in mouse tumor xenograft in the MiaPaCa-2 cancer cell model.

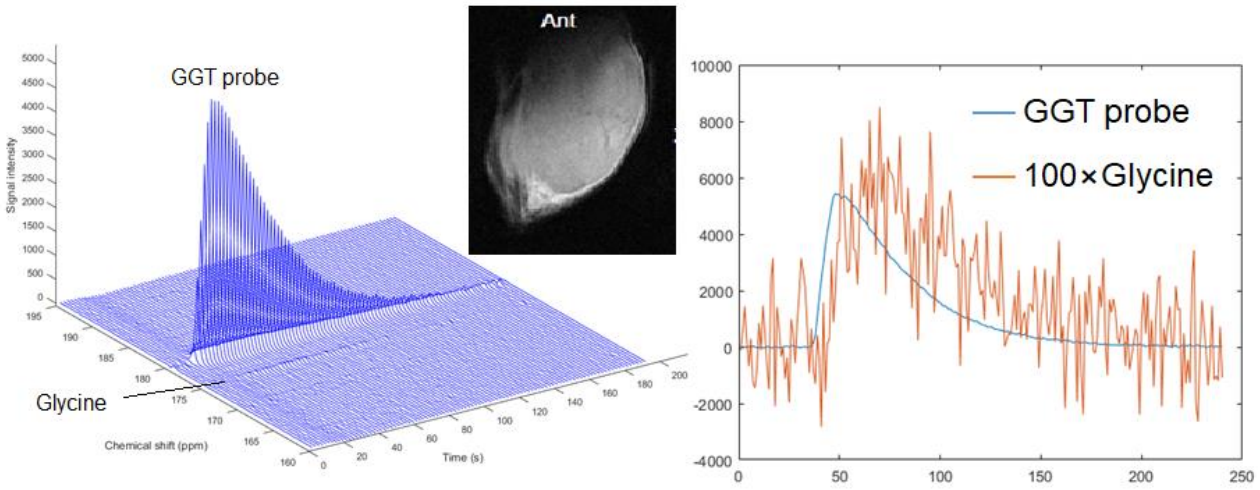


*Figure 35 – γ-Glu-[1-$^{13}$C]Gly injected into mouse with MiaPaCa-2 tumor. GGT activity was detected as glycine was formed from γ-Glu-[1-$^{13}$C]Gly, showing the potential for in vivo applications of the probe.*

In summary, the formulation of the γ-Glu-[1-$^{13}$C]Gly was increased from the original 1 M to 2.6 M leading to higher polarization useful for *in vivo* studies. The initial demonstration of the use *in vivo* was performed, showing the feasibility for γ-Glu-[1-$^{13}$C]Gly to be used as a bioprobe in biological systems with overexpressed GGT enzyme, correlating with tumor malignancy. The distinct change in ppm from substrate to product serves as a readout of the activity levels of GGT. Further studies will involve more *in vivo* data to investigate the scope of biological applications.

## 5.6 Discussion and conclusion of part III

Three novel bioprobes for HP experiments were presented: NAC, αKG and γ-Glu-[1-$^{13}$C]Gly. They were all optimized for highest possible DNP build-up for further *in vivo* studies. By manipulating with the pH of the sample, a high concentration could be achieved and the bioprobes became self-glassing, making the need for glassing agent unnecessary. This is advantageous for *in vivo* experiments, where biological tolerance of glycerol can pose an issue.

For each probe, a biological system was considered. Biodistribution experiment with NAC showed HP signal in the brain, meaning that either NAC itself or a derivative such as cysteine, did cross the BBB. A suitable biological system for NAC is still to be found. However, it would be interesting to determine whether NAC crosses the BBB, since literature describes contradictory results. αKG formulation was optimized, but it was not tested on any biological system. The potential for αKG to serve as a probe for the oncometabolite 2HG is promising, since the biochemistry of 2HG is unique and connected to certain cancers. The final probe, γ-Glu-[1-$^{13}$C]Gly, was optimized and tested *in vivo* on MiaPaCa-2 xenograft on mouse. The experiment showed a conversion of the probe to its glycine residue, showing promising results for applying this to other biological systems.

Development of new bioprobes allows for investigation of interesting metabolic patterns, which may be readout of a pathological state and therefore serve as a diagnostic tool. However, challenges are involved when developing a new probe for *in vivo* use. The metabolism of the probe needs to take place within a time frame determined by the molecule $T_1$. The components of the sample need to be tolerated by the animal, and the HP signal should be sufficient for the molecule to reach the place of interest despite the decay of HP signal on its way through the blood stream. Chemical modifications of molecules involving specific labeling, deuterations etc., are useful tools to improve readout of these experiments, opening a research area in the field of probe development for HP experiments.

# 6. Overall conclusion

Lifestyle diseases are expanding global health problems that are contributing to the global burden of chronic diseases. To link diet to metabolic outcome, it is necessary to understand the metabolic fate and interaction of the nutritional components in living organisms. The objective of this project was to study perturbed metabolism using dissolution Dynamic Nuclear Polarization (dDNP) in several disease models *in vitro*:

In the first part of the thesis, dDNP is used to probe slow biochemical reactions in combination with Stable Isotope Resolved Metabolomics (SIRM). By application of this method, the timeframe of the experiment can be extended from minutes to hours or longer. This part was based on two papers:

Paper I concern the development of the stable isotope-resolved analysis combined with dDNP. The paper describes technical optimization of the experiment (polarization time, polarization medium etc.) and the extraction protocol for cell experiments. The paper furthermore discusses the possibility of quantification by introducing signal loss coefficient (SLC), a set up specific parameter. The analysis is eventually demonstrated on incubations ranging from 0-30 min performed on two different cancer cell lines, PC3 and MCF7, which shows cell line specific metabolic profiles, that develop with incubation time. The paper demonstrates how dDNP can be used for studying slow biochemical reaction which is not possible with the classical dDNP experiments, where the timeframe is limited to minutes.

In paper II, this approach is applied to investigate early handling of excess fuel in insulin producing β-cells before they reach a glucotoxic state which is a pathogenic factor in type 2 diabetes. Glucose-derived pyruvate is found to correlate with a high fuel burden for the cells and is hypothesized to be a potential biomarker in the development of insulin impairment. In conclusion, this study shows that β-cells actively use different metabolic pathways to reduce excess metabolites formed due to uncontrolled glycolysis. Glycerol- and fatty acid metabolism is the most likely candidate for this deviation pathway. Further studies are needed to elucidate this fundamentally important and relatively overlooked defense mechanism important for protecting the β-cell against glucotoxicity.

In the second part of the thesis, dDNP was applied to study real time kinetics using hyperpolarized [1-$^{13}$C]pyruvate to visualize metabolism in cancer cells. The biological model represented pancreatic cancer, demonstrated by two different cell lines representing different stages of the cancer. For this

purpose, a bioreactor with a home-built flow cell was constructed and tested. Adherence of cells to avoid anoikis, quantification of cells on microcarriers, flow stress experiments etc. were all important factors that needed to be optimized before a longitudinal experiment involving treatment with TH-302 could be performed. It was demonstrated that the cells grown on microcarriers showed pyruvate to lactate conversion in the flow cell. Furthermore, the bioreactor was found suitable for longitudinal cell studies over several hours, but also revealed that flow stress is an important limitation for many cell systems on microcarriers.

The third part of the thesis concerns three different bioprobes (NAC, αKG and GGT probe) for novel applications, *in vivo* and *in vitro*. Designing novel probes requires a fine interplay between chemistry, physics and biology. The formulation and solid-state build up for each sample was optimized for *in vivo* applications. NAC was further tested *in vivo* to explore biological distribution, since literature describes contradictory results. HP signal was observed in the brain using a head-coil, which was an interesting result. αKG polarization was optimized, but the application on relevant biological system is still to be conducted. GGT probe was optimized in terms of solid-state build up as well, and was tested on mouse xenograft showing conversion, suggesting it is capable of being a bioprobe for HP experiments. These results will appear in several publications, which are currently in preparation.

In conclusion, this study showed the versatility of dDNP for metabolic research and potential diagnostic applications demonstrated by the polarization of $^{13}C$ labeled substrates *in vitro*. However, dDNP has a much wider application range, involving other nuclei, *in vivo* applications and capability of clinical translation, with many more applications yet to be explored.

# 5. References


[1] B. A. Swinburn, G. Sacks, K. D. Hall, K. McPherson, D. T. Finegood, M. L. Moodie and S. L. Gortmaker, "The global obesity pandemic: shaped by global drivers and local environments," *Lancet*, vol. 378, pp. 804-814, 2011.

[2] R. A. DeFronzo, E. Ferrannini, L. Groop, R. R. Henry, W. H. Herman, J. J. Holst, F. B. Hu, C. R. Kahn, I. Raz, G. I. Shulman, D. C. SImonson, M. A. Testa and R. Weiss, "Type 2 diabetes mellitus," *Nat. Rev.*, vol. 1, pp. 1-22, 2015.

[3] E. Giovannucci and D. Michaud, "The Role of Obesity and Related Metabolic Disturbances in Cancers of the Colon, Prostate, and Pancreas," *Gastroenterol.*, vol. 132, pp. 2208-2225, 2007.

[4] H.-C. Lee and Y.-H. Wei, "Mitochondrial DNA Instability and Metabolic Shift in Human Cancers," *Int. J. Mol. Sci.*, vol. 10, pp. 674-701, 2009.

[5] U. Martinez-Outschoorn, F. Sotgia and M. P. Lisanti, "Tumor Microenvironment and Metabolic Synergy in Breast Cancers: Critical Importance of Mitochondrial Fuels and Function," *Semin. Oncol.*, vol. 41, no. 2, pp. 195-216, 2014.

[6] K. S. Reddy and M. B. Katan, "Diet, nutrition and the prevention of hypertension and cardiovascular diseases," *Public Health Nutr.*, vol. 7, pp. 167-186, 2004.

[7] C. Hawkes, "Uneven dietary development: linking the policies and processes of globalization with the nutrition transition, obesity and diet-related chronic diseases," *Global. Health.*, vol. 2, no. 1, 2006.

[8] R. J. DeBerardinis and C. B. Thompson, "Cellular Metabolism and Disease: What Do Metabolic Outliers Teach Us?," *Cell*, vol. 148, pp. 1132-1144, 2012.

[9] M. G. V. Heiden, L. C. Cantley and C. B. Thompson, "Understanding the Warburg Effect: The Metabolic Requirements of Cell Proliferation," *Science*, vol. 324, pp. 1029-1033, 2009.

[10] J. Kurhanewicz, D. B. Vigneron, K. Brindle, E. Y. Chekmenev, A. Comment, C. H. Cunningham, R. J. DeBerardinis, G. G. Green, M. O. Leach, S. S. Rajan, R. R. Rizi, B. D. Ross, W. S. Warren and C. R. Malloy, "Analysis of Cancer Metabolism by Imaging Hyperpolarized Nuclei: Prospects for Translation to Clinical Research," *Neoplasia*, vol. 13, pp. 81-97, 2011.

[11] S. J. Nelson, J. Kurhanewicz, D. B. Vigneron, P. E. Z. Larson, A. L. Harzstark, M. Ferrone, M. van Criekinge, J. W. Chang, R. Bok, I. Park, G. Reed, V. K. Weinberg, J. H. Ardenkjær-Larsen, A. P. Chen, R. E. Hurd, L.-I. Odegardstuen, F. J. Robb, J. Tropp and J. A. Murray, "Metabolic Imaging of Patients with Prostate Cancer Using Hyperpolarized [1-13C]Pyruvate," *Sci. Transl. Med.*, vol. 5, no. 198, pp. 1-11, 2013.

[12] C. H. Schilling, S. Schuster, B. O. Palsson and R. Heinrich, "Metabolic Pathway Analysis: Basic Concepts and Scientific Applications in the Post-genomic Era," *Biotechnol. Prog.*, vol. 15, pp. 296-303, 1999.

[13] G. Wu, "Amino acids: metabolism, functions, and nutrition," *Amino Acids*, vol. 37, pp. 1-17, 2009.

[14] A. Efeyan, W. C. Comb and D. M. Sabatini, "Nutrient-sensing mechanisms and pathways," *Nature*, vol. 517, pp. 302-310, 2015.

[15] I. Göhring, V. V. Sharoyko, S. Malmgren, L. E. Andersson, P. Spégel, D. G. Nicholls and H. Mulder, "Chronic High Glucose and Pyruvate Levels Differentially Affect Mitochondrial

Bioenergetics and Fuel-stimulated Insulin Secretion from Clonal INS-1 832/13 Cells," *J. Biol. Chem.*, vol. 289, no. 6, pp. 3786-3798, 2014.

[16] R. P. Robertson, J. Harmon, P. O. Tran, Y. Tanaka and H. Takahashi, "Glucose Toxicity in beta-Cells: Type 2 Diabetes, Good Radicals Gone Bad, and the Glutathione Connection," *Diabetes,* vol. 52, pp. 581-587, 2003.

[17] V. Poitout and R. P. Robertson, "Glucolipotoxicity: Fuel Excess and Beta-Cell Dysfunction," *Endocrine Reviews,* vol. 29, no. 3, pp. 351-366, 2008.

[18] O. Warburg, " On the Origin of Cancer Cells," *Science,* vol. 123, pp. 309-314, 1956.

[19] K. Garber , "Energy Boost: The Warburg Effect Returns in a New Theory of Cancer," *J. Natl. Cancer Inst.,* vol. 96, pp. 1805-1806, 2004.

[20] N. M. Zacharias, H. R. Chan, N. Sailasuta, B. D. Ross and P. Bhattacharya, "Real Time Molecular Imaging of TCA Cycle Metabolism in vivo By Hyperpolarized 1-13C Diethyl Succinate," *J. Am. Chem. Soc.,* vol. 134, no. 2, pp. 934-943, 2012.

[21] M. Li, X. Wang, J. Aa, W. Qin, W. Zha, Y. Ge, L. Liu, T. Zheng, B. Cao, J. Shi, C. Zhao, X. Wang, X. Yu, G. Wang and Z. Liu, "GC/TOFMS analysis of metabolites in serum and urine reveals metabolic perturbation of TCA cycle in db/db mice involved in diabetic nephropathy," *Am. J. Physiol. Renal. Physiol.,* vol. 304, pp. F1317-F1324, 2013.

[22] N. Raimundo, B. E. Baysal and G. S. Shadel, "Revisiting the TCA cycle: signaling to tumor formation," *Trends Mol. Med.,* vol. 17, pp. 641-649, 2011.

[23] J.-P. Bayley and P. Devilee, "Warburg tumours and the mechanisms of mitochondrial tumour suppressor genes. Barking up the right tree?," *Curr. Opin. Genet. Dev.,* vol. 20, pp. 324-329, 2010.

[24] M. A. Schroeder, H. J. Atherton, D. R. Ball, M. A. Cole, L. C. Heather, J. L. Griffin, K. Clarke, G. K. Radda and D. J. Tyler, "Real-time assessment of Krebs cycle metabolism using hyperpolarized 13C magnetic resonance spectroscopy," *FASEB J.,* vol. 23, no. 8, pp. 2529-2538, 2009.

[25] H. R. Cross, K. Clarke, L. H. Opie and G. K. Radda, "Is Lactate-induced Myocardial Ischaemic Injury Mediated by Decreased pH or Increased Intracellular Lactate?," *J. Mol. Cell. Cardiol.,* vol. 27, pp. 1369-1381, 1995.

[26] O. E. Owen, S. C. Kalhan and R. W. Hanson, "The Key Role of Anaplerosis and Cataplerosis for Citric Acid Cycle Function," *J. Biol. Chem.,* vol. 277, no. 34, pp. 30409-30412, 2002.

[27] A. Zhang, H. Sun, G. Yan, P. Wang, Y. Han and X. Wang, "Metabolomics in diagnosis and biomarker discovery of colorectal cancer," *Cancer Lett.,* vol. 345, pp. 17-20, 2013.

[28] K. Suhre, C. Meisinger, A. Döring, E. Altmaier, P. Belcredi, C. Gieger, D. Chang, M. V. Milburn, W. E. Gall, K. M. Weinberger, H.-W. Mewes, M. Hrabé de Angelis, H.-E. Wichmann, F. Kronenberg, J. Adamiski and T. Illig, "Metabolic Footprint of Diabetes: A Multiplatform Metabolomics Study in an Epidemiological Setting," *PLOS ONE,* vol. 5, no. 11, p. e13953, 2010.

[29] J. B. German, B. D. Hammock and S. M. Watkins, "Metabolomics: building on a century of biochemistry to guide human health," *Metabolomics,* vol. 1, no. 1, pp. 3-9, 2005.

[30] W. B. Dunn and D. I. Ellis, "Metabolomics: Current analytical platforms and methodologies," *Trend Anal. Chem.,* vol. 24, no. 4, pp. 285-295, 2005.

[31] T. W. Fan and A. N. Lane, "Applications of NMR spectroscopy to systems biochemistry," *Prog. Nucl. Magn. Reson. Spectrosc.*, Vols. 92-93, pp. 18-53, 2016.

[32] K. R. Keshari and D. M. Wilson, "Chemistry and biochemistry of 13C hyperpolarized magnetic resonance using dynamic nuclear polarization," *Chem. Soc. Rev.*, vol. 43, pp. 1627-1659, 2014.

[33] M. Goldman, H. Johanneson, O. Axelsson and M. Karlsson, "Hyperpolarization of 13C through order transfer from parahydrogen: A new contrast agent for MRI," *Magn. Reson. Imaging*, vol. 23, pp. 153-157, 2005.

[34] K. Golman and S. Petersson, "Metabolic Imaging and Other Applications of Hyperpolarized 13C1," *Acad. Radiol.*, vol. 13, no. 8, pp. 932-942, 2006.

[35] W. Edelstein, G. Glover, C. Hardy and R. Redington, "The Intrinsic Signal-to-Noise Ratio in NMR Imaging," *Magn. Reson. Med.*, vol. 3, pp. 604-618, 1986.

[36] J. H. Ardenkjær-Larsen, H. Johanneson, J. S. Petersson and J. Wolber, "Hyperpolarized Molecules in Solution," in *In Vivo NMR Imaging*, Humana Press, 2011, pp. 205-226.

[37] A. Abragam and M. Goldman, "Principles of dynamic nuclear polarisation," *Rep. Prog. Phys.* , vol. 41, pp. 395-467, 1978.

[38] D. Shimon, Y. Hovav, A. Feintuch, D. Goldfarb and S. Vega, "Dynamic nuclear polarization in the solid state: a transition between the cross effect and the solid effect," *Phys. Chem. Chem. Phys.*, vol. 14, pp. 5729-5743, 2012.

[39] R. E. Hurd, Y.-F. Yen, A. Chen and J. H. Ardenkjær-Larsen, "Hyperpolarized 13C Metabolic Imaging Using Dissolution Dynamic Nuclear Polarization," *J. Magn. Reson. Imaging*, vol. 36, pp. 1314-1328, 2012.

[40] J. H. Ardenkjær-Larsen, B. Frindlund, A. Gram, G. Hansson , L. Hansson, M. H. Lerche, R. Servin, M. Thaning and K. Golman, "Increase in signal-to-noise ratio of >10,000 times in liquid-state NMR," *Proc. Natl. Acad. Sci. U.S.A.*, vol. 100, no. 18, pp. 10158-10163, 2003.

[41] M. Duijvestijn, R. Wind and J. Smidt, "A Quantitative Investigation of the Dynamic Nuclear Polarization Effect by Fixed Paramagnetic Centra of Abundant and Rare Spins in Solids at Room Temperature," *Physica* , vol. 138B, pp. 147-170, 1986.

[42] M. K. Hornstein, V. S. Bajaj, K. E. Kreischer, R. G. Griffin and R. J. Temkin, "CW Second Harmonic Results at 460 GHz of a Gyrotron Oscillator for Sensitivity Enhanced NMR," *the Joint 30th International Conference on Infrared and Millimeter Waves and 13th International Conference on Terahertz Electronics*, vol. 2, pp. 437-438, 2005.

[43] S. Bowen and J. H. Ardenkjær-Larsen, "Enhanced performance large volume dissolution-DNP," *J. Magn. Reson.*, vol. 240, pp. 90-94, 2014.

[44] J. H. Ardenkjær-Larsen, A. M. Leach, N. Clarke, J. Urbahn, D. Anderson and T. W. Skloss, "Dynamic Nuclear Polarization Polarizer for Sterile Use Intent," *NMR Biomed.*, vol. 24, pp. 927-932, 2011.

[45] A. Comment and M. E. Merritt, "Hyperpolarized Magnetic Resonance as a Sensitive Detector of Metabolic Function," *Biochem.*, vol. 53, no. 47, pp. 7333-7357, 2014.

[46] M. M. Chaumeil, C. Najac and S. M. Ronen, "Studies of Metabolism Using 13C MRS of Hyperpolarized Probes," *Methods. Enzymol.*, vol. 561, pp. 1-54, 2015.

[47] J. A. Bastiaansen, H. A. Yoshihara, Y. Takado, R. Gruetter and A. Comment, "Hyperpolarized 13C lactate as a substrate for in vivo metabolic studies in skeletal muscle," *Metabolomics*, vol. 10, pp. 986-994, 2014.

[48] A. P. Chen, J. Kurhanewicz, R. Bok, D. Xu, D. Joun, V. Zhang, S. J. Nelson, R. E. Hurd and D. B. Vigneron, "Feasibility of using hyperpolarized [1-13C]lactate as a substrate for in vivo metabolic 13C MRSI studies," *Magn. Reson. Imag.*, vol. 26, pp. 721-726, 2008.

[49] S. Hu, M. Zhu, H. A. Yoshihara, D. M. Wilson, K. R. Keshari, P. Shin, G. Reed, C. von Morze, R. Bok, P. E. Larson, J. Kurhanewicz and D. B. Vigneron, "In vivo measurement of normal rat intracellular pyruvate and lactate levels after injection of hyperpolarized [1-13C]alanine," *Magn. Reson. Imag.*, vol. 29, pp. 1035-1040, 2011.

[50] G. J. Kelloff, P. Choyke and D. S. Coffey, "Challenges in Clinical Prostate Cancer: Role of Imaging," *AJR Am. J. Roentgenol.*, vol. 192, pp. 1455-1470, 2009.

[51] C. H. Cunningham, J. Y. Lau, A. P. Chen, B. J. Geraghty, W. J. Perks, I. Roifman, G. A. Wright and K. A. Connelly, "Hyperpolarized 13C Metabolic MRI of the Human Heart, Initial Experience," *Circ. Res.*, vol. 119, no. 11, pp. 1177-1182, 2016.

[52] M. H. Lerche, P. R. Jensen, M. Karlsson and S. Meier, "NMR Insights into the Inner Workings of Living Cells," *Anal. Chem.* , vol. 87, no. 1, pp. 119-132, 2015.

[53] M. H. Lerche, S. Meier, P. R. Jensen, S. O. Hustvedt, M. Karlsson, J. O. Duus and J. H. Ardenkjær-Larsen, "Quantitative dynamic nuclear polarization-NMR on blood plasma for assays of drug metabolism," *NMR Biomed.*, vol. 24, no. 1, pp. 96-103, 2011.

[54] C. E. Christensen, M. Karlsson, J. R. Winther, P. R. Jensen and M. H. Lerche, "Non-invasive In-cell Determination of Free Cytosolic [NAD+]/[NADH] Ratios Using Hyperpolarized Glucose Show Large Variations in Metabolic Phenotypes," *J. Biol. Chem.*, vol. 289, no. 4, pp. 2344-2352, 2014.

[55] J. N. Dumez, J. Milani, B. Vuichoud, A. Bornet, J. Lalande-Martin, I. Tea, M. Yon , M. Maucourt, C. Deborde, A. Moing, L. Frydman, G. Bodenhausen, S. Jannin and P. Giraudeau, "Hyperpolarized NMR of plant and cancer cell extracts at natural abundance," *Analyst*, vol. 140, no. 17, pp. 5860-5863, 2015.

[56] P. R. Jensen and S. Meier, "Hyperpolarised Organic Phosphates as NMR Reporters of Compartmental pH," *Chem. Commun.*, vol. 52, pp. 2288-2291, 2016.

[57] M. G. Vander Heiden, S. Y. Lunt, T. L. Dayton, B. P. Fiske, W. J. Israelsen, K. R. Mattani, N. I. Vokes, G. Stephanopoulos, L. C. Cantley, C. M. Metallo and J. W. Locasale, "Metabolic Pathway Alterations that Support Cell Proliferation," *Symp. Quant. Biol.*, vol. 76, pp. 325-334, 2011.

[58] M. Karlsson, P. R. Jensen, J. O. Duus, S. Meier and M. H. Lerche, "Development of Dissolution DNP-MR Substrates for Metabolic Research," *Appl. Magn. Reson.*, vol. 43, pp. 223-236, 2012.

[59] J. H. Ardenkjær-Larsen, S. Macholl and H. Jóhannesson, "Dynamic Nuclear Polarization with Trityls at 1.2 K," *Appl. Magn. Reson.*, vol. 34, pp. 509-522, 2008.

[60] S. Bowen and C. Hilty, "Rapid sample injection for hyperpolarized NMR spectroscopy," *Phys. Chem. Chem. Phys.*, vol. 12, no. 22, pp. 5755-5770, 2010.

[61] J. Milani, B. Vuichoud, A. Bornet, P. Miéville, R. Mottier, S. Jannin and G. Bodenhausen , "A magnetic tunnel to shelter hyperpolarized fluids," *Rev. Sci. Instrum.*, vol. 86, no. 2, p. 024101, 2015.

[62] C. J. Nolan, P. Damm and M. Prentki, "Type 2 diabetes across generations: from pathophysiology to prevention and management," *Lancet*, vol. 378, pp. 169-181, 2011.

[63] V. Poitout and R. Robertson, "Glucolipotoxicity: Fuel Excess and b-Cell Dysfunction," *Endocr. Rev.*, vol. 29, no. 3, pp. 351-366, 2008.

[64] C. Fernandez, U. Fransson, E. Hallgard, P. Spégel, C. Holm, M. Krogh, K. Wårell, P. James and H. Mulder, "Metabolomic and Proteomic Analysis of Clonal Insulin-Producing beta-cell Line (INS-1 832/13)," *J. Proteome Res.,* vol. 7, pp. 400-411, 2008.

[65] M. Wallace, H. Whelan and L. Brennan, "Metabolomic analysis of pancreatic beta cells following exposure to high glucose," *Biochim. Biophys. Acta.,* vol. 1830, pp. 2583-2590, 2013.

[66] Y. Mugabo, S. Zhao, J. Lamontagne, A. Al-Mass, M.-L. Peyot, B. E. Corkey, E. Joly, S. Murthy Madiraju and M. Prentki, "Metabolic fate of glucose and candidate signaling and excess-fuel detoxification pathways in pancreatic beta-cells," *J. Biol. Chem.,* vol. 292, no. 18, pp. 7407-7422, 2017.

[67] L. Brennan, M. Corless, C. Hewage, J. Malthouse, N. McClenaghan, P. Flatt and P. Newsholme, "13C NMR analysis reveals a link between L-glutamine metabolism, D-glucose metabolism and γ-glutamyl cycle activity in a clonal pancreatic beta-cell line," *Diabetologia,* vol. 46, pp. 1512-1521, 2003.

[68] P. Spégel, S. Malmgren, V. V. Sharoyko, P. Newsholme, T. Koeck and H. Mulder, "Metabolomic analyses reveal profound differences in glycolytic and tricarboxylic acid cycle metabolism in glucose-responsive and -unresponsive clonal β-cell lines," *Biochem. J.,* vol. 435, pp. 277-284, 2011.

[69] D. Lu, H. Mulder, P. Zhao, S. C. Burgess, M. V. Jensen, S. Kamzolova, C. B. Newgard and A. D. Sherry, "13C NMR isotopomer analysis reveals a connection between pyruvate cycling and glucose-stimulated insulin secretion (GSIS)," *PNAS,* vol. 99, pp. 2708-2713, 2002.

[70] S. M. Ronnebaum, O. Ilkayeva, S. C. Burgess, J. W. Joseph, D. Lu, R. D. Stevens, T. C. Becker, A. D. Sherry, C. B. Newgard and M. V. Jensen, "A Pyruvate Cycling Pathway Involving Cytosolic NADP-dependent Isocitrate Dehydrogenase Regulates Glucose-stimulated Insulin Secretion," *J. Biol. Chem.* , vol. 281, no. 41, pp. 30593-30602, 2006.

[71] A. De Vos, H. Heimberg, E. Quartier, P. Huypens, L. Bouwens, D. Pipeleers and F. Schuit, "Human and Rat Beta Cells Differ in Glucose Transporter but Not in Glucokinase Gene Expression," *J. Clin. Invest.,* vol. 95, no. 5, pp. 2489-2495, 1995.

[72] S. J. Ashcroft, L. C. C. Weerasinghe and P. J. Randle, "Interrelationship of Islet Metabolism, Adenosine Triphosphate Content and Insulin Release," *Biochem. J.,* vol. 132, pp. 223-231, 1973.

[73] C. B. Newgard and J. D. McGarry, "Metabolic Coupling Factors in Pancreatic Beta-Cell Signal Transduction," *Annu. Rev. Biochem.,* vol. 64, pp. 689-719, 1995.

[74] J. Henquin, M. Ravier, M. Nenquin, J. Jonas and P. Gilon, "Hierarchy of the beta-cell Signals Controlling Insulin Secretion," *Eur. J. Clin. Invest.,* vol. 33, pp. 742-750, 2003.

[75] M. Gembal, P. Gilon and J.-C. Henquin, "Evidence That Glucose Can Control Insulin Release Independently from Its Action on ATP-sensitive K+ Channels in Mouse B Cells," *J. Clin. Invest.,* vol. 89, pp. 1288-1295, 1992.

[76] S. Farfari, V. Schulz, B. Corkey and M. Prentki, "Glucose-Regulated Anaplerosis and Cataplerosis in Pancreatic beta-Cells, Possible Implication of a Pyruvate/Citrate Shuttle in Insulin Secretion," *Diabetes,* vol. 49, pp. 718-726, 2000.

[77] K. Eto, Y. Tsubamoto, Y. Terauchi, T. Sugiyama, T. Kishimoto, N. Takahashi, N. Yamauchi, N. Kubota, S. Murayama, T. Aizawa, Y. Akanuma, S. Aizawa, H. Kasai, Y. Yazaki and T. Kadowaki, "Role of NADH Shuttle System in Glucose-Induced Activation of

Mitochondrial Metabolism and Insulin Secretion," *Science*, vol. 283, no. 5404, pp. 981-985, 1999.

[78] M. V. Jensen, J. W. Joseph, O. Ilkayeva, S. Burgess, D. Lu, S. M. Ronnebaum, M. Odegaard, T. C. Becker, A. D. Sherry and C. B. Newgard, "Compensatory Responses to Pyruvate Carboxylase Suppression in Islet beta-Cells," *J. Biol. Chem.*, vol. 281, pp. 22342-22351, 2006.

[79] B. E. Corkey, M. C. Glennon, K. S. Chen, J. T. Deeney, F. M. Matschinsky and M. Prentki, "A Role for Malonyl-CoA in Glucose-stimulated Insulin Secretion from Clonal Pancreatic Beta-Cells," *J. Biol. Chem.*, vol. 264, pp. 21608-21612, 1989.

[80] J. W. Joseph, M. V. Jensen, O. Ilkayeva, F. Palmieri, C. Alárcon, C. J. Rhodes and C. B. Newgard, "The Mitochondrial Citrate/Isocitrate Carrier Plays a Regulatory Role in Glucose-stimulated Insulin Secretion," *J. Biol. Chem.*, vol. 281, pp. 35624-35632, 2006.

[81] M. J. MacDonald, L. A. Fahien, L. J. Brown, N. M. Hasan, J. D. Buss and M. A. Kendrick, "Perspective: emerging evidence for signaling roles of mitochondrial anaplerotic products in insulin secretion," *Am. J. Physiol. Endocrinol. Metab.*, vol. 288, pp. E1-E15, 2005.

[82] M. Prentki, F. M. Matschinsky and S. M. Madiraju, "Metabolic Signaling in Fuel-Induced Insulin Secretion," *Cell Metab.* , vol. 18, pp. 162-185, 2013.

[83] U. Krus, O. Kotova, P. Spegel, E. Hallgard, V. Sharoyko, A. Vedin, T. Moritz, M. C. Sugden, T. Koeck and H. Mulder, "Pyruvate Dehydrogenase Kinase 1 Controls Mitochondrial Metabolism and Insulin Secretion in INS-1 832/13 Clonal Beta-Cells," *Biochem. J.*, vol. 429, pp. 205-213, 2010.

[84] K.-G. Park, K.-M. Lee, H.-Y. Seo, J.-H. Suh, H.-S. Kim, L. Wang, K.-C. Won, H.-W. Lee, J.-Y. Park, K.-U. Lee, J.-G. Kim, B.-W. Kim, H.-S. Choi and I.-K. Lee, "Glucotoxicity in the INS-1 Rat Insulinoma Cell Line Is Mediated by the Orphan Nuclear Receptor Small Heterodimer Partner," *Diabetes*, vol. 56, pp. 431-437, 2007.

[85] F. Schuit, A. De Vos, S. Farfari, K. Moens, D. Pipeleers, T. Brun and M. Prentki, "Metabolic Fate of Glucose in Purified Islet Cells," *J. Biol. Chem.*, vol. 272, no. 30, pp. 18572-18579, 1997.

[86] M. V. Jensen, J. W. Joseph, S. M. Ronnebaum, S. C. Burgess, A. D. Sherry and C. B. Newgard, "Metabolic cycling in control of glucose-stimulated insulin secretion," *Am. J. Physiol. Endocrinol. Metab.*, vol. 295, pp. E1287-E1297, 2008.

[87] A. Wiederkehr and C. B. Wollheim, "Mitochondrial signals drive insulin secretion in the pancreatic b-cell," *Mol. Cell. Endocrinol.*, vol. 353, pp. 128-137, 2012.

[88] J. V. Rocheleau, W. S. Head, W. E. Nicholson, A. C. Powers and D. W. Piston, "Pancreatic Islet Beta-Cells Transiently Metabolize Pyruvate," *J. Biol. Chem.*, vol. 277, no. 34, pp. 30914-30920, 2002.

[89] C. Nolan and M. Prentki, "The islet b-cell: fuel responsive and vulnerable," *Trends. Endocrinol. Metab.*, vol. 19, pp. 285-291, 2008.

[90] N. Sekine, V. Cirulli, R. Regazzi, L. J. Brown, E. Gine, J. Tamarit-Rodriguez, M. Girotti, S. Marie, M. J. MacDonald, C. B. Wollheim and G. A. Rutter, "Low Lactate Dehydrogenase and High Mitochondrial Glycerol Phosphate Dehydrogenase in Pancreatic P-Cells," *J. Biol. Chem.*, vol. 269, no. 7, pp. 4895-4902, 1994.

[91] C. E. Gleason, M. Gonzalez, J. S. Harmon and R. P. Robertson, "Determinants of glucose toxicity and its reversibility in the pancreatic islet beta-cell line, HIT-T15," *Am. J. Physiol. Endocrinol. Metab.*, vol. 279, pp. E997-1002, 2000.

[92] S. E. Bohndiek, M. I. Kettunen, D.-e. Hu, B. W. Kennedy, J. Boren, F. A. Gallagher and K. M. Brindle, "Hyperpolarized [1-13C]-Ascorbic and Dehydroascorbic Acid: Vitamin C as a Probe for Imaging Redox Status in Vivo," *J. Am. Chem. Soc.*, vol. 133, pp. 11795-11801, 2011.

[93] S. E. Day, M. I. Kettunen, F. A. Gallagher, D.-E. Hu, M. Lerche, J. Wolber, K. Golman, J.-H. Ardenkjær-Larsen and K. M. Bindle, "Detecting tumor response to treatment using hyperpolarized 13C magnetic resonance imaging and spectroscopy," *Nat.Med.*, vol. 13, pp. 1382-1387, 2007.

[94] F. A. Gallagher, M. I. Kettunen, S. E. Day, M. Lerche and K. M. Brindle , "13C MR Spectroscopy Measurements of Glutaminase Activity in Human Hepatocellular Carcinoma Cells Using Hyperpolarized13C-Labeled Glutamine," *Magn. Reson. Med.* , vol. 60, pp. 253-257, 2008.

[95] K. R. Keshari, J. Kurhanewicz, R. E. Jeffries, D. M. Wilson, B. J. Dewar, M. Van Criekinge, M. Zierhut, D. B. Vigneron and J. M. Macdonald, "Hyperpolarized 13C Spectroscopy and an NMR-Compatible Bioreactor System for the Investigation of Real-Time Cellular Metabolism," *Magn. Reson. Med.*, vol. 63, pp. 322-329, 2010.

[96] A. Mancuso, A. Zhu, N. J. Beardsley, J. D. Glickson, S. Wehrli and S. Pickup, "Artificial Tumor Model Suitable for Monitoring 31P and 13C NMR Spectroscopic Changes During Chemotherapy-Induced Apoptosis in Human Glioma Cells," *Magn. Reson. Med.*, vol. 54, pp. 67-78, 2005.

[97] R. Sriram, M. van Criekinge, A. Hansen, Z. J. Wang, D. B. Vigneron, D. M. Wilson, K. R. Keshari and J. Kurhanewicz, "Real-time measurement of hyperpolarized lactate production and efflux as a biomarker of tumor aggressiveness in an MR compatible 3D cell culture bioreactor," *NMR Biomed.*, vol. 28, pp. 1141-1149, 2015.

[98] S. Lauritsen, L. B. Bertelsen, P. Daugaard, C. Laustsen, N. Nielsen, J. V. Nygaard and H. Stødkilde-Jørgensen, "Bioreactor for quantification of cell metabolism by MR-hyperpolarization," *Biomed. Phys. Eng. Express*, vol. 1, no. 4, p. 047003, 2015.

[99] V. Breukels, K. F. Jansen, F. H. van Heijster, A. Capozzi, J. M. van Bentum, J. A. Schalken, A. Comment and T. W. Scheenen, "Direct dynamic measurement of intracellular and extracellular lactate in small-volume cell suspensions with 13C hyperpolarised NMR," *NMR Biomed.*, vol. 28, pp. 1040-1048, 2015.

[100] J. M. Brown and W. R. Wilson, "EXPLOITING TUMOUR HYPOXIA IN CANCER TREATMENT," *Nature Rev. Canc.*, vol. 4, pp. 437-447, 2004.

[101] J. W. Wojtkowiak, H. C. Cornell, S. Matsumoto, K. Saito, Y. Takakusagi, P. Dutta, M. Kim, X. Zhang, R. Leos, K. M. Bailey, G. Martinez, M. C. Lloyd, C. Weber, J. B. Mitchell, R. M. Lynch, A. F. Baker, R. A. Gatenby, K. A. Rejniak, C. Hart, M. C. Krishna and R. J. Gillies, "Pyruvate sensitizes pancreatic tumors to hypoxia-activated prodrug TH-302," *Cancer Metab.*, vol. 3, no. 2, pp. 1-13, 2015.

[102] "ATCC: The Global Bioresource Center," ATCC, [Online]. Available: https://www.lgcstandards-atcc.org/?geo_country=dk. [Accessed 01 08 2018].

[103] G. J. Weiss, J. R. Infante, E. G. Chiorean, M. J. Borad, J. C. Bendell, J. R. Molina, R. Tibes, R. K. Ramanathan, K. Lewandowski, S. F. Jones, M. E. Lacouture, V. K. Langmuir, H. Lee, S. Kroll and H. A. Burris III, "Phase 1 Study of the Safety, Tolerability, and Pharmacokinetics of TH-302, a Hypoxia-Activated Prodrug, in Patients with Advanced Solid Malignancies," *Clin. Cancer Res.*, vol. 17, no. 9, pp. 2997-3004, 2011.

[104] F. Meng, J. W. Evans, D. Bhupathi, M. Banica, L. Lan, G. Lorente, J.-X. Duan, X. Cai, A. M. Mowday, C. P. Guise, A. Maroz, R. F. Anderson, A. V. Patterson, G. C. Stachelek, P. M. Glazer, M. D. Matteucci and C. P. Hart, "Molecular and Cellular Pharmacology of the Hypoxia-Activated Prodrug TH-302," *Mol. Canc. Ther.*, vol. 11, no. 3, pp. 740-751, 2012.

[105] S. M. Frisch and H. Francis, "Disruption of Epithelial Cell-Matrix Interactions Induces Apoptosis," *J. Cell Biol.*, vol. 124, no. 4, pp. 619-629, 1994.

[106] A. Vanwezel, "Growth of Cell-strains and Primary Cells on Micro-carriers in Homogeneous Culture," *Nature*, vol. 216, pp. 64-65, 1967.

[107] F. Pampaloni, E. G. Reynaud and E. H. Stelzer, "The third dimension bridges the gap between cell culture and live tissue," *Nat. Rev. Mol. Cell Biol.* , vol. 8, no. 10, pp. 839-845, 2007.

[108] T. Mosmann, "Rapid Colorimetric Assay for Cellular Growth and Survival: Application to Proliferation and Cytotoxicity Assays," *J. Immunol. Methods*, vol. 65, pp. 55-63, 1983.

[109] T. L. Riss, R. A. Moravec, A. L. Niles, S. Duellman, H. A. Benink, T. J. Worzella and L. Minor, Cell Viability Assays, Eli Lilly & Company and the National Center for Advancing Translational Sciences; 2004, 2013.

[110] K. R. Keshari, R. Sriram, B. L. Koelsch, M. Van Criekinge, D. M. Wilson, J. Kurhanewicz and Z. J. Wang, "Hyperpolarized 13C-pyruvate magnetic resonance reveals rapid lactate export in metastatic renal cell carcinomas," *Cancer Res.*, vol. 73, no. 2, pp. 529-538, 2012.

[111] A. Lodi, S. M. Woods and S. M. Ronen, "Treatment with the MEK inhibitor U0126 induces decreased hyperpolarized pyruvate to lactate conversion in breast, but not prostate, cancer cells," *NMR Biomed.*, vol. 26, pp. 299-306, 2012.

[112] K. Golman, R. in't Zandt, M. Lerche, R. Pehrson and J. H. Ardenkjaer-Larsen, "Metabolic Imaging by Hyperpolarized 13C Magnetic Resonance Imaging for In vivo Tumor Diagnosis," *Cancer Res.*, vol. 66, no. 22, pp. 10855-10860, 2006.

[113] K. Golman, J. S. Petersson, P. Magnusson, E. Johansson, P. Åkeson, C.-M. Chai, G. Hansson and S. Månsson, "Cardiac Metabolism Measured Noninvasively by Hyperpolarized13C MRI," *Magn. Res. Med.*, vol. 59, pp. 1005-1013, 2008.

[114] M. E. Merritt, C. Harrison, C. Storey, F. M. Jeffrey, A. D. Sherry and C. R. Malloy, "Hyperpolarized 13C allows a direct measure of flux through a single enzyme-catalyzed step by NMR," *PNAS*, vol. 104, no. 50, pp. 19773-19777, 2007.

[115] M. A. Schroeder, L. E. Cochlin, L. C. Heather, K. Clarke, G. K. Radda and D. J. Tyler, "In vivo assessment of pyruvate dehydrogenase flux in the heart using hyperpolarized carbon-13 magnetic resonance," *PNAS*, vol. 105, no. 33, pp. 12051-12056, 2008.

[116] S. Kohler, Y. Yen, J. Wolber, A. Chen, M. Albers, R. Bok, V. Zhang, J. Tropp, S. Nelson, D. Vigneron, J. Kurhanewicz and R. Hurd, "In Vivo13Carbon Metabolic Imaging at 3T With Hyperpolarized13C-1-Pyruvate," *Magn. Reson. Med.*, vol. 58, pp. 65-69, 2007.

[117] C. Laustsen, J. A. Østergaard, M. H. Lauritzen, R. Nørregaard, S. Bowen, L. V. Søgaard, A. Flyvbjerg, M. Pedersen and J. H. Ardenkjær-Larsen, "Assessment of early diabetic renal changes with hyperpolarized [1-13C]pyruvate," *Diabetes Metab. Res. Rev.*, vol. 29, pp. 125-129, 2013.

[118] T. Xu, D. Mayer, M. Gu, Y.-F. Yen, S. Josan, J. Tropp, A. Pfefferbaum, R. Hurd and D. Spielman, "Quantification of in vivo metabolic kinetics of hyperpolarized pyruvate in rat kidneys using dynamic 13C MRSI," *NMR Biomed.*, vol. 24, pp. 997-1005, 2011.

[119] M. J. Albers, R. Bok, A. P. Chen, C. H. Cunningham, M. L. Zierhut, V. Y. Zhang, S. J. Kohler, J. Tropp, R. E. Hurd, Y.-F. Yen, S. J. Nelson, D. B. Vigneron and J. Kurhanewicz, "Hyperpolarized 13C Lactate, Pyruvate, and Alanine: Noninvasive Biomarkers for Prostate Cancer Detection and Grading," *Cancer Res.*, vol. 20, pp. 8607-8615, 2008.

[120] F. A. Gallagher, M. I. Kettunen, D.-E. Hu, P. R. Jensen, R. i. Zandt, M. Karlsson, A. Gisselsson, S. K. Nelson, T. H. Witney, S. E. Bohndiek, G. Hansson, T. Peitersen, M. H. Lerche and K. M. Brindle, "Production of hyperpolarized [1,4-13C2]malate from [1,4-13C2]fumarate is a marker of cell necrosis and treatment response in tumors," *PNAS*, vol. 106, no. 47, pp. 19801-19806, 2009.

[121] S. Meier, P. R. Jensen and J. Ø. Duus, "Real-time detection of central carbon metabolism in living Escherichia coli and its response to perturbations," *FEBS Lett.*, vol. 585, pp. 3133-3138, 2011.

[122] S. Meier, M. Karlsson, P. R. Jensen, M. H. Lerche and J. Ø. Duus, "Metabolic pathway visualization in living yeast by DNP-NMR," *Mol. BioSyst.*, vol. 7, pp. 2834-2836, 2011.

[123] D. M. Wilson, R. E. Hurd, K. Keshari, M. V. Criekinge, A. P. Chen, S. J. Nelson, D. B. Vigneron and J. Kurhanewicz, "Generation of hyperpolarized substrates by secondary labeling with [1,1-13C] acetic anhydride," *PNAS*, vol. 106, no. 14, pp. 5503-5507, 2009.

[124] C. von Morze, R. Bok, J. Sands, J. Kurhanewicz and D. Vigneron, "Monitoring urea transport in rat kidney in vivo using hyperpolarized $^{13}C$ magnetic resonance imaging," *Am. J. Physiol. Renal. Physiol.*, vol. 302, no. 12, pp. F1658-F1662, 2012.

[125] W. M. Pardridge, "Drug transport across the blood–brain barrier," *J. Cereb. Blood Flow Metab.*, vol. 32, pp. 1959-1972, 2012.

[126] H. Allouche-Arnon, T. Wade, L. F. Waldner, V. N. Miller, J. Gomori, R. Katz-Brull and C. A. McKenzie, "In vivomagnetic resonance imaging of glucose – initial experience," *Contrast Media Mol. Imaging*, vol. 8, pp. 72-82, 2013.

[127] T. B. Rodrigues, E. M. Serrao, B. W. Kennedy, D.-e. Hu, M. I. Kettunen and K. M. Brindle, "Magnetic resonance imaging of tumor glycolysis using hyperpolarized 13C-labeled glucose," *Nat. Med.*, vol. 3, no. 1, pp. 93-97, 2014.

[128] J. H. Ardenkjær-Larsen, S. Macholl and H. Jóhannesson, "Dynamic Nuclear Polarization with Trityls at 1.2 K," *Appl. Magn. Reson.*, vol. 34, pp. 509-522, 2008.

[129] L. Lumata, S. Ratnakar, A. Jindal, M. Merritt, A. Comment, C. Malloy, A. Sherry and Z. Kovacs, "BDPA: An Efficient Polarizing Agent for Fast Dissolution Dynamic Nuclear Polarization NMR Spectroscopy," *Chem. Eur. J.*, vol. 17, pp. 10825-10827, 2011.

[130] F. Montanari, S. Quici, H. Henry-Riyad, T. T. Tidwell, A. Studer and T. Vogler, "2,2,6,6-Tetramethylpiperidin-1-oxyl," *e-EROS*, pp. 1-9, 2007.

[131] L. Lumata, M. E. Merritt, C. R. Malloy, A. Sherry and K. Zoltan, "Impact of Gd3+ on DNP of [1-13C]Pyruvate Doped with Trityl OX063, BDPA, or 4-Oxo-TEMPO," *J. Phys. Chem. A*, vol. 116, pp. 5129-5138, 2012.

[132] J. Heckmann, W. Meyer, E. Radtke and G. Reicherz, "Electron spin resonance and its implication on the maximum nuclear polarization of deuterated solid target materials," *Phys. Rev. B*, vol. 74, p. 134418, 2006.

[133] L. Lumata, Z. Kovacs, A. D. Sherry, C. Malloy, S. Hill, J. van Tol, L. Yu, L. Song and M. E. Merritt, "Electron spin resonance studies of trityl OX063 at a concentration optimal for DNP," *Phys. Chem. Chem. Phys.*, vol. 15, pp. 9800-9807, 2013.

[134] L. Lumata, S. J. Ratnakar, A. Jindal, M. Merritt, A. Comment, C. Malloy, A. D. Sherry and Z. Kovacs, "BDPA: An Efficient Polarizing Agent for Fast Dissolution Dynamic Nuclear Polarization NMR Spectroscopy," *Chem. Eur. J.*, vol. 17, pp. 10825-10827, 2011.

[135] K. Golman, R. I. Zandt and M. Thaning, "Real-time metabolic imaging," *PNAS*, vol. 103, no. 30, pp. 11270-11275, 2006.

[136] P. R. Jensen, M. Karlsson, S. Meier, J. Ø. Duus and M. H. Lerche, "Hyperpolarized Amino Acids for In Vivo Assays of Transaminase Activity," *Chem. Eur. J.*, vol. 15, pp. 10010-10012, 2009.

[137] L. Lumata, M. Merritt, C. R. Malloy, A. Sherry and Z. Kovacs, "Impact of Gd3+ on DNP of [1-13C]Pyruvate Doped with Trityl OX063, BDPA, or 4-Oxo-TEMPO," *J. Phys. Chem. A*, vol. 116, pp. 5129-5138, 2012.

[138] C. Ward, H. Venkatesh, M. Chaumeil, A. Brandes, M. VanCriekinge, H. Dafni, S. Sukumar, S. Nelson, D. Vigneron, J. Kurhanewicz, C. James, D. Haas-Kogan and S. Ronen, "Noninvasive Detection of Target Modulation following Phosphatidylinositol 3-Kinase Inhibition Using Hyperpolarized 13C Magnetic Resonance Spectroscopy," *Cancer Res.*, vol. 70, no. 4, pp. 1296-1305, 2010.

[139] J. E. Raftos, S. Whillier, B. E. Chapman and P. W. Kuchel, "Kinetics of uptake and deacetylation of N-acetylcysteine by human erythrocytes," *Int. J. Biochem. Cell. Biol.*, vol. 39, pp. 1698-1706, 2007.

[140] G. Wu, Y.-Z. Fang, S. Yang, J. R. Lupton and N. D. Turner, "Glutathione Metabolism and Its Implications for Health," *J. Nutr.*, vol. 134, no. 3, pp. 489-492, 2004.

[141] A. Kisaoglu, B. Ozogul, M. I. Turan, I. Yilmaz, I. Demiryilmaz, S. S. Atamanalp, E. Bakan and H. Suleyman, "Damage induced by paracetamol compared with N-acetylcysteine," *J. Chin. Med. Assoc.*, vol. 39, pp. 1698-1706, 2007.

[142] G. F. Rushworth and I. L. Megson, "Existing and potential therapeutic uses for N-acetylcysteine: The need for conversion to intracellular glutathione for antioxidant benefits," *Pharmacol. Ther.*, vol. 141, pp. 150-159, 2014.

[143] V. Uttamsingh, D. Keller and M. Anders, "Acylase I-Catalyzed Deacetylation of N-Acetyl-L-cysteine and S-Alkyl-N-acetyl-L-cysteines," *Chem. Res. Toxicol.*, vol. 11, pp. 800-809, 1998.

[144] I. E. Dhouib, M. Jallouli, A. Annabi, N. Gharbi, S. Elfazaa and M. M. Lasram, "A minireview on N-acetylcysteine: An old drug with new approaches," *Life Sci.*, vol. 151, pp. 359-363, 2016.

[145] Y. Samuni, S. Goldstein, O. M. Dean and M. Berk, "The chemistry and biological activities of N-acetylcysteine," *Biochim. Biophys. Acta*, vol. 1830, pp. 4117-4129, 2013.

[146] A. Sheffner, E. Medler, K. Bailey, D. Gallo, A. Mueller and H. Sarett, "METABOLIC STUDIES WITH ACETYLCYSTEINE," *Biochem. Pharmacol.*, vol. 15, pp. 1523-1535, 1966.

[147] D. P. Arfsten, E. W. Johnson, E. R. Wilfong, A. E. Jung and A. J. Bobb, "Distribution of Radio-Labeled N-Acetyl-L Cysteine in Sprague-Dawley Rats and Its Effect on Glutathione Metabolism Following Single and Repeat Dosing by Oral Gavage," *Cutan. Ocul. Toxicol.*, vol. 26, pp. 113-134, 2007.

[148] E. A. Neuwelt, M. A. Pagel, B. P. Hasler, T. G. Deloughery and L. L. Muldoon, "Therapeutic Efficacy of Aortic Administration of N-Acetylcysteine as a Chemoprotectant

against Bone Marrow Toxicity after Intracarotid Administration of Alkylators, with or without Glutathione Depletion in a Rat Model," *Cancer Res.*, vol. 61, pp. 7868-7874, 2001.

[149] K. Yen, M. Bittinger, S. Su and V. Fantin, "Cancer-associated IDH mutations: biomarker and therapeutic opportunities," *Oncogene*, vol. 29, pp. 6409-6417, 2010.

[150] J. Popovici-Muller, J. O. Saunders, F. G. Salituro, J. M. Travins, S. Yan, F. Zhao, S. Gross, L. Dang, K. E. Yen, H. Yang, K. S. Straley, S. Jin, K. Kunii, V. R. Fantin, S. Zhang, Q. Pan, D. Shi, S. A. Biller and S. M. Su, "Discovery of the First Potent Inhibitors of Mutant IDH1 That Lower Tumor 2-HG in Vivo," *ACS Med. Chem. Lett.*, vol. 3, pp. 850-855, 2012.

[151] O. C. Andronesi, I. C. Arrillaga-Romany, K. I. Ly, W. Bogner, E. M. Ratai, K. Reitz, A. J. Iafrate, J. Dietrich, E. R. Gerstner, A. S. Chi, B. R. Rosen, P. Y. Wen, D. P. Cahill and T. T. Batchelor, "Pharmacodynamics of mutant-IDH1 inhibitors in glioma patients probed by in vivo 3D MRS imaging of 2-hydroxyglutarate," *Nat. Commun.*, vol. 9, no. 1, p. 1474, 2018.

[152] J. W. Keillor, R. Castonguay and C. Lherbet, "Gamma-Glutamyl Transpeptidase Substrate Specificity and Catalytic Mechanism," *Methods. Enzymol.*, vol. 401, pp. 449-467, 2005.

[153] T. Nishihara, H. Yoshihara, H. Nonaka, Y. Takakusagi, F. Hyodo, K. Ichikawa, E. Can, J. Bastiaansen, Y. Takado, A. Comment and S. Sando, "Direct Monitoring of g-Glutamyl Transpeptidase Activity In Vivo Using aHyperpolarized13C-Labeled Molecular Probe," *Angew. Chem.*, vol. 128, pp. 10784-10787, 2016.

[154] J. Whitfeld, "Gamma Glutamyl Transferase," *Crit. Rev. Clin. Lab. Sci.*, vol. 38, no. 4, pp. 262-355, 2001.

[155] M. H. Hanigan, "Gamma-glutamyl transpeptidase: redox regulation and drug resistance.," *Adv. Cancer Res.*, vol. 122, pp. 104-141, 2014.

[156] M. H. Lerche, D. Yigit, A. B. Frahm, J. H. Ardenkjær-Larsen, R. M. Malinowski and P. R. Jensen, "Stable Isotope-Resolved Analysis with Quantitative Dissolution Dynamic Nuclear Polarization," *Anal. Chem.*, vol. 90, pp. 674-678, 2018.

[157] R. M. Malinowski, S. M. Ghiasi, T. Mandrup-Poulsen, M. H. Lerche, J. H. Ardenkjær-Larsen and P. R. Jensen, "Pancreatic b-cells respond with early metabolic switch to fuel pressure," *Submitted to J. Biol. Chem.*.

# Paper I

Stable Isotope-Resolved Analysis with Quantitative Dissolution Dynamic Nuclear Polarization

Lerche, M.H.; Yigit, D.; Frahm. A.B.; Ardenkjær-Larsen, J.H.; **Malinowski, R.M**.; Jensen, P.R.

Published in Analytical Chemistry, ACS

analytical chemistry

Technical Note

Cite This: Anal. Chem. 2018, 90, 674−678

pubs.acs.org/ac

# Stable Isotope-Resolved Analysis with Quantitative Dissolution Dynamic Nuclear Polarization

Mathilde H. Lerche, Demet Yigit,[†] Anne B. Frahm,[†] Jan Henrik Ardenkjær-Larsen, Ronja M. Malinowski, and Pernille R. Jensen*

Center for Hyperpolarization in Magnetic Resonance, Department of Electrical Engineering, Technical University of Denmark, Ørsteds Plads, 2800 Kongens Lyngby, Denmark

Supporting Information

**ABSTRACT:** Metabolite profiles and their isotopomer distributions can be studied noninvasively in complex mixtures with NMR. The advent of dissolution Dynamic Nuclear Polarization (dDNP) and isotope enrichment add sensitivity and resolution to such metabolic studies. Metabolic pathways and networks can be mapped and quantified if protocols that control and exploit the ex situ signal enhancement are created. We present a sample preparation method, including cell incubation, extraction and signal enhancement, to obtain reproducible and quantitative dDNP (qdDNP) NMR-based stable isotope-resolved analysis. We further illustrate how qdDNP was applied to gain metabolic insights into the phenotype of aggressive cancer cells.

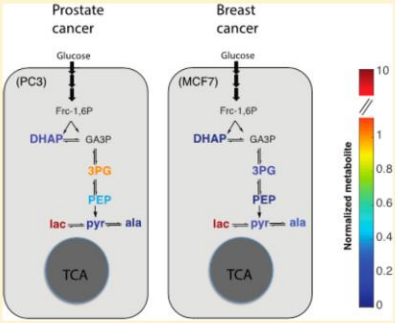


An increasing quest for systems approaches to biochemical understanding in living organisms makes NMR analysis of metabolism still more attractive. In conjunction with stable isotope labeling, NMR provides the possibility to directly determine metabolite composition of complex mixtures and to perform in situ analysis of pathway dynamics from live cells and whole organisms.[1] Augmented sensitivity and resolution of the NMR signals can be gained by ex situ signal enhancement, for example, obtained with dissolution Dynamic Nuclear Polarization (dDNP).[2] The well-established real-time kinetic dDNP NMR experiment offers detection of the direct conversion of a hyperpolarized substrate in a cell suspension with subsecond resolution.[3] This type of experiment allows the determination of rate constants within a 1 min time window after addition of the substrate to the cell suspension. This transient experiment, however, requires high up-take and turnover rates for its success.

Changing the order of events in the described DNP signal enhanced experiment could eliminate any restriction on time scale. Such an experiment would involve incubation of live cells or whole organisms with stable isotope labeled substrates, extraction of metabolites and quantitative dDNP NMR of the extracts. Such complementary strategy has previously been applied for therapeutic drug monitoring in animals by analyzing systemic and excreted metabolites in blood and urine,[4] for characterization of physical parameters of metabolites[5] and as metabolomics approach for component analysis of plant and breast cancer cells.[6] In general, the complementary strategy of dDNP on metabolite extracts, benefit from the high sensitivity and resolution provided by hyperpolarized samples in high-field NMR spectrometers, the quantification by comparison with an internal standard, and the capability to monitor slow metabolic transformations.

Here we are focused on obtaining dynamic labeling patterns using dissolution DNP NMR for quantification of relative pathway activities. We demonstrate a robust protocol for quantitative dissolution DNP (qdDNP) sensitivity enhanced isotope tracer analysis by NMR. Living cancer cells are incubated with uniformly $^{13}$C-labeled glucose at different time points, metabolites are extracted, hyperpolarized, and subsequently analyzed with NMR allowing reconstruction of cancer type specific metabolic pathways.

## EXPERIMENTAL SECTION

**Sample Preparation To Evaluate Polarization, Solubility, and Concentration.** Stock solutions of five test compounds were made, $^{13}C_1$-pyruvate (27 mM), $^{13}C_1$-lactate (34 mM), $^{13}C_1$-alanine (54 mM), $^{13}C_1$-acetate (35 mM), and $^{13}$C-HP001 (50 mM, 1.1-bis (hydroxymethyl) cyclopropane)). A polarization medium was made of 314 mg Milli-Q-water, 70 mg trityl radical OX063, 1227 mg glycerol, and 28.8 mg Gadoteridol (100 $\mu$mol/g). A total of 5 $\mu$L of each stock solutions were mixed with 100 $\mu$L of polarization medium, 25 $\mu$L of Milli-Q water, and 11.58 mg [U-$^{13}$C,D] glucose (60 $\mu$mol) or 1.80 mg [U-$^{13}$C,D] glucose (10 $\mu$mol). The 150 $\mu$L sample was transferred to a sample cup.

Received: July 17, 2017
Accepted: December 4, 2017
Published: December 4, 2017





DOI: 10.1021/acs.analchem.7b02779
Anal. Chem. 2018, 90, 674−678

**Cancer Cell Growth.** Human prostate adenocarcinoma cells (PC3) and human mammary adenocarcinoma cells (MCF7) were grown to approximately 90%. Cells were grown in flasks (175 $cm^2$) in an environment with 5% $CO_2$, at 37 °C in RPMI-1640 medium with FBS and antibiotics. Cells were harvested by trypsination, washed, and resuspended in 40 mM phosphate buffer pH 7.3 to a concentration of 20 million cells/mL.

**Metabolite Samples and Cell Extracts.** A total of 500 $\mu$L of cell suspension (10 mio. cells) in 2 mL Eppendorf tubes were placed in a shaking thermostat at 37 °C. 100 $\mu$L of [U-$^{13}$C,D] glucose (120 mM) was added and the cells were incubated for 0, 1, 3, 10, or 30 min, respectively. Following incubation, the entire cell suspension was quenched with perchloric acid (PCA): 400 $\mu$L of ice cold 2.2 M PCA solution was added to 600 $\mu$L of cell suspension and placed on ice for at least 10 min. Soluble metabolites were extracted by centrifugation (10 min, 10000 rpm, 4 °C). Supernatant was pH neutralized with KOH, centrifuged, and freeze-dried. The lyophilized samples were dissolved with 150 $\mu$L of polarization medium (70 mg OX063, 1227 mg glycerol, 944 mg Milli-Q water, 28.8 mg Gadoteridol (100 $\mu$mol/g)), and 5 $\mu$L of HP001 (50 mM) was added as an internal standard.

**Metabolite Samples, Unlabeled.** Signal loss coefficient (SLC) measured using unlabeled metabolites consisted of 75 $\mu$mol of each compound (3-phosphoglycerate (3PG), dihydroxyacetone phosphate (DHAP), or phosphoenolpyruvate (PEP)) mixed with 450 $\mu$L of polarization medium as described under cell extracts, 15 $\mu$L of HP001 (50 mM), and 5.4 mg [U-$^{13}$C,D] glucose. Difference in pH dependency of the chemical shift for 3PG and 6PG[7] was used to identify 3PG as the observed metabolite (Figure S3).

**Dynamic Nuclear Polarization.** qdDNP was performed at 3.35 T and 1.4 K in a HyperSense polarizer with microwave irradiation at $f_{\mu w}$ = 94 GHz and $P_{\mu w}$ = 100 mW. Technical samples were polarized for 30, 90, or 240 min, respectively. Metabolite samples were polarized for 90 min. All samples were dissolved with 5 mL of phosphate buffer (40 mM, pH 7.4) and transferred to a 9.4 T NMR spectrometer into a 5 mm NMR tube in approximately 12 s.

**NMR Spectroscopy, qdDNP.** All samples were measured in a 9.4 T Varian spectrometer at 37 °C. $^{13}$C 1D NMR spectra of metabolite samples were acquired with a 70° pulse. $^{13}$C 1D NMR spectra of technical samples were obtained with a series of 5° pulses acquired every 3 s.

**NMR Spectroscopy, Thermal NMR.** A 75 $\mu$L aliquot of DNP sample was dissolved in 400 $\mu$L of phosphate buffer (40 mM, pH 7.3), 75 $\mu$L of $D_2O$ and 15 $\mu$L of Omniscan. $^{13}$C 1D NMR spectra were recorded on a Bruker 800 MHz spectrometer with cryoprobe using a delay of 2 s and 4096 scans.

**Data Processing.** NMR spectra were processed with MNova. Statistical analysis was done with Python using SciPy.[8,9]

## RESULTS AND DISCUSSION

**Optimization of DNP Sample Preparation.** Quantification of biological extracts requires a general and robust polarization matrix compatible with an ensemble of different metabolites. A mixture of 50% water/50% glycerol was used with the trityl radical OX063 and a gadolinium−DOTA complex as described in general principles by Karlsson et al.[10] HP001 was chosen as internal reference compound due to its favorable properties such as spectral position, long $T_1$ on the quaternary carbon, high solubility, and chemical stability.[4] To simulate the conditions in a metabolite sample, [U-$^{13}$C,D] glucose was added along with the standard compound to the polarization matrix.

The samples were polarized for 30, 90, and 240 min to find the best time point for dissolution (Figure 1). For each time point, the solid-state polarization is repeatable (a.u. 2817 ± 114, 5311 ± 74, and 5716 ± 57 for, respectively, 30, 90, and 240 min). After 90 min, 93% of the maximal achievable polarization is reached. This time point was therefore chosen for samples where optimal SNR is important. It is evident that reducing the polarization time to 30 min can increase the throughput of the method. In this case, about 50% of the maximal polarization can be achieved. After dissolution, the integral of the standard compound (HP001) follows the solid-state build-up as expected (Figure 1, red symbols). The polarization matrix used here is optimized with respect to radical, Gd-complex, and $^{13}$C concentration. A relatively broad maximum around 15 mM OX063 has been found in the literature for polarization matrices.[10] Addition of gadolinium increases the polarization at 3.35 T with 60% (Table S2). Ludwig et al.[11] have suggested that $^{13}$C labeled additives can increase the polarization by increasing the spin diffusion. In accordance with this we observe a 50% decrease of the polarization if the [U-$^{13}$C,D] glucose is replaced by natural abundance glucose (Table S2). To obtain maximum signal in the solid state 60 $\mu$mol of [U-$^{13}$C,D] glucose was applied but even at 10 $\mu$mol [U-$^{13}$C,D] glucose 83% of the maximum polarization can be achieved (Table S2). At optimum conditions, a liquid state polarization of 20% on glucose C1 was obtained after 240 min polarization, followed by dissolution and 12 s manual transfer time. This corresponds approximately to a solid-state polarization of 44% ($T_1$ = 15 s, 9.4 T).

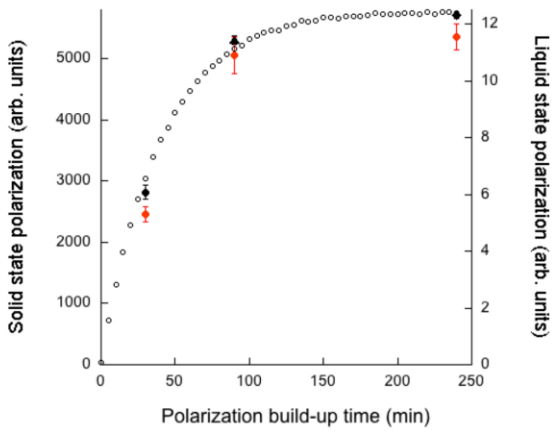


**Figure 1.** Solid-state polarization buildup of $^{13}$C signal in the general polarization matrix consisting of 50% water, 50% glycerol, OX063 radical, and Gd-complex (black symbols, $n$ = 3). The corresponding liquid state polarization of the standard compound HP001 (red symbols) is shown as comparison ($n$ = 3 for 30 and 90 min and $n$ = 2 for 240 min polarization time).

**Quantification of Metabolites.** The liquid state polarization level was measured for four often-occurring metabolites (lactate, acetate, alanine, and pyruvate) polarized at three different time points (30, 90, and 240 min). The absolute


DOI: 10.1021/acs.analchem.7b02779
Anal. Chem. 2018, 90, 674−678

integrals are reproducible for a given polarization time (Figure 2), but over longer time periods, the stability of the

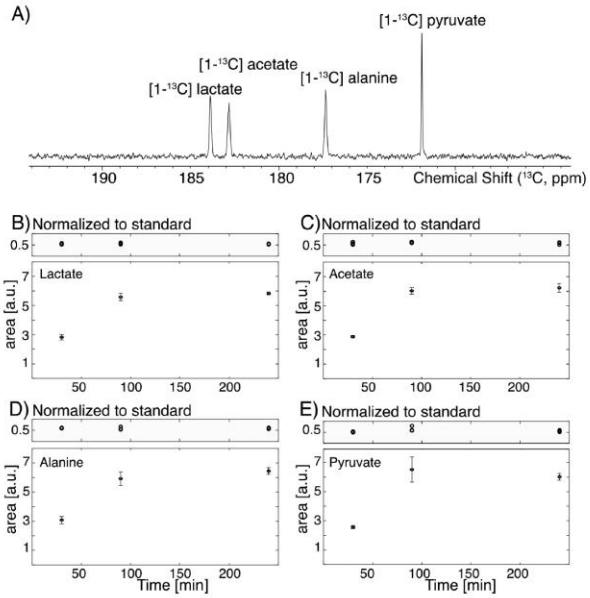


**Figure 2.** (A) Example of spectrum after dissolution of four metabolites after 90 min polarization. (B–E) Measured integrals of the dissolved samples after 30–240 min polarization. Top panels show ratio to internal standard (HP001).

polarizer can influence these.[12] For the method to be robust the quantification of the metabolites is thus based on the ratio to an internal standard (HP001). This ratio is stable and independent of the polarization time for each metabolite with a coefficient of variation of 4.5% ($^{13}C_1$-lactate), 7.4% ($^{13}C_1$-acetate), 6.1% ($^{13}C_1$-alanine), and 15.7% ($^{13}C_1$-pyruvate), $n = 9$. Transport of the sample from the polarizer to the NMR spectrometer represents in many cases an uncontrolled magnetic environment. For our current setup with a 12 s transfer time, the method is limited to quaternary and deuterated carbon positions. Other laboratories have minimized losses of polarization in the sample transfer step by implementation of magnetic and temperature controlled transfer lines.[13,14] Although these solutions are important for optimization of assay sensitivity and reproducibility, robust quantification of metabolites demands that individual signal decay is taken into account.[12] To account for signal decay during transfer for all identified metabolites, a signal loss coefficient (SLC) was determined relative to the internal standard and compared to the ratio obtained with conventional thermal $^{13}C$ NMR (Table 1). For the tested compounds the SLC varies from 55 to 108%. Alanine has the lowest SLC. This could be expected based on a short $T_1$ at 9.4 T (22 s, Table S3) and the observation that amino acids are sensitive to the dissolution process.[15] The line width of the four molecules in Figure 2A (2.9 Hz vs 10.1 Hz for pyruvate and alanine, respectively) reveals that pyruvate has a longer $T_2$ than the other three molecules. Due to these metabolite specific relaxation behaviors the SLC must be determined for each metabolite to be able to calculate absolute concentrations.

**Identification and Quantification of Characteristic Metabolites in Cancer Cells.** Breast cancer cells (MCF7) and prostate cancer cells (PC3) were incubated with [U-$^{13}$C,D] glucose for 1, 3, 10, and 30 min ($n = 3$). The entire cell suspensions were arrested and soluble metabolites were extracted and analyzed as discussed above. A distinct cell type dependent metabolic pattern is showing itself already at 10 min incubation time but is highly evident after 30 min incubation with [U-$^{13}$C,D] glucose, Figure 3. For comparison, a thermal NMR spectrum acquired on a 600 MHz spectrometer overnight on an identical sample only reveals lactate (MCF7, 30 min, Figure S1).

**Table 1. Signal Loss Coefficient (SLC): Metabolite Ratios Relative to the Standard HP001 from the DNP Experiment is Calibrated to the Values Obtained with Thermal NMR (SLC = DNP ratio/NMR ratio)**

| compound (Com) | DNP ratio (Com/HP001) | NMR ratio (Com/HP001) | SLC (%) |
|---|---|---|---|
| lactate, C1 | 0.55 ± 0.03 | 0.67 ± 0.07 | 82 ± 8 |
| acetate, C1 | 0.58 ± 0.04 | 0.61 ± 0.04 | 95 ± 6 |
| alanine, C1 | 0.60 ± 0.04 | 1.08 ± 0.01 | 55 ± 4 |
| pyruvate, C1 | 0.57 ± 0.09 | 0.53 ± 0.01 | 108 ± 9 |

Both cell types produce large amounts of lactate (about 20 times more than the other observed metabolites), confirming their glycolytic phenotype. While this production is constant over time in MCF7 cells it is decreasing in PC3 cells. Lactate production per minute is halved at 30 min compared to 1 min incubation time, $p < 0.01$ (Figure S2). No equivalent change in glucose consumption between the cell types is found based on the remaining glucose signal. The change in lactate production thus hints to a changed metabolism significant at 30 min incubation time.

Amounts of identified metabolites can be calculated for the two cell types allowing a direct comparison of fluxes. A signal loss coefficient (SLC) for identified metabolites was obtained with dDNP NMR on unlabeled metabolites polarized under the same conditions as for the metabolite extracts. A list of SLC values for identified metabolites is given in Table 2. Difference in sample preparation such as increased concentration and different labeling schemes do not influence the calculated SLC (Tables S4 and S5). Amounts of metabolites identified at 30 min incubation time in the two cell types were quantified (Figure 4) using the SLC values given in Tables 1 and 2.

Whereas breast cancer cells produce almost entirely pyruvate (pyr) and its downstream metabolites alanine (ala) and lactate (lac), prostate cancer cells accumulate phosphoenolpyruvate (pep) and dihydroxyacetone phosphate (DHAP). 3-Phosphoglycerate (3PG) although produced by both cell types is 6× higher in the long incubation times for prostate cancer cells as shown in Figure 3C. This high increase in 3PG follows the relative decrease in lactate production in PC3 cells at long incubation times and may reflect alternative use of glucose metabolism such as, for example, buildup of amino acids. This interpretation is supported by the both upstream and downstream accumulation of glycolytic intermediates.

## ■ CONCLUSIONS

By inverting the steps involved in a real-time cellular dDNP experiment, and incubating living cells with an isotope enriched substrate before subjecting the metabolite(s) to hyperpolarization, we prolong the time window from a few minutes to hours. The time frame will be dependent on the biological model rather than on the $T_1$ of the tracer. We show in this work that


DOI: 10.1021/acs.analchem.7b02779
Anal. Chem. 2018, 90, 674–678

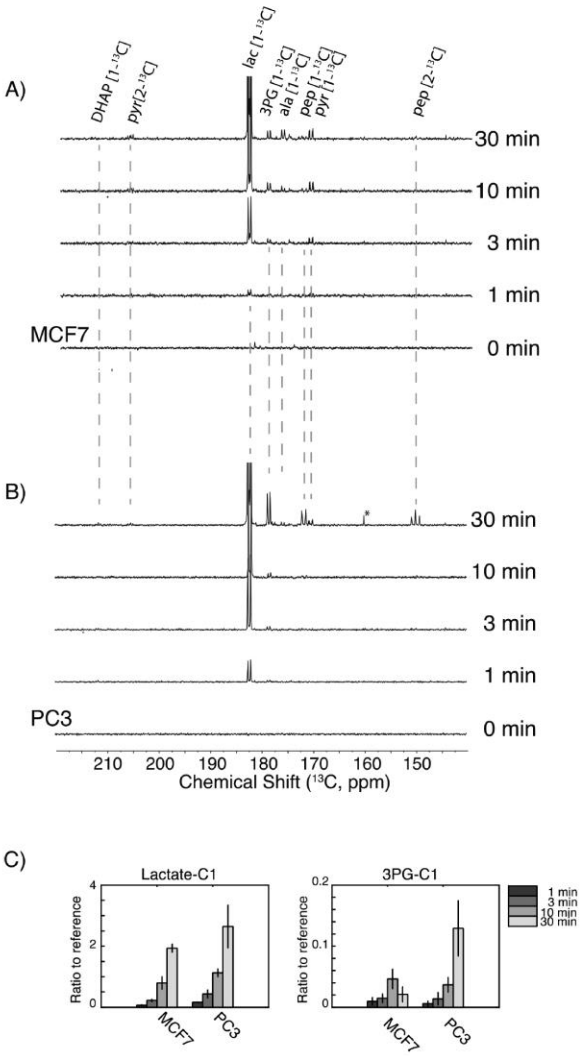


**Figure 3.** (A, B) Example of dDNP-NMR spectra of metabolite extracts from two cancer cell lines (MCF7, breast cancer and PC3, prostate cancer). The cells have been incubated with [U-$^{13}$C,D] glucose for time points 0, 1, 3, 10, and 30 min. Chemical shifts are referenced to HP001 at 23.7 ppm and metabolite assignments are performed as described in Supporting Information (Table S6). (C) Lactate and 3-phosphoglycerate production as a function of time relative to an internal standard ($n$ = 3).

**Table 2. Signal Loss Coefficients (SLC) for Metabolites Identified in Addition to Table 1**

| compound | DNP ratio (Com/HP001) | NMR ratio (Com/HP001) | SLC (%) |
|---|---|---|---|
| 3PG, C1 | 0.49 ± 0.01 | 0.94 ± 0.02 | 52 ± 4 |
| DHAP, C2 | 0.37 ± 0.004 | 0.32 ± 0.02 | 116 ± 1 |
| pep, C1 | 1.30 ± 0.01 | 1.22 ± 0.09 | 107 ± 9 |
| pep, C2 | 1.42 ± 0.01 | 1.18 ± 0.04 | 120 ± 4 |

NMR analysis of hyperpolarized metabolite extracts following substrate incubation can be quantitative provided that an internal standard is applied in combination with laboratory dependent calibrations. The former is straightforwardly added to the analyte and the latter is determined as one-time corrections unique for each metabolite.

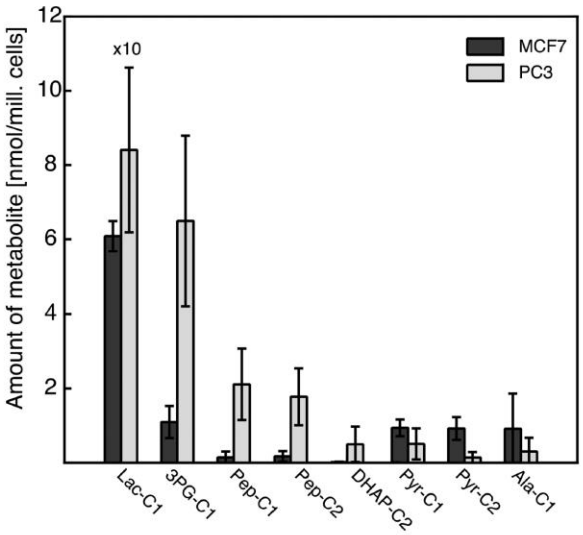


**Figure 4.** Quantitative metabolic fingerprint from 30 min incubation of MCF7 and PC3 cell line with [U-$^{13}$C,D] glucose ($n$ = 3).

In combination, the extended time scale and quantitative signal enhancement of extracts allow metabolite driven hypotheses in cellular biochemistry. In the example discussed here, the metabolic pattern of MCF7 cells support a highly glycolytic phenotype with accumulated downstream metabolites of pyruvate, lactate and alanine. The metabolic pattern of PC3 cells is more complex: Both DHAP and pep accumulate supporting that the active isoform of pyruvate kinase (PKM2) in cancer is inhibited in aggressive prostate cancer cells.[16] The accumulation of 3PG suggests alternative use of energy production such as activation of the serine/glycine pathway resulting in an apparent decrease in lactate formation at long incubation times.

The presented work describes a method by which, in cell, metabolite analysis can be performed with high sensitivity and high accuracy and precision. Such a method is a means to bring biological insight from a new level of measurable metabolites.

## ■ ASSOCIATED CONTENT

### Supporting Information

The Supporting Information is available free of charge on the ACS Publications website at DOI: 10.1021/acs.analchem.7b02779.

Additional tables and figures in support of sample preparation, SLC, lactate production and assignment of metabolites especially 6PG versus 3PG (PDF).

## ■ AUTHOR INFORMATION

### Corresponding Author

*E-mail: peroje@elektro.dtu.dk.

### ORCID

Pernille R. Jensen: 0000-0003-4359-848X

### Author Contributions

†These authors contributed equally. All authors have given approval of the final version of the manuscript.



DOI: 10.1021/acs.analchem.7b02779
Anal. Chem. 2018, 90, 674−678

### Notes

The authors declare no competing financial interest.

## ■ ACKNOWLEDGMENTS

The authors gratefully acknowledge funding by the Danish National Research Foundation (Grant DNRF124) and Sebastian Meier for NMR data acquisition at the NMR Center·DTU.

## ■ REFERENCES

(1) Fan, T. W.; Lane, A. N. *Prog. Nucl. Magn. Reson. Spectrosc.* **2016**, *92*−*93*, 18−53.
(2) Ardenkjaer-Larsen, J. H.; Fridlund, B.; Gram, A.; Hansson, G.; Hansson, L.; Lerche, M. H.; Servin, R.; Thaning, M.; Golman, K. *Proc. Natl. Acad. Sci. U. S. A.* **2003**, *100* (18), 10158−63.
(3) Lerche, M. H.; Jensen, P. R.; Karlsson, M.; Meier, S. *Anal. Chem.* **2015**, *87* (1), 119−32.
(4) Lerche, M. H.; Meier, S.; Jensen, P. R.; Hustvedt, S. O.; Karlsson, M.; Duus, J. O.; Ardenkjaer-Larsen, J. H. *NMR Biomed.* **2011**, *24* (1), 96−103.
(5) Christensen, C. E.; Karlsson, M.; Winther, J. R.; Jensen, P. R.; Lerche, M. H. *J. Biol. Chem.* **2014**, *289* (4), 2344−52.
(6) Dumez, J. N.; Milani, J.; Vuichoud, B.; Bornet, A.; Lalande-Martin, J.; Tea, I.; Yon, M.; Maucourt, M.; Deborde, C.; Moing, A.; et al. *Analyst* **2015**, *140* (17), 5860−3.
(7) Jensen, P. R.; Meier, S. *Chem. Commun.* **2016**, *52*, 2288−2291.
(8) Python Software Foundation. Python Language Reference, version 3.5. Available at http://www.python.org.
(9) Jones, E.; Oliphant, E.; Peterson, P. SciPy: Open Source Scientific Tools for Python, http://www.scipy.org/ (date 2017-Sep-17).
(10) Karlsson, M.; Jensen, P. R.; Duus, J. O.; Meier, S.; Lerche, M. H. *Appl. Magn. Reson.* **2012**, *43* (1−2), 223−236.
(11) Ludwig, C.; Marin-Montesinos, I.; Saunders, M. G.; Günther, U. L. *J. Am. Chem. Soc.* **2010**, *132* (8), 2508−9.
(12) Bornet, A.; Maucourt, M.; Deborde, C.; Jacob, D.; Milani, J.; Vuichoud, B.; Ji, X.; Dumez, J. N.; Moing, A.; Bodenhausen, G.; Jannin, S.; Giraudeau, P. *Anal. Chem.* **2016**, *88* (12), 6179−83.
(13) Bowen, S.; Hilty, C. *Phys. Chem. Chem. Phys.* **2010**, *12* (22), 5766−70.
(14) Milani, J.; Vuichoud, B.; Bornet, A.; Miéville, P.; Mottier, R.; Jannin, S.; Bodenhausen, G. *Rev. Sci. Instrum.* **2015**, *86* (2), 024101.
(15) Jensen, P. R.; Karlsson, M.; Meier, S.; Duus, J. O.; Lerche, M. H. *Chem. - Eur. J.* **2009**, *15*, 10010−2.
(16) Vander Heiden, M. G.; Lunt, S. Y.; Dayton, T. L.; Fiske, B. P.; Israelsen, W. J.; Mattaini, K. R.; Vokes, N. I.; Stephanopoulos, G.; Cantley, L. C.; Metallo, C. M.; Locasale, J. W. *Cold Spring Harbor Symp. Quant. Biol.* **2011**, *76*, 325−34.



DOI: 10.1021/acs.analchem.7b02779
*Anal. Chem.* 2018, 90, 674−678

**SUPPORTING INFORMATION**

# Stable isotope-resolved analysis with quantitative dissolution dynamic nuclear polarization

Mathilde H. Lerche[1], Demet Yigit[1]*, Anne B. Frahm[1]*, Jan Henrik Ardenkjær-Larsen[1], Ronja M. Malinowski[1] and Pernille R. Jensen[1#].

[1]Center for Hyperpolarization in Magnetic Resonance, Department of Electrical Engineering, Technical University of Denmark, Ørsteds Plads, 2800 Kgs. Lyngby, Denmark.

## 1. Details of experimental methods

# 1. Details of experimental methods

## 1.1 LIQUID STATE POLARIZATION OBTAINED FOR OPTIMIZATION OF SAMPLE PREPARATION

*Table S1. Liquid state polarization for HP001 in dissolved samples following three different solid state polarization times (n=3 for 30 and 90 min and n=2 for 240 min).*

| Polarization time | Condition | Integral HP001 [a.u] |
|---|---|---|
| 30 min | 60 µmol 13C glucose | 5.12 ± 0.56 |
| 90 min | 60 µmol 13C glucose | 10.04 ± 0.11 |
| 240 min | 60 µmol 13C glucose | 10.82 ± 0.40 |

*Table S2 Liquid state polarization for HP001. All numbers are normalized to standard technical sample conditions (60 µmol [U-$^{13}$C,D] glucose, 150 µl polarization medium).*

| Polarization time | Condition | HP001 signal area |
|---|---|---|
| 90 min | 60 µmol $^{13}$C glucose | 1 |
| 90 min | 60 µmol $^{12}$C glucose | 0.48 |
| 90 min | 60 µmol $^{13}$C glucose without Gd | 0.38 |
| 90 min | 10 µmol $^{13}$C glucose | 0.83 |
| 90 min | 10 µmol $^{13}$C glucose 50% radical with Gd | 0.26 |

## 1.2 LIQUID STATE T1 FOR SELECTED METABOLITES

*Table S3. $T_1$ of $^{13}$C from carboxylic acid moieties of four small metabolites. Measured with dissolution DNP NMR, with the sample condition (radical and Gd3+ concentrations) described in materials and methods in the main article.*

| Compound | $T_1$ dDNP [s], (n=6); 9.4 T, 37 °C |
|---|---|
| HP001 | 58.4 ± 2.6 |
| Lactate, C1 | 27.9 ± 1.3 |
| Acetate, C1 | 32.1 ± 1.1 |
| Alanine, C1 | 21.3 ± 1.4 |
| Pyruvate, C1 | 40.2 ± 1.4 |

### 1.3 LIQUID STATE $T_1$ AND POLARIZATION FOR ACETATE UNDER DIFFERENT CONDITIONS AND $^{13}$C-LABELING

The influence of the sample composition such as concentration and $^{13}$C labeling on liquid state polarization was tested. Three samples were made according to the procedure from the experimental section consisting of either: [1-$^{13}$C] acetate (0.25 µmol), [1,2-$^{13}C_2$] acetate (0.25 µmol) or [1-$^{13}$C] acetate (0.25 µmol) plus natural abundance acetate (25.8 µmol i.e. 0.28 µmol $^{13}$C (1.1%)). In addition 1.8 mg [U-$^{13}$C] glucose, 150 µl polarization medium and HP001 (0.250 µmol). The samples were polarized for 90 min and dissolved in 5 ml phosphate buffer (40 mM, pH 7.4).

*Table S4. DNP recovery of carboxylic acid moieties of acetate compared to reference compound (HP001).*

| Compound | DNP Ratio to HP001 | Sample $^{13}$C acetate-C1 [µmol] | Sample $^{13}$C acetate-na [µmol] | Ratio/ µmol $^{13}$C acetate |
|---|---|---|---|---|
| [1-$^{13}$C] acetate | 0.54 | 0.25 | 0 | 2.2 |
| [1,2-$^{13}C_2$] acetate | 0.50 | 0.25 | 0 | 2.0 |
| [1-$^{13}$C] acetate+ n.a. acetate | 1.34 | 0.25 | 0.28 | 2.5 |

n.a = natural abundance.

The influence of $^{13}$C labelling scheme on $T_1$ was measured by inversion recovery at 9.4 T at 37 °C. Two samples were made consisting of either: [1-$^{13}$C] acetate (100 mM) or [1,2-$^{13}C_2$] acetate (100 mM) in 400 µl dissolution buffer (phosphate buffer (40 mM, pH 7.4), 15 µl polarization medium and 100 µl $D_2O$).

*Table S5. $T_1$ of $^{13}$C from carboxylic acid moieties of acetate. Measured with inversion recovery at 9.4 T and 37 °C.*

| Compound | $T_1$ [s] (9.4 T, 37 °C) |
|---|---|
| [1-$^{13}$C] acetate | 26.3 ± 0.5 |
| [1,2-$^{13}C_2$] acetate | 25.4 ± 0.6 |

### 1.4 COMPARISON TO HIGH FIELD NMR 600 MHZ SPECTROMETER

Two samples of MCF7 cells were incubated with [U-$^{13}$C,D] glucose for 30 min and the metabolites extracted as described in the experimental section. One sample was hyperpolarized according to the protocol and one sample was diluted in 500 µl phosphate buffer (40 mM, pH 7.3), 75 µl $D_2O$ and 15 µl omniscan. Omniscan was added to allow fast pulsing with only 1.5 s between each scan. The spectrum was acquired for 13 h on Bruker 600 MHz DRX spectrometer equipped with a TXI SmartProbe.

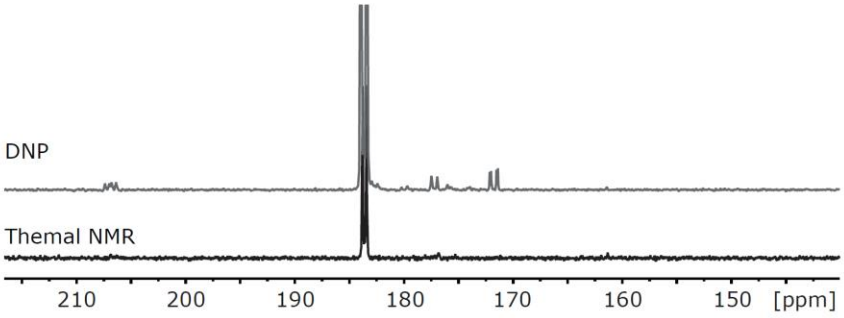


*Figure S1. Comparison between qd DNP and 1D $^{13}C$ NMR spectrum on a 600 MHz instrument using 13h acquisition time.*

### 1.5 LACTATE PRODUCTION AS FUNCTION OF TRACER INCUBATION TIME

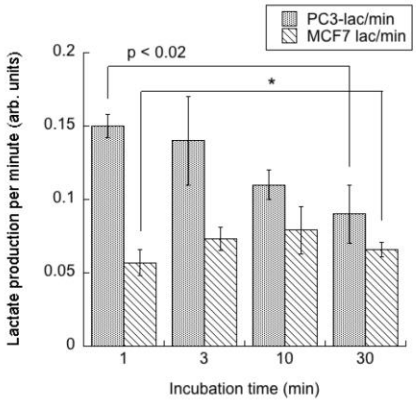


*Figure S2. Lactate production per minute at four different incubation times (1,3,10 and 30 minutes) for two different cell types, breast cancer cells (MCF7) and prostate cancer cells (PC3) (n=3).*
** indicates that the production change is insignificant for MCF7 between incubation times 1 min and 30 min. In contrast PC3 cells produce significantly less lactate per minute at 30 min. incubation compared to 1 min incubation time ($p < 0.02$).*

### 1.6 METABOLITE ASSIGNMENTS

*Table. S6. Metabolite assignments based on chemical shifts.*

| Compound | Chemical shift (ppm) relative to HP001 at 23.7 ppm |
|---|---|
| Lactate | C1:183.2; C2:68.7; C3:20.6 |
| Alanine | C1:176.7; C2:51.8; C3:17.2 |
| Pyruvate | C1:171.2; C2:206.3; C3:27.4 |
| DHAP | C2:212.6 |
| DHA | C2:210.3 |
| PEP | C1:172.5; C2:150.8; C3:100.7 |
| 3-PG | C1:179.4 |

*Metabolite assignment based on additional pH shift.*

The signal at 179.4 ppm in Table S4 is assigned to C1 in 3-phosphoglycerate (3PG). This assignment cannot be done based on the chemical shift at pH 7.4 alone due to close proximity with the metabolite 6-phosphogluconate (C1). The assignment can be done utilizing the difference in pH dependency of the chemical shift in the two compounds (Figure S3). Samples were prepared as described in materials for cell extracts and unlabeled compounds. The samples were dissolved in either phosphate buffer pH=7.3 (40 mM) or acetate buffer pH = 5.0 (40 mM) which reach final pH = 5.3.

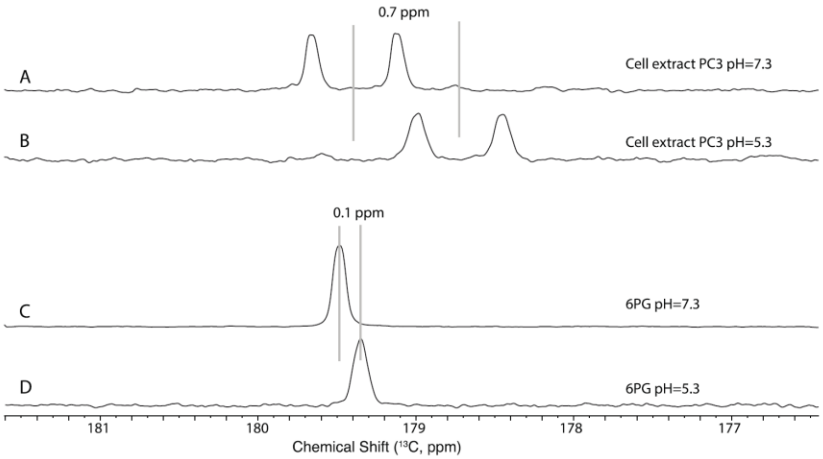


*Figure S3. $^{13}C$ spectra of hyperpolarized cell extracts at pH 7.3 and 5.3 (A,B). In comparison $^{13}C$ spectra of 6PG hyperpolarized under the same conditions as the cell extracts (C,D). Grey bars indicate chemical shift difference between peaks.*

The chemical shift dependency of the metabolite signal at 179.4 ppm from hyperpolarized samples is larger than observed from 6PG under the same condition. The reported chemical shift dependency of the NMR signal from 3PG and 6PG[1] is confirmed (Figure S4) and allows unambiguous assignment of the peak at 179.4 ppm to 3PG.

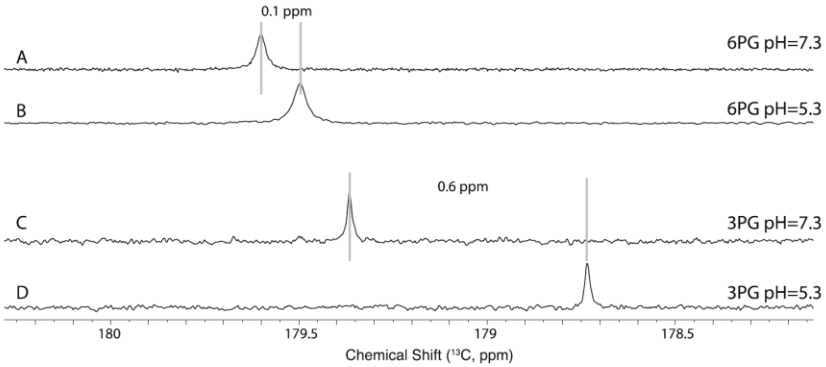


*Figure S4 Thermal $^{13}C$ spectra of 6PG and 3PG obtained at pH 7.3 and 5.3 ppm. Grey bars indicate chemical shift difference between peaks.*

[1] Jensen, P.R. and Meier, S. Chem. Comm. 2016, 52; 2288-2291.

# Paper II

Pancreatic β-cells respond with early metabolic switch to fuel pressure

**Malinowski, R.M**.; Ghiasi, S.M.; Mandrup-Poulsen, T.; Lerche M.H.; Ardenkjær-Larsen, J.H.; Jensen, P.R.

Submitted to Journal of Biological Chemistry, JBC

Pancreatic β-cells respond with early metabolic switch to fuel pressure

**Ronja M. Malinowski[1], Seyed M. Ghiasi[2], Thomas Mandrup-Poulsen[2], Mathilde H. Lerche[1], Jan H. Ardenkjær-Larsen[1], Pernille R. Jensen[1*]**

[1]Dept. of Electrical Engineering, Technical University of Denmark, Kgs. Lyngby, Dennmark
[2]Dept. of Biomedical Sciences, University of Copenhagen, Copenhagen, Denmark

Running title: *Metabolic switch in INS-1 cells*

* To whom correspondence should be addressed: Pernille R. Jensen, Department of Electrical Engineering, Technical University of Denmark, Oersteds Pl. Bldg. 349, Room 120, 2800 Kgs. Lyngby. Telephone: (+45)45253688; E-mail: peroje@elektro.dtu.dk

**Keywords:** INS-1 cells, metabolomics, excess-fuel handling, DNP, $^{13}$C NMR.

**ABSTRACT(250 words)**

Pancreatic β-cells become irreversible damaged by long-term exposure to excessive glucose concentration and lose their ability to produce glucose stimulated insulin secretion (GSIS). The β-cells are not able to control glucose uptake and they are therefore left vulnerable for endogenous toxicity from metabolites produced in excess amount as function of increased glucose availability. The β-cells possess metabolic pathways designed to handle excess fuel but little is known about these. We present a study of β-cell metabolism under increased fuel pressure using a stable isotope resolved metabolomics approach to investigate early metabolic events that lead up to β-cell dysfunction. The method is based on a recently described combination of $^{13}$C metabolomics combined with signal enhanced NMR via dissolution dynamic nuclear polarization(dDNP). We find a switch in the central carbon metabolism even after short exposure times. When the cells are exposed to normal glucose concentrations a divergence pathway is active directing metabolites produced in the upper part of glycolysis away from the end product, pyruvate. For higher glucose concentrations, the ability to diverge the metabolism is diminished and eventually lost. This metabolic switch is taking place before GSIS is affected.

## INTRODUCTION

It is well understood that glucotoxicity is a pathogenic factor leading to pancreatic β-cell failure in type 2 diabetes [1] [2]. Glucotoxicity can be defined as irreversible cell damage caused by chronic exposure to supraphysiological glucose concentrations [3]. The metabolism of β-cells is particular compared to other cell types. They are designed to sense blood glucose in a narrow concentration range and respond with insulin secretion. Hence, the β-cell cannot shield itself from toxicity by blocking glucose uptake and therefore rely on other metabolic protection mechanisms to avoid toxicity [4]. There are thus two different metabolic functions at play when the β-cells are exposed to excessive glucose concentration: 1) Metabolism of glucose and other nutrients that triggers insulin secretion. Multiple mechanisms are taking place via different metabolic products from glucose metabolism that

generates the so-called metabolic coupling factors (MCF), a topic which is still not fully understood [5]. 2) Initial handling of excessive fuel to avoid toxicity. It has been suggested, that under excessive fuel exposure, glucose carbons are diverted into glycerol release and lipid synthesis as a protection mechanism to fuel surfeit [6]. These two aspects of glucose metabolism in β-cells function in an interplay that are yet to be fully understood.

Metabolomics offer a systems level view of cell metabolism and is well suited for unbiased investigations of cell metabolism. The method has been used in a number of studies investigating β-cell metabolism comprising both mass spectrometry and nuclear magnetic resonance as detection modalities [7]. Stable Isotope Resolved Metabolomics (SIRM) is an approach that measures isotope-filtered selection of molecules for elucidation of the dynamics and compartmentation of metabolic pathways and networks [8]. [U-$^{13}$C,D]glucose can for instance be used as a metabolic tracer to probe the glycolysis where $NAD^+$-dependent oxidation of glucose to pyruvate is taking place. The metabolic transformations of the tracer lead to distinct labeling patterns in metabolic intermediates. In this way, metabolic fluxes can be measured from temporal profiles of metabolite concentration changes. In conjunction with the use of stable isotope tracers, $^{13}$C-NMR is a method of choice for exploring metabolic reprogramming in major metabolic diseases such as cancer and diabetes [9] [10]. $^{13}$C-NMR has a number of unparalleled advantages for metabolic studies; it is quantitative, versatile and specific. The relative insensitivity of the method can be compensated when combined with hyperpolarization in the form of dissolution dynamic nuclear polarization [11]. Such a combined method of hyperpolarized $^{13}$C-NMR for analysis of SIRM has recently been published [12].

In this study, we use the hyperpolarized $^{13}$C NMR method to gain information on how the β-cells handle increased fuel pressure before reaching glucotoxicity. Our data show that a division of carbon flow from the glycolysis is used as an initial protection strategy. Under increasing fuel pressure, this metabolic ability of the β-cell is lost.

**RESULTS**

*Hyperpolarized SIRM of β-cells–* To select conditions where β-cells are challenged by high fuel pressure before functional impairment, exposure time and concentration of glucose need to be defined. A literature survey was used to classify the functional state of β-cells based on their insulin release response to various levels of glucose load (time and concentration), Figure 1. Basal glucose concentrations are within the range of 3-5 mM corresponding to normal blood glucose concentration. Up to glucose concentration of 11.7 mM insulin secretion is increased compared to the basal level at long exposure time. Conditions where insulin releases are reduced compared to the basal level are termed glucotoxic. Whereas the literature is sparse when it comes to higher concentrations and short exposure times, it is clear that it is possible to provoke the cells into a glucotoxic state with 17 mM glucose at long exposure times (24 h or longer). Accordingly 11.7 mM and 17 mM glucose were chosen to represent "normal" and "high" glucose loading. With the time frame of 2-8 h these conditions do not reach a glucotoxic state and are therefore considered early events (Fig. 1).

The metabolic fingerprint of β-cells INS1 was obtained using hyperpolarized SIRM [12]. The protocol involved incubation of live cells in solution with [U-$^{13}$C,D]glucose, quenching and extraction of intra- and extracellular soluble metabolites and quantification of the extracted metabolites relative to an internal standard. An

example of the carbonyl region from a 1D $^{13}C$ spectrum from β-cells under "normal" conditions (4 h with 11.7 mM glucose) is shown in Figure 2. The insert shows the full spectrum with the signals from the uniformly labelled substrate, glycerol added to ease the hyperpolarization process and a signal from the reference used for quantification. The carbonyl carbons of four metabolites could be identified as: 2-$^{13}C$-pyruvate, 205.8 ppm; 1-$^{13}C$-lactate, 183.4 ppm; 5-$^{13}C$-glutamate, 182.2 ppm; 1-$^{13}C$-alanine, 176.8 ppm; 1-$^{13}C$-glutamate, 175.6 ppm and 1-$^{13}C$-pyruvate, 171.2 ppm. The identification was based on the carbonyls distinct chemical shifts (referenced to the internal standard) and the coupling constants originating from the $^{13}C$-$^{13}C$ couplings since all metabolites are derived from uniformly $^{13}C$ labelled glucose.

*Effect of glucose concentration on metabolic fingerprint of β-cells*- To investigate the short term metabolic events under varying concentrations of glucose, INS1 β-cells were incubated for 4 h with "basal" 3 mM, "normal" 11.7 mM and "high" 17 mM levels of [U-$^{13}C$,D]glucose. It is clear from a mere comparison of the 1D $^{13}C$ NMR spectra that the metabolic fingerprint of β-cells respond to changes in glucose availability and all measured metabolites increase with increased glucose availability (Fig. 3A).

The accumulated insulin release and insulin content at the three glucose concentrations were measured from supernatants and cell pellets, respectively (Fig. 3B). Insulin release was increased when glucose availability is changed from 3 to 11.7 mM ($p=0.13$) confirming that the β-cells at 11.7 mM glucose levels are responding as expected (Fig. 3B). No difference in insulin release was measured between 11.7 and 17 mM ($p=0.6$). An inverse relation was measured for insulin content ($p=0.3$ for 3 mM vs 17 mM).

A dose response curve showing the sum of all metabolites was constructed for a range of concentrations between 3 and 35 mM glucose with incubation time of 4 h (Figure 4A). An increase relationship was seen in the sum of $^{13}C$-metabolic products, with an initial linear slope up to 17 mM glucose. This increased metabolite production was directly reflected in an increased glucose consumption (Fig. 4B). At "very high" glucose concentration (35 mM) the β-cell metabolism saturated for both metabolic products and glucose consumption. The individual metabolites followed the same trend except lactate, which was saturated at 7 mM and pyruvate, which increased (Fig. S1).

In summary these data show that β-cells respond normally when it comes to insulin excretion at all tested glucose concentrations (3-35 mM). Correspondingly, the β-cells produce energy metabolites directly proportional to an increasing glucose up take until the 35 mM challenge where both metabolite production and glucose uptake is saturated.

*Effect of exposure time on metabolic fingerprint of β-cells* -Fuel pressure is the product of glucose concentration and exposure time. It was further investigated how the metabolic output changed with incubation time 2-8 h, for the two glucose concentrations, 11.7 mM and 17 mM (Fig. 5A). Lactate was accumulating over time for both glucose concentrations and it showed a significantly larger production at 17 mM compared to 11.7 mM after 8 h ($p < 0.05$). Changes in glutamate and alanine with incubation time were not significant ($p > 0.05$) for 11.7 mM, whereas both glutamate ($p = 0.01$) and alanine ($p = 0.002$) levels increased significantly over time when β-cells were exposed to 17 mM glucose. An unexpected metabolic response was observed when the amount of produced pyruvate was quantified over time. Initially, pyruvate concentration increased to 106±18 nmol (11.7 mM) and 183±55 nmol (17 mM) at 2 h incubation time. Hereafter, however, this metabolite was depleted over time to

reach 7±4 nmol (11.7 mM) and 75±70 nmol (17 mM) at 8 h incubation time. During the whole experiment period glucose consumption rate was linear (0.52 mM/h for 11.7 mM and 0.68 mM/h for 17 mM) (Fig. S2). Accumulated insulin release and insulin content were measured for the same time points and there were no measured change over the 8 h period for any of the concentrations (Fig. 5B; supernatant p=0.6 for 11.7 mM, p=0.9 for 17 mM 8 h vs 0 h; content p=0.9 for 11.7 mM, p=0.6 for 17 mM 8 h vs 0 h).

The sum of pyruvate and lactate accumulation over the time period 2-8 h did not change significantly with exposure to any of the glucose concentrations (158±21 nmol for 11.7 mM and 285±63 nmol for 17 mM, p>0.05 for 2 vs 8 h incubation) indicating that a pseudo-steady state for the $^{13}$C-metabolites are established within 2 h and sustained up until 8 h (Fig. 6A and 6B). The individual amounts of pyruvate and lactate on the other hand changed over the time course. Lactate was produced with a constant rate of 0.31 nmol/min for 11.7 mM and 0.55 nmol/min for 17 mM. Pyruvate on the other hand was generated as the most abundant metabolite in the first 2 h after which it decreased with the rate of 0.26 nmol/min for 11.7 mM and 0.33 nmol/min for 17 mM. The stable sum of $^{13}$C metabolites suggests that no metabolic bottlenecks appear in the glycolysis upstream pyruvate and that metabolic pathways in the crossroad between glycolysis and energy metabolism do not change within the studied 8 h. To investigate whether it was possible to perturb this pseudo-steady state the β-cells were challenged with a "very high" glucose concentration (35 mM) over the time frame 2-8 h (Fig. 6C). At this glucose concentration, the metabolic sum of lactate and pyruvate was no longer constant with time but increased significantly over the time course with a lactate production of 0.98 nmol/min and a pyruvate production of 1.85 nmol/min.

No significant change was measured in glucose stimulated insulin secretion (GSIS) neither as function of time (2-8 h) or concentration (11.7-35 mM) (Fig. 6D-F; p=0.8 for 11.7 mM, p=0.5 for 17 mM and p=0.4 for 35 mM ΔGSIS 2 h vs 8 h). The β-cells are under increased fuel pressure under these conditions but not glucotoxic since the GSIS is not decreased. Also no change in cell viability was detected throughout the time course (Tab. S1).

Taken together the data indicate that the β-cells cannot control intake of glucose. However, they can accumulate pyruvate until a certain threshold after which the cells start to respond with change in metabolism to reduce the pyruvate pool and in this way adjust the glycolysis flux. This ability is lost at very high glucose concentrations. These metabolic changes are at all challenge conditions observed in normal functioning β-cells judged by their ability to excrete insulin.

*β-cells use metabolic switch under high fuel pressure –*

$^{13}$C flux analysis of glucose metabolism in β-cells was based on a constant lactate production and pyruvate metabolism in the investigated concentration and time frame (Fig. 6A-C). The corresponding glucose consumption was also constant (Fig. S2). After 2 h incubation a transient accumulation of pyruvate occurs. Increased amount of pyruvate is observed as function of glucose concentration (106 nmol to 233 nmol) whereas the lactate production is relatively constant (42 nmol to 55 nmol) (Fig. 7). At prolonged exposure times the rate of pyruvate production increases as a function of glucose concentration from -0.3 nmol/min to 1.85 nmol/min for 11.7 and 17 mM compared to 35 mM glucose concentration. This implies that β-cells under glucose concentrations up to 17 mM over time metabolically diverge the initially produced pyruvate to e,g. release the pressure on the TCA cycle from metabolites generated by the steady

uncontrolled glucose uptake. This ability of the β-cell is unchanged at normal and high glucose concentrations but at very high glucose concentration (35 mM) this ability to diverge pyruvate is not used. A relative quantification of this metabolic divergence scaled to the condition at 2 h is illustrated by an arrow X in Fig. 7. This metabolic switch occurs even though the β-cells are not glucotoxic since GSIS was not decreased (Fig. 6D-F) and no change in cell viability could be observed (Tab. S1).

**DISCUSSION**

We have studied the energy metabolism of β-cells exposed to glucose concentrations ranging from 3-35 mM over the time course of 2-8 h with the aim of investigating early metabolic events of excess fuel handling and observed a significant pyruvate accumulation over a large span of glucose concentrations from 3 to 35 mM. The pyruvate pool increased 5.7 fold when comparing 11.7 mM with 35 mM glucose (at 4 h exposure time). And even more pronounced at longer exposure times (>100 fold). An increase in the pyruvate pool has previously been seen when β-cells have been exposed to increased glucose concentration from 2.8 mM to 16.7 mM at short exposure times 1 h [4] and at long exposure times (48 h) [1]. But the switch in $^{13}C$ flux as revealed by the changed pyruvate metabolism observed over time is to our knowledge not observed before.

Pyruvate is not considered a direct metabolic coupling factor (MCF) for insulin response since it cannot increase GSIS [13]. Indirectly pyruvate cycling generates NADPH, which is considered a MCF since is correlates with GSIS [14] [15]. In a screen for metabolic pathways that are important for excess fuel handling Mugabo et al. searched for metabolites that did not correlate with insulin secretion but continued to increase above concentrations of 17 mM glucose [4]. They found that glycerol production and lipid synthesis fulfilled this criterion. In our study pyruvate as the only metabolite increase after 17 mM glucose and therefore potentially qualify as an important biomarker for excess fuel handling. Three main pathways are active for pyruvate metabolism in β-cells; glucose oxidation via TCA, anaplerosis via pyruvate cycling and glycerolipid/fatty acid cycling [6]. We do not observe change in TCA cycle activity measured by the constant glutamate production; pyruvate cycling is coupled to NADPH and through this to GSIS. Since we do not observe any change in GSIS this pathway is also assumed constant. We therefore suggest the glycerolipid/fatty acid cycling as the pathway coupled to the observed change in pyruvate metabolism. In normal functioning β-cells NADH formed from glycolysis will not be lost in the reduction of pyruvate to lactate but rather transferred to the mitochondria as a substrate of the respiratory chain [16]. This assures a tight coupling between glycolysis and mitochondrial metabolism essential for glucose sensing. Under glucose load up to 17 mM (Fig. 7) our data show a constant glucose consumption and initial accumulation of pyruvate, which would lead to an accumulation of NADH. This excess of NADH is not reduced by LDH shown by a constant rate of lactate production. Also the TCA cycle activity is unchanged over time as observed by an unchanged glutamate formation. Therefore another NADH dependent reaction is likely to take place in the β-cell. This diverging pathway is here reflected in the observed decreased pyruvate production rate. In β-cells an active NADH shuttle system via the glucolytic enzyme 3-phosphate dehydrogenase (GAPDH) participates in the coupling between the glycolysis and mitochondria by transferring NADH [17]. DHAP is coupled to the cytosolic glycerolipid/fatty acid cycle using NADH as co-substrate. An up-regulation of this pathway can explain the observed decrease in pyruvate

production rate since the glycolysis flux to pyruvate is then diverged upstream at the point of 3PG and thereby reducing NADH formation (Fig. S4).

The chosen glucose load in this study never results in glucotoxicity since no decreased insulin response is observed. The studied metabolic changes are thus prior to failure of the β-cell. Most reported studies focus on one time point and several glucose concentrations. However, when the metabolism as done here is studied over time it is evident that an initially accumulated pyruvate pool will diminish as a diverging metabolic pathway is up regulated on the hour time scale. As the glucose concentration is further increased the ability of the β-cell to diverge pyruvate is eventually lost. This points to a switch in β-cell metabolism when exposed to excess fuels. We suggest that under excess fuel conditions the β-cell first protects itself by modulating the pyruvate pool while up-regulating divergence pathways. Importantly this initial regulation takes place before mitochondrial processes affect insulin secretion.

Our study is performed with SIRM combined with hyperpolarized $^{13}C$ NMR. The method showed high sensitivity, high specificity and permitted absolute quantification of energy metabolites. An increased sensitivity obtained by hyperpolarized $^{13}C$-NMR made direct detection of $^{13}C$-isotope enriched metabolites possible for time resolved β-cell metabolism. The employed $^{13}C$-isotopically enriched glucose allowed an unambiguous identification of the glycolytic end-product, pyruvate, and evidence for lactate dehydrogenase and transaminase activity by identification of lactate and alanine and also mitochondrial activity confirmed by the presence of glutamate. Absolute quantification of the identified metabolites led to a proposed model for how the β-cell metabolically can control effects of being challenged by a high glucose load. Importantly the model also indicated that this metabolic strategy of the β-cell is lost before the cells enter a glucotoxic state and that this lost functionality can be measured by the build-up of an unsustainable high pyruvate pool.

In conclusion this study shows that the β-cells use different metabolic pathways to reduce excess metabolites formed from uncontrolled glycolysis. Glycerol and fatty acid metabolism is the most lileky candidate for this deviation pathway. Further studies are needed to elucidate this fundamentally important and relatively overlooked defense mechanism for protecting the β-cell against glucotoxicity.

## EXPERIMENTAL PROCEDURES

*Cell Culture* INS-1 cells [obtained from Prof. Claes B. Wollheim] were cultured in Gibco RPMI 1640 Medium, GlutaMAX Suplement (Thermo Fisher Scientific) with 10% Fetal Bovine Serum (FBS) (Sigma-Aldrich), 1% Penicillin-Streptomycin (Sigma-Aldrich) and 500 µL of 50 mM 2-Mercaptoethanol (Thermo Fisher Scientific). This culture medium contains 11 mM glucose. The culture was maintained at 37 ºC under humidified (5% $CO_2$, 95% air) conditions. Cell number and viability were measured by an automatic cell counter (EVE, NanoEntek). Cells were subcultured in 175 $cm^2$ flasks at a density of 10 x $10^6$ cells.

*Glucose Utilization.* Glucose utilization was measured by Glucose (GO) Assay Kit (Sigma Aldrich), standard curve based on [U-$^{13}C$,D]glucose. Absorbance was measured at wavelength 540 nm on a BioTek EPOCH 2 microplate reader (Holm & Halby, Brøndby, Denmark).

*Glucose-Stimulated Insulin Secretion (GSIS).* Cells were seeded in a 24-well plate (0.3 x $10^6$) 48 h prior to the experiment. Initially, the cells were

pre-incubated at various concentrations (7 – 35 mM Glucose in 40 mM phosphate buffer) for 2 – 8 h. The media were discarded, and the cells were incubated with 2 mM Glc in Krebs Ringer Hepes Buffer (KRHB) for 1 h. After this, GSIS was performed (1 h 2 mM Glc, then 1 h 16.7 mM Glc in KRHB), all supernatants were collected for ELISA, and the cells were finally lysed with NP-40 buffer (Life Technologies) for insulin content measurements.

*Insulin ELISA.* Supernatants (1:1000 dilution for accumulated insulin release and 1:100 for GSIS experiments) and cell lysate (1:2000 dilution) were used for measurement of accumulated insulin and insulin content respectively using competitive insulin ELISA assay [18] in duplicates with the modification that an enzyme substrate 1-step Ultra TMB (3,3', 5,5;-tetramethylbenzidine) (Life Technologies) was used here.

*Metabolism experiments.* Cells were trypsinized and counted. Ten x $10^6$ cells were placed in 167 µL phosphate-buffer (40 mM, pH 7.4) in an Eppendorf tube. Phosphate-buffer containing the isotope labelled substrate [U-$^{13}$C,D] glucose (Sigma Aldrich) was added (333 µL) and the Eppendorf tube was placed on a thermomixer (Hettich Benelux) at 37 °C, 500 rpm, for the period of time indicated. The reaction was stopped by addition of 200 µL 2.2 M of ice-cold perchloric acid (for hyperpolarization experiments) or by immersing the tube in liquid nitrogen (for glucose utilization). The extracts for hyperpolarization were processed as described in [12] and freeze-dried.

*Hyperpolarization and NMR acquisition* The freeze-dried extract was dissolved in 50 µL ultra-pure water, mixed with 92.5 mg polarizing medium (967 mg glycerol, 38 mg OX063, 4.18 mg Omniscan) and 5 µL 50 mM [1-$^{13}$C] HP001 (1.1-bis (hydroxymethyl) cyclopropane) was used as internal reference. The sample was polarized for 1.5 h on HyperSense (Oxford Instruments), after which it was dissolved in 5 mL phosphate buffer (40 mM, EDTA 100 mg/L) brought to a temperature of 175 ºC. The dissolved sample was quickly transferred to a 400 MHz NMR (Agilent Technologies, USA). Acquisition started 10 s post dissolution using a 90º flip angle and no $^1$H decoupling.

*Data analysis.* NMR data were analysed using TopSpin 3.2 and presented as means ± SD. Insulin data are presented as means ± SEM. For all data types comparisons between different groups were carried out by ANOVA analysis, followed by Student's paired *t* test using the GraphPad Prism version 6 (La Jolla, USA). Bonferroni-corrected *P-values* $\leq$ 0.05 were considered as significant.

**ACKNOWLEDGEMENTS**

The authors gratefully acknowledge funding by Danish National Research Foundation (grant DNFR124). Innovation Fund Denmark (grant 1308-00028B) and Christian Kjeldsen for support of NMR data acquisition at the DTU NMR center. SMG was supported by grants from the Danish Diabetes Academy, Zealand Pharma, and the Dept. of Biomedical Sciences, University of Copenhagen.

**CONFLICT OF INTEREST**

The authors declare that they have no conflict of interest with the contents of this article.

**Bibliography**

[1] I. Göhring, V. V. Sharoyko, S. Malmgren, L. E. Andersson, P. Spégel, D. G. Nicholls and H. Mulder, "Chronic High Glucose and Pyruvate Levels Differentially Affect Mitochondrial Bioenergetics and Fuel-stimulated Insulin Secretion from Clonal INS-1 832/13 Cells," *J. Biol. Chem.,* vol. 289, no. 6, pp. 3786-3798, 2014.

[2] V. Poitout and R. Robertson, "Glucolipotoxicity: Fuel Excess and b-Cell Dysfunction," *Endocr. Rev.,* vol. 29, no. 3, pp. 351-366, 2008.

[3] R. P. Robertson, J. Harmon, P. O. Tran, Y. Tanaka and H. Takahashi, "Glucose Toxicity in beta-Cells: Type 2 Diabetes, Good Radicals Gone Bad, and the Glutathione Connection," *Diabetes,* vol. 52, no. 3, pp. 581-587, 2003.

[4] Y. Mugabo, S. Zhao, J. Lamontagne, A. Al-Mass, M.-L. Peyot, B. E. Corkey, E. Joly, S. Murthy Madiraju and M. Prentki, "Metabolic fate of glucose and candidate signaling and excess-fuel detoxification pathways in pancreatic beta-cells," *J. Biol. Chem.,* vol. 292, no. 18, pp. 7407-7422, 2017.

[5] M. V. Jensen, J. W. Joseph, S. M. Ronnebaum, S. C. Burgess, A. D. Sherry and C. B. Newgard, "Metabolic cycling in control of glucose-stimulated insulin secretion," *Am. J. Physiol. Endocrinol. Metab.,* vol. 295, no. 6, p. E1287–E1297, 2008.

[6] C. Nolan and M. Prentki, "The islet b-cell: fuel responsive and vulnerable," *Trends. Endocrinol. Metab.,* vol. 19, no. 8, pp. 285-291, 2008.

[7] J. R. Gooding, M. J. Jensen and C. B. Newgard, "Metabolomics applied to the pancreatic islet," *Arch. Biochem. Biophys.,* vol. 589, pp. 120-130, 2016.

[8] R. C. Bruntz, A. N. Lane, R. M. Higashi and T. W. Fan, "Exploring cancer metabolism using stable isotope-resolved metabolomics (SIRM)," *J. Biol. Chem.,* vol. 292, no. 28, pp. 11601-11609, 2017.

[9] T. M. Fan, P. K. Lorkiewicz, K. Sellers, H. N. Moseley, R. M. Higashi and A. N. Lane, "Stable isotope-resolved metabolomics and applications for drug development," *Pharmacol. Ther.,* vol. 133, no. 3, pp. 366-391, 2012.

[10] K. M. Sas, A. Karnovsky, G. Michailidis and S. Pennathur, "Metabolomics and Diabetes: Analytical and Computational Approaches," *Diabetes,* vol. 64, no. 3, pp. 718-732, 2015.

[11] J. H. Ardenkjær-Larsen, B. Frindlund, A. Gram, G. Hansson, L. Hansson, M. H. Lerche, R. Servin, M. Thaning and K. Golman, "Increase in signal-to-noise ratio of > 10,000 times in liquid-state NMR," *PNAS,* vol. 100, no. 18, pp. 10158-10163, 2003.

[12] M. H. Lerche, D. Yigit, A. B. Frahm, J. H. Ardenkjær-Larsen, R. M. Malinowski and P. R. Jensen,

"Stable Isotope-Resolved Analysis with Quantitative Dissolution Dynamic Nuclear Polarization," *Anal. Chem.,* vol. 90, no. 1, pp. 674-678, 2018.

[13] J. V. Rocheleau, W. S. Head, W. E. Nicholson, A. C. Powers and D. W. Piston, "Pancreatic Islet Beta-Cells Transiently Metabolize Pyruvate," *J. Biol. Chem.,* vol. 277, no. 34, pp. 30914-30920, 2002.

[14] S. M. Ronnebaum, O. Ilkayeva, S. C. Burgess, J. W. Joseph, D. Lu, R. D. Stevens, T. C. Becker, A. D. Sherry, C. B. Newgard and M. V. Jensen, "A Pyruvate Cycling Pathway Involving Cytosolic NADP-dependent Isocitrate Dehydrogenase Regulates Glucose-stimulated Insulin Secretion," *J. Biol. Chem. ,* vol. 281, no. 41, pp. 30593-30602, 2006.

[15] D. Lu, H. Mulder, P. Zhao, S. C. Burgess, M. V. Jensen, S. Kamzolova, C. B. Newgard and A. D. Sherry, "13C NMR isotopomer analysis reveals a connection between pyruvate cycling and glucose-stimulated insulin secretion (GSIS)," *PNAS,* vol. 99, no. 5, pp. 2708-2713, 2002.

[16] A. Wiederkehr and C. B. Wollheim, "Mitochondrial signals drive insulin secretion in the pancreatic b-cell," *Mol. Cell. Endocrinol.,* vol. 353, no. 1-2, pp. 128-137, 2012.

[17] K. Eto, Y. Tsubamoto, Y. Terauchi, T. Sugiyama, T. Kishimoto, N. Takahashi, N. Yamauchi, N. Kubota, S. Murayama, T. Aizawa, Y. Akanuma, S. Aizawa, H. Kasai, Y. Yazaki and T. Kadowaki, "Role of NADH Shuttle System in Glucose-Induced Activation of Mitochondrial Metabolism and Insulin Secretion," *Science,* vol. 283, no. 5404, pp. 981-985, 1999.

[18] J. Kekow, K. Ulrichs, W. Muller-Ruchholtz and W. Gross, "Measurement of rat insulin. Enzyme-linked immunosorbent assay with increased sensitivity, high accuracy, and greater practicability than established radioimmunoassay," *Diabetes,* vol. 37, no. 3, pp. 321-326, 1988.

[19] C. Fernandez, U. Fransson, E. Hallgard, P. Spégel, C. Holm, M. Krogh, K. Wårell, P. James and H. Mulder, "Metabolomic and Proteomic Analysis of Clonal Insulin-Producing beta-cell Line (INS-1 832/13)," *J. Proteome Res.,* vol. 7, no. 1, pp. 400-411, 2008.

[20] I. Goehring, N. Sauter, G. Catchpole, A. Assmann, L. Shu, K. Zien, M. Moehlig, A. Pfeiffer, J. Oberholzer, L. Willmitzer, J. Spranger and K. Maedler, "Identification of an intracellular metabolic signature impairing beta cell function in the rat beta cell line INS-1E and human islets," *Diabetologia,* vol. 54, no. 10, pp. 2584-2594, 2011.

[21] H. Hohmeier, H. Mulder, G. Chen, R. Henkel-Rieger, M. Prentki and C. Newgard, "Isolation of INS-1–Derived Cell Lines With Robust ATP-Sensitive K+ Channel-Dependent and -Independent Glucose-Stimulated Insulin Secretion," *Diabetes,* vol. 49, no. 3, pp. 424-430, 2000.

[22] K.-G. Park, K.-M. Lee, H.-Y. Seo, J.-H. Suh, H.-S. Kim, L. Wang, K.-C. Won, H.-W. Lee, J.-Y. Park, K.-U. Lee, J.-G. Kim, B.-W. Kim, H.-S. Choi and I.-K. Lee, "Glucotoxicity in the INS-1 Rat Insulinoma Cell Line Is Mediated by the Orphan Nuclear Receptor Small Heterodimer Partner," *Diabetes,* vol. 56, no. 2, pp. 431-437, 2007.

[23] N. E. Simpson, N. Khokhlova, J. A. Oca-Cossio and I. Constantinidis, "Insights into the role of anaplerosis in insulin secretion: a 13C NMR study," *Diabetologia,* vol. 49, no. 6, pp. 1338-1348, 2006.

[24] P. Spégel, S. Malmgren, V. V. Sharoyko, P. Newsholme, T. Koeck and H. Mulder, "Metabolomic analyses reveal profound differences in glycolytic and tricarboxylic acid cycle metabolism in glucose-responsive and -unresponsive clonal β-cell lines," *Biochem. J.,* vol. 435, no. 1, pp. 277-284, 2011.

[25] M. Wallace, H. Whelan and L. Brennan, "Metabolomic analysis of pancreatic beta cells following exposure to high glucose," *Biochim. Biophys. Acta,* vol. 1830, no. 3, pp. 2583-2590, 2013.

FIGURES

**FIG1**

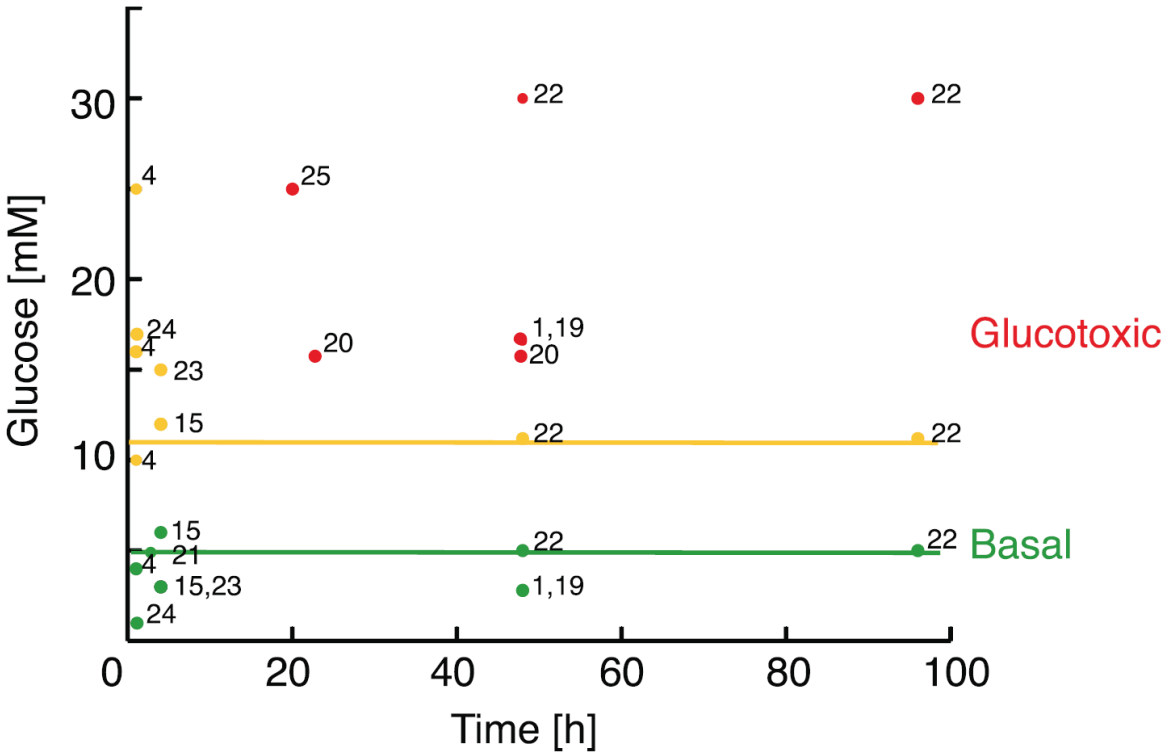


Figure 1. Literature survey of insulin response to glucose loading in β-cells. Green represents basal blood glucose concentration (5 mM); yellow represent glucose conditions where insulin response is increased compared to the basal condition. The yellow line is drawn at 11.1 mM glucose, which is the diagnostic level of diabetes; red represents glucotoxic conditions where insulin secretion is reduced compared to the basal condition. Numbers refers to literature references.

**FIG. 2**

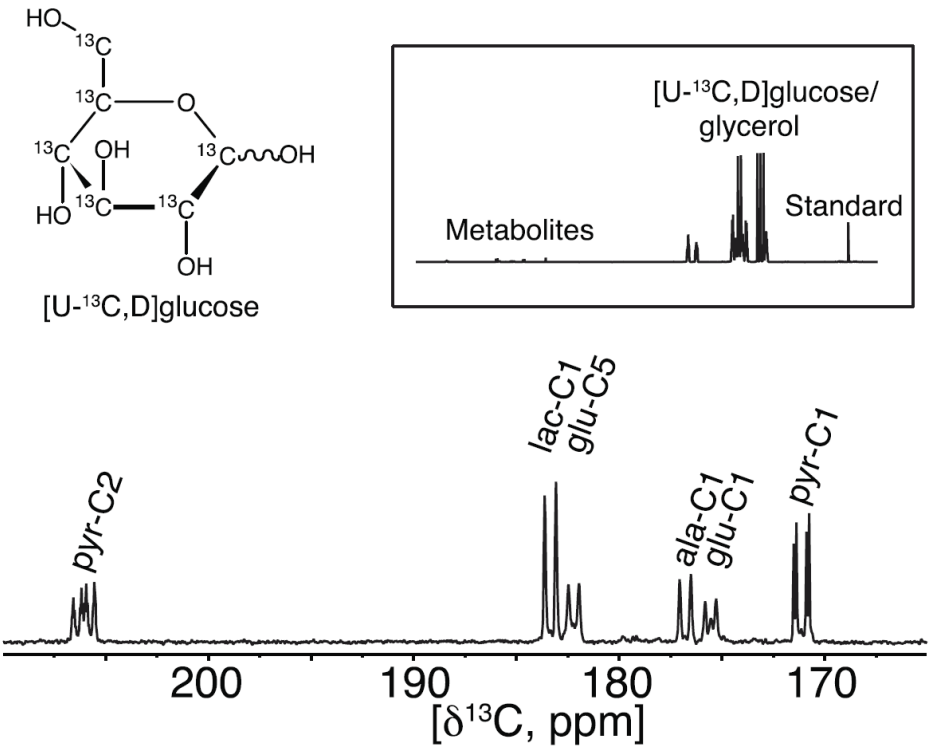


**Figure 2.** ) $^{13}C$ 1D spectrum of hyperpolarized metabolites after 4 h of incubation with 11.7 mM [U-$^{13}C$,D] glucose. The metabolites were polarized for 90 min. after which they were subjected to rapid dissolution in hot phosphate buffer. Four metabolites were observed with distinct carbonyl shifts at: 2-$^{13}C$-pyruvate (205.8 ppm), 1-$^{13}C$-lactate (183.4 ppm), 5-$^{13}C$-glutamate (182.2 ppm), 1-$^{13}C$-alanine (176.8 ppm), 1-$^{13}C$-glutamate (175.6 ppm) and 1-$^{13}C$-pyruvate (171.2 ppm). The full spectrum can be seen on the insert. Other components in the sample are glucose, glycerol to mediate the hyperpolarization and an internal standard for quantification.

**FIG. 3**

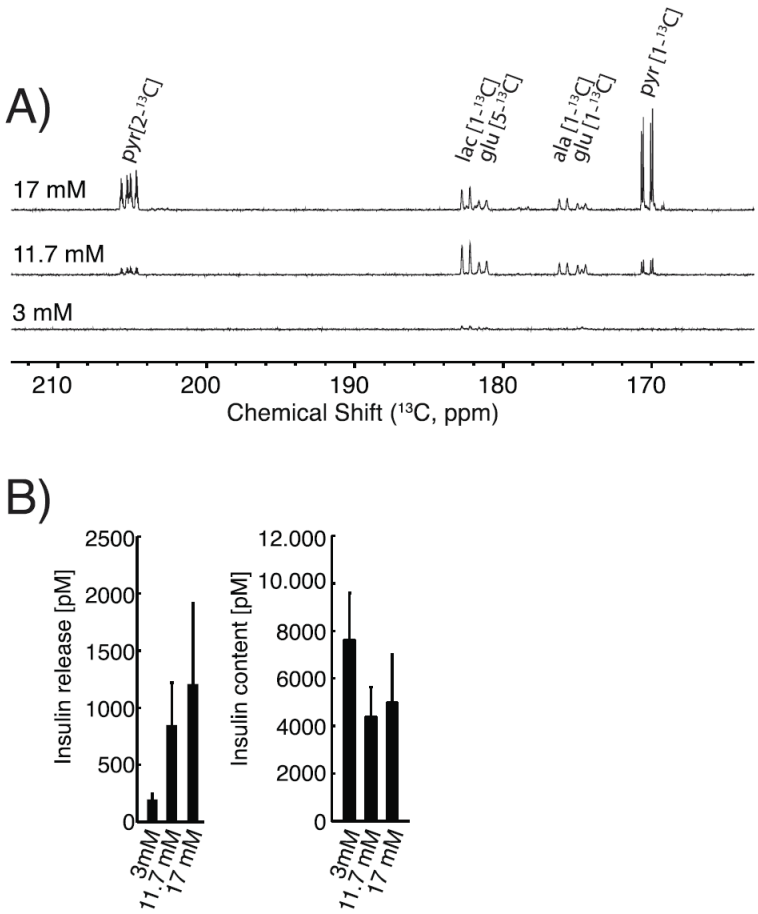


**Figure 3**. A) $^{13}C$ 1D spectrum of hyperpolarized metabolites after 4 h of incubation with 3, 11.7 and 17 mM [U-$^{13}C$,D] glucose. The metabolites were polarized for 90 min after which they were subjected to rapid dissolution in hot phosphate buffer B) Corresponding accumulated insulin ELISA on extract supernatant and cell lysate from 3 – 17 mM glucose, n=4.

## FIG. 4

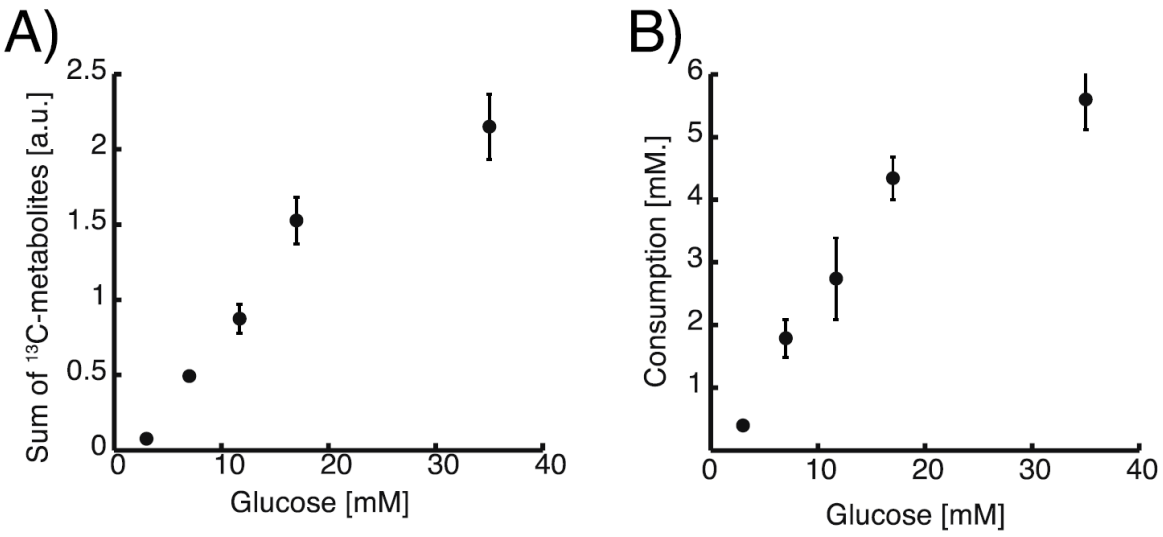


**Figure 4**. A) Sum of measured metabolites relative to an internal standard as function of glucose concentration (3 – 35 mM) after 4 h of incubation, n=4. B) Glucose consumption (mM) as function of glucose concentration after 4 h of incubation measured by a UV-assay, n=4.

# FIG. 5

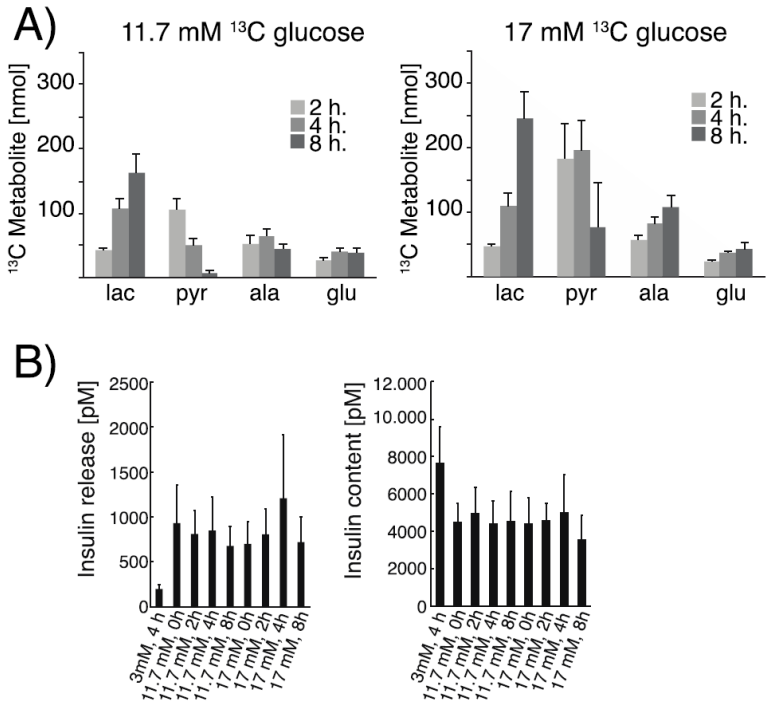


**Figure 5**. A) The observed metabolites quantified with regard to the internal standard. Cells were incubated for 2 – 8 h with respectively 11.7 mM and 17 mM [U-$^{13}$C,D] glucose (n = 4). B) Corresponding accumulated insulin release and content (n = 4).

# FIG. 6

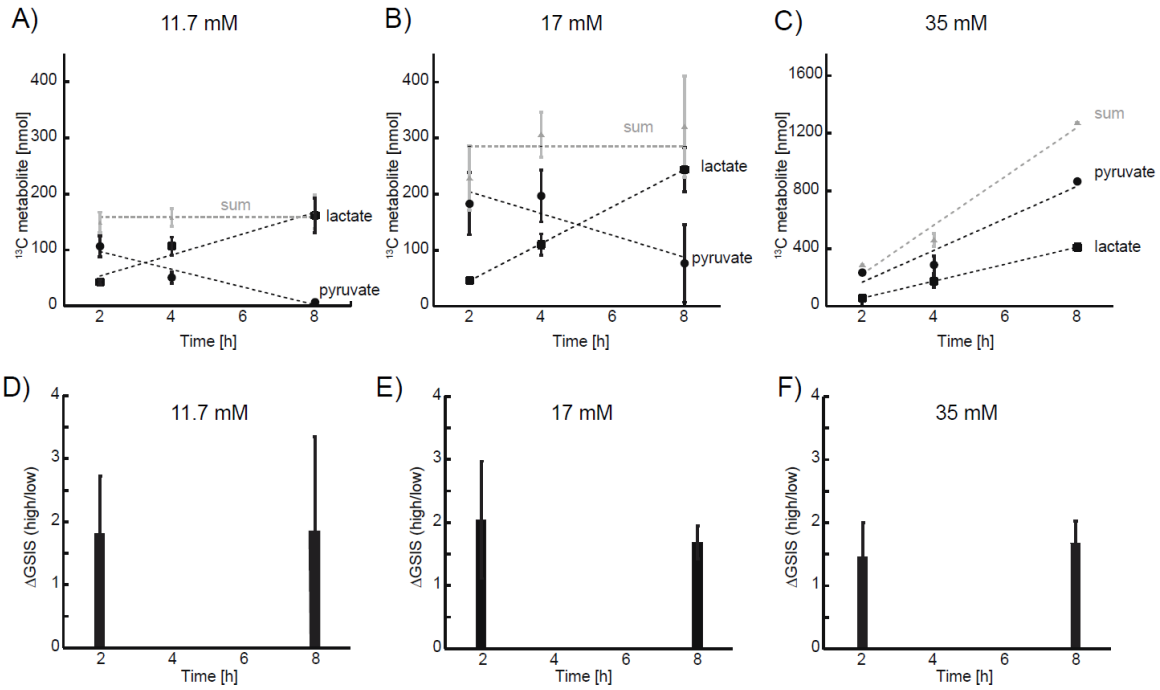


**Figure 6.** A-C) The two main metabolites; lactate and pyruvate together with their sum as function of glucose concentration (11.7, 17 and 35 mM). D-F) The corresponding glucose stimulated insulin secretion (GSIS) as a ratio between high and low glucose stimulation (2 and 17 mM glucose respectively) from GSIS experiment carried out after either 2 or 8 h of incubation with the three glucose concentrations.

# FIG. 7

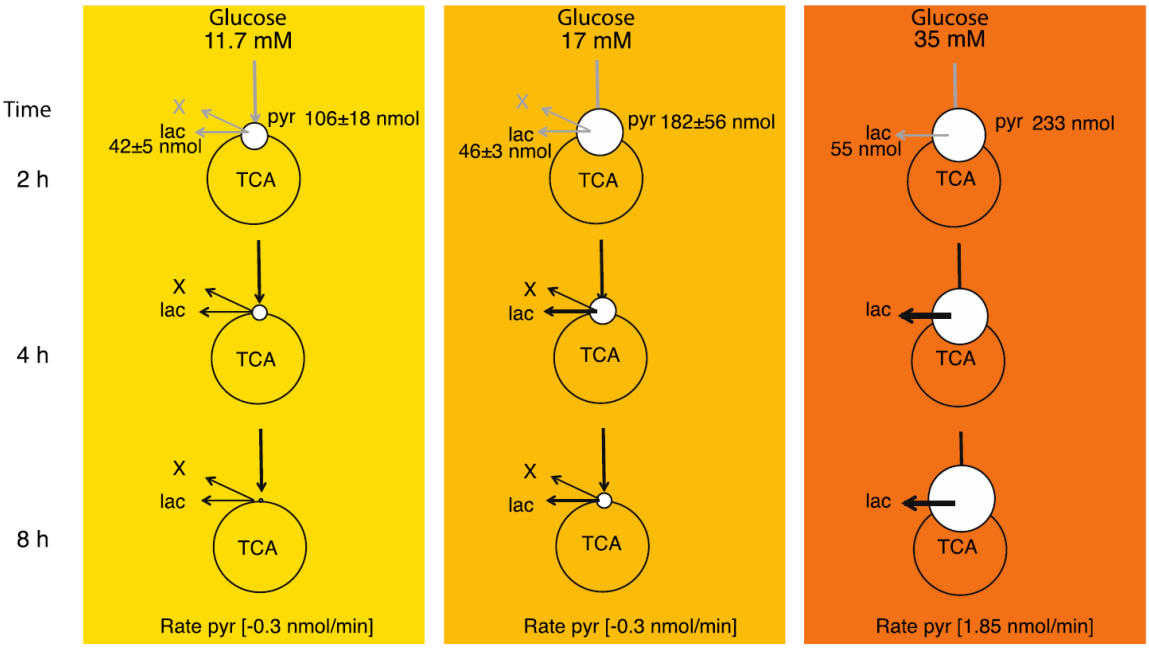


**Figure 7.** Schematic representation of β-cell metabolism under increasing fuel pressure (11.7 to 35 mM glucose) in the time span of 2-8 h. Measured amounts of pyruvate and lactate (nmol) after 2 h incubation are stated for the three glucose concentrations. After 2 h incubation there is: Constant glucose consumption, constant production of glutamate (TCA cycle), constant production of lactate but large plasticity in the pyruvate pool (white circle). To account for the loss in observed pyruvate a divergence pathway away from the central glycolysis must take place. This divergence pathway (X) has the rate corresponding to the determined loss of pyruvate (0.3 nmol/min) for 11.7 and 17 mM glucose. At very high fuel pressure (35 mM) this metabolic pathway is not used anymore and pyruvate accumulates. Grey arrows indicate undetermined rates from 0-2 h. All data are scaled relative to the mildest conditions at 11.7 mM and 2 h for visualization (see Tab. S2 for actual numbers).

SUPPLEMENTARY INFORMATION

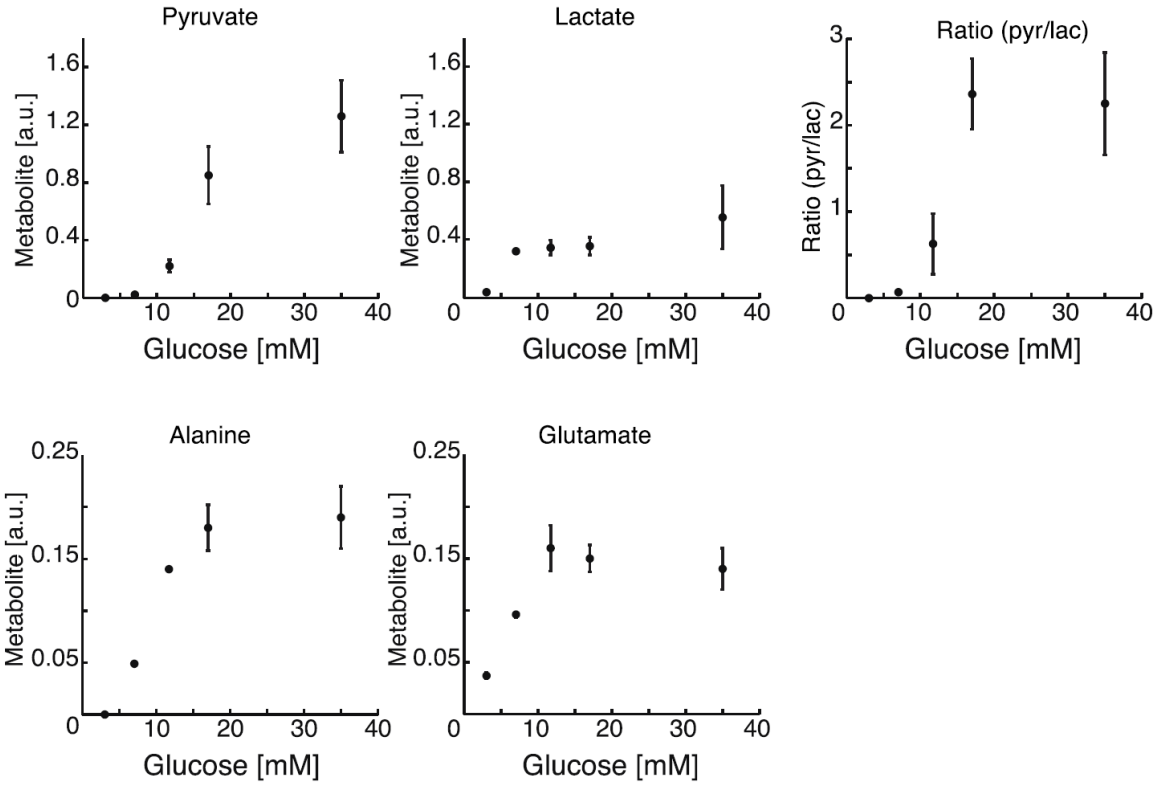


**Figure S1.** Amount of individual metabolites after incubation time of 4 h with glucose concentration from 3-35 mM determined by dDNP-NMR. The amount is given as a ratio to an internal standard, n=4.

Figure S2

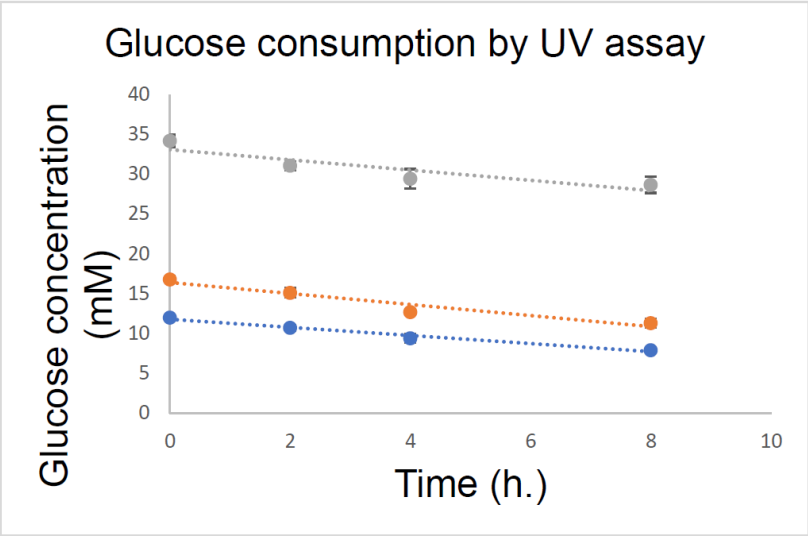


**Figure S2.** Glucose consumption during 8 h. incubation at start glucose concentrations of 11.7, 17 and 35 mM respectively measured by UV-assay, n=4.

Table S1

**Table S1.** Average cell viability during 8 h. of experiment under the three conditions, n=2. The viability was measured by an automatic cell counter (EVE, NanoEntek) as ratio between viable and non-viable cells after trypan blue staining.

| Cell viability | | | |
|---|---|---|---|
| Glucose concentration | 2 hours | 4 hours | 8 hours |
| 11.7 mM | 94 % | 94 % | 90 % |
| 17 mM | 94 % | 94 % | 92 % |
| 35 mM | 93 % | 94 % | 94 % |

Table S2

**Tab. 2S.** Average metabolite amount measured by dDNP NMR. To these data linear fits have been presented in figure 6A-C. The fitted slopes are used for the numbers presented under Calculated. *The slope in the obtained fits for pyruvate at 11.7 and 17 mM glucose are very similar (-0.26 nmol/min and 0.33 nmol/min, respectively) and here the average of these two numbers were used for simplicity.

| | **Measured average [nmol]** | | **Calculated* [nmol]** | |
|---|---|---|---|---|
| | Pyruvate | Lactate | Pyruvate | Lactate |
| 11.7 mM glucose | | | | |
| 2 h | 106 | 43 | | |
| 4 h | 51 | 107 | 70 | 80 |
| 8 h | 7 | 162 | 34 | 117 |
| | | | | |
| 17 mM | | | | |
| 2 h | 183 | 46 | | |
| 4 h | 197 | 110 | 147 | 112 |
| 8 h | 76 | 244 | 111 | 178 |
| | | | | |
| 35 mM | | | | |
| 2 h | 233 | 55 | | |
| 4 h | 287 | 174 | 456 | 172 |
| 8 h | 865 | 409 | 678 | 290 |

Figure S3

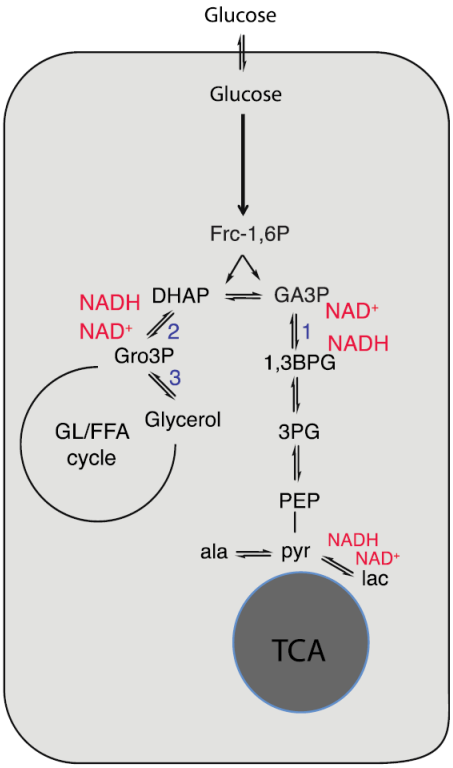


**Fig. S3**. Schematic illustration of β-cell metabolism highlighting the crossroad between glycolysis, lipid synthesis and energy metabolism (TCA). Two enzymes in the upper glycolysis use the cofactors $NAD^+$/NADH; Glyceraldehyde-3phosphate-dehydrogenase (GAPDH),1; Glycerol-3phosphate-dehydrogenase (G3PDH), 2. In addition a newly found enzyme shortcuts the production of glycerol; Glycerol-3phosphate-phosphatase (G3PP), 3. Although this enzyme is not $NAD^+$/NADH dependent it is highlighted due to its importance for insulin secretion and response to metabolic stress[1].

[1] Mugabo et al. Proc Natl Acad Sci U S A. 2016;113(4):E430-9.

# Paper III

Dissolution Dynamic Nuclear Polarization capability study with fluid path

**Malinowski, R.M**.; Lipsø, K.W.; Lerche, M.H.; Ardenkjær-Larsen, J.H.

Published in Journal of Magnetic Resonance, JMR

Journal of Magnetic Resonance 272 (2016) 141–146

Contents lists available at ScienceDirect

Journal of Magnetic Resonance

journal homepage: www.elsevier.com/locate/jmr

# Dissolution Dynamic Nuclear Polarization capability study with fluid path

Ronja M. Malinowski [a], Kasper W. Lipsø [a], Mathilde H. Lerche [a,b], Jan H. Ardenkjær-Larsen [a,c,*]

[a] Department of Electrical Engineering, Technical University of Denmark, Kgs. Lyngby, Denmark
[b] Albeda Research, Ole Maaloes vej 3, 2200 København N, Denmark
[c] GE Healthcare, Denmark

ARTICLE INFO

*Article history:*
Received 11 August 2016
Revised 20 September 2016
Accepted 21 September 2016
Available online 22 September 2016

*Keywords:*
Hyperpolarization
Dynamic Nuclear Polarization
Dissolution-DNP
Polarizer

ABSTRACT

Signal enhancement by hyperpolarization is a way of overcoming the low sensitivity in magnetic resonance; MRI in particular. One of the most well-known methods, dissolution Dynamic Nuclear Polarization, has been used clinically in cancer patients. One way of ensuring a low bioburden of the hyperpolarized product is by use of a closed fluid path that constitutes a barrier to contamination. The fluid path can be filled with the pharmaceuticals, i.e. imaging agent and solvents, in a clean room, and then stored or immediately used at the polarizer. In this study, we present a method of filling the fluid path that allows it to be reused. The filling method has been investigated in terms of reproducibility at two extrema, high dose for patient use and low dose for rodent studies, using [1-13C]pyruvate as example. We demonstrate that the filling method allows high reproducibility of six quality control parameters with standard deviations 3–10 times smaller than the acceptance criteria intervals in clinical studies.



## 1. Introduction

Increase of the NMR signal of molecules by hyperpolarization is a technique, which has many applications in the field of NMR spectroscopy and imaging. The most commonly used method is dissolution-Dynamic Nuclear Polarization (d-DNP) [1], in which the hyperpolarized nuclear spins are transferred from the solid state to the liquid state by a quick dissolution while retaining the nuclear spin polarization.

In this study, the d-DNP technique will be demonstrated by hyperpolarization of pyruvate; being a key intersection in various metabolic pathways, [1-$^{13}$C]pyruvate is by far the most common molecule for studies with d-DNP [2,3]. It has an advantageously long relaxation time $T_1$ and high polarization levels can be achieved [4]. Other molecules can be used to probe biological pathways as well; [U-$^{13}$C;U-$^{2}$H]glucose [5], [1,4-$^{13}C_2$]fumarate [6], [1-$^{13}$C]bicarbonate [7] among many other biologically relevant molecules. Similarly, hyperpolarized $^{13}$C-labelled biologically inert molecules have been applied for angiography and perfusion studies [8,9]. Besides the bioprobe, an electron paramagnetic agent (EPA) should be present to enable Dynamic Nuclear Polarization. The commonly used EPAs for hyperpolarization are OXO63 [10], BDPA [11] and TEMPO [12]. In this study, AH111501 is used, a stable trityl radical, which precipitates in low pH and can be removed by filtration in the receiver previous to the neutralization step. In 2013, the first clinical study with hyperpolarized [1-$^{13}$C] pyruvate was published, demonstrating technical feasibility and showing promising results in the phase I trial on patients with prostate cancer [13].

Studies on the performance of the d-DNP process with the aim of demonstrating efficient dissolution, i.e. high concentration and large volume with minimal loss of polarization have been published [14,15]. The principle of dissolution in these studies is the use of a solvent that is heated to an elevated temperature to create a vapor pressure that can drive the flow of solvent past the cold, polarized sample. In the case of aqueous dissolutions, a temperature of 180 °C is typically used, creating a vapor pressure of 10 bar. Another principle of dissolution was introduced in 2011 [16], where the concept of a closed fluid path (FP) was presented. The primary objective of the closed FP was to secure a sterile environment throughout the polarization and dissolution process [16]. In terms of dissolution capability, two key principal differences between the FP and previous designs should be noted: (1) the solvent is not driven by the vapor pressure at the given temperature, but by a syringe, (2) the independent inlet and outlet tubes are replaced by two concentric tubes with the inlet as the inner lumen and with return flow in the outer lumen. From the first point follows that solvent temperature can be controlled independently

* Corresponding author at: Technical University of Denmark, Ørsteds Plads, Bldg. 349, Room 126, 2800 Kgs. Lyngby, Denmark.
*E-mail address:* jhar@elektro.dtu.dk (J.H. Ardenkjær-Larsen).

http://dx.doi.org/10.1016/j.jmr.2016.09.015
1090-7807/

of solvent flow rate. In [17] it was shown that a syringe and solvent temperature of 130 °C and piston drive pressure of 16 bar was optimal for the dissolution. These conditions are extreme for most plastic materials, but is tolerated by e.g. polyphenylsulfones or polyetheretherketones. The second point is expected to affect dissolution efficiency, but was introduced to facilitate a dynamic seal that allows sample introduction into the cryostat through an air lock without raising the pressure of the 1 K sample space to atmospheric pressure. The FP consists of two major parts: part A, which contains sample and solvent, and allows the hyperpolarized solution to leave the polarizer through an open ended tube, and part B, that consists of a receiver connecting to the exit tube of part A, allowing non-contact quality control of the dissolved product. Part B also includes a filter that removes the EPA in-line with the dissolution process. The EPA precipitates in aqueous solution at acidic pH and can be removed effectively by mechanical filtration.

The objective of this work was to study the dissolution capability of the FP for two different sample sizes of [1-$^{13}$C]pyruvic acid. (1) A sample of 1.47 g, producing a human dose, dissolved in dissolution medium (DM) and neutralized with Neutralization Medium (NM) to a target concentration of 250 mM [1-$^{13}$C]pyruvate using the SPINlab polarizer and quality control system (involving FP part A and B). (2) A sample of 40 mg, producing a small animal dose, dissolved in DM to a target concentration of 80 mM, using a home-built polarizer involving only part A of the FP.

## 2. Materials and methods

### 2.1. Polarizer

Large samples were polarized on a SPINlab (GE Healthcare), Fig. 1, operating at 5 T and 0.85 K. Small samples were polarized on a home built polarizer [1] operating at 6.7 T and 1.1–1.2 K modified to accommodate the fluid path dissolution system.

### 2.2. Sample

[1-$^{13}$C]pyruvic acid (PA) (GE Healthcare, Norway) containing 15 mM AH111501 (EPA), 94.9% purity (GE Healthcare, USA).

### 2.3. Dissolution medium (DM)

Large sample: Ultra pure water (CHROMASOLV®Plus HPLC grade, Sigma Aldrich) with 0.1 g/L ethylenediaminetetraacetic acid disodium salt dihydrate (EDTA) (VWR).

Small sample: 0.2 M tris-hydroxymethyl aminomethane (TRIS base) (VWR) with 0.1 g/L EDTA.

### 2.4. Neutralization Medium (NM)

Large samples: 0.72 M NaOH (MERCK), 0.4 M TRIS base, 0.1 g/L EDTA.

Small sample: NaOH (10 M).

### 2.5. Fluid path (FP)

The FP (type 1293, GE Healthcare, USA) used for this study is shown in Fig. 1. Part A of the fluid path consists of a vial which can hold up to 2 mL of sample, the dynamic seal that allows the tubing to move inside the polarizer under vacuum, the co-axial tubing for DM inlet and outlet, the valve that opens the inlet and outlet simultaneously and the dissolution syringe that can hold up to 60 mL of solvent. Fig. 2B and C shows the vial with the position of the inner tube. The inner tube has a nozzle to provide a more efficient dissolution as demonstrated in [15,17]. Part B of the FP, Fig. 1, consists of the transfer tube, the EPA filter, receiver vessel with quality control (QC) appendage, the sterile assurance filter and a Medrad 65 mL MR syringe (Bayer, Denmark). On first use of the FP, the vial was attached to the outer tube by the use


**Fig. 1.** (A) SPINlab polarizer. The polarizer operates at 5 T and 0.9 K [16]. The polarizer has four independent channels that allow simultaneous polarization of up to four samples (fluid paths). The QC module (cylindrical black unit) is seen to the right of the photo below the touch screen. (B) Fluid Path (FP). Part A: (1) vial, (2) dynamic seal, (3) co-axial tube, (4) valve, (5) dissolution syringe. Part B: (6) transfer tube, (7) EPA filter, (8) receiver vessel, (9) QC appendage, (10) sterile assurance filter, (11) Medrad 65 mL MR syringe. Part A loads into the polarizer (behind the sliding door). The vial is inserted into one of the four airlock and the dissolution syringe is inserted into the corresponding heater-pressure module. After some pump-flush cycles, the airlock gate-valve will open and the vial can be pushed through the dynamic seal to the 0.9 K sample space. Part B is initially loaded into the corresponding warmer module seen to the lower right in (A). Shortly before dissolution part B is moved from the warmer to the QC module.

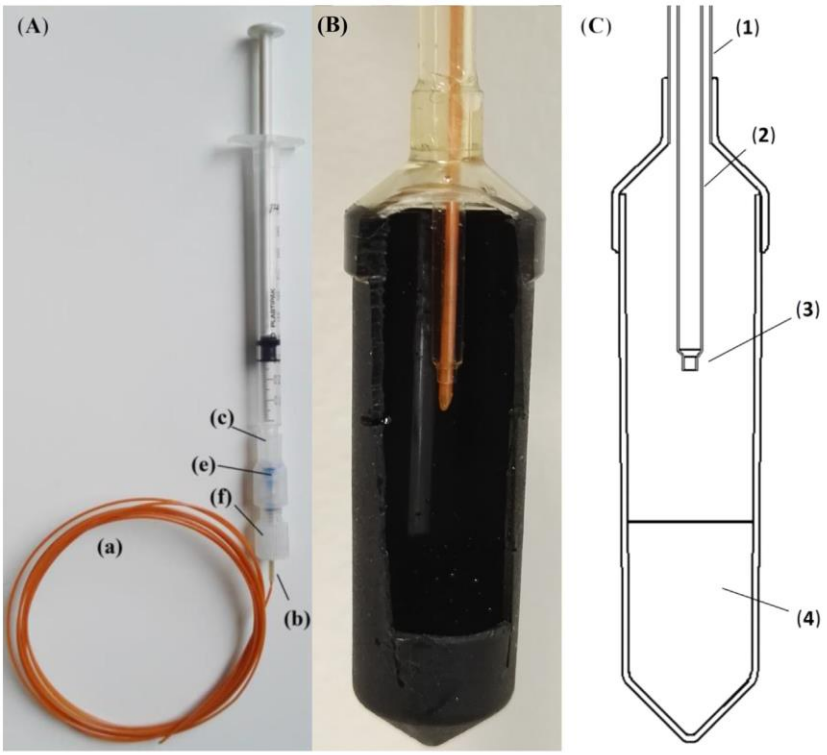


**Fig. 2.** (A) PEEK tube (a), sleeve (b), adapter (c), ferrule (e) and screw (f) assembled to result in the filling tube used for filling of the FP. (B) Filling tube placed in correct position in a demonstrational set-up (C) section of a vial with sample; (1) outer lumen, (2) inner tube, (3) nozzle, (4) sample (pyruvic acid).

of UV adhesive (Dymax 1161-M). On reuse, the FP part A was cleaned with 40 mL washing buffer (10% NM in distilled water), and then twice with 40 mL distilled water. Initially, the FP was thoroughly examined for any potential defects or irregularities. The FP was placed on a pressure check fixture and briefly flushed with Helium gas to secure unhindered flow. Reused FPs containing visible moisture were flushed for 10 min, or until dry, with compressed air or helium gas. Part B is not reused since it contains a small amount of HPTS (8-hydroxypyrene-1,3,6-trisulfonic acid, trisodium salt) dye used for the optical pH determination.

### 2.6. Filling tube for sample addition

For adding the sample, a syringe with a filling tube (Mikrolab Aarhus A/S, PEEK O.D. 1/32″ I.D. 0.5 mm, 1.5 m, VI JRT5620M3) attached through an adapter, a ferrule and a screw (Tefzel P628, Tefzel P200 and Tefzel P215, Mikrolab Aarhus A/S, Denmark) were used. To fit into the adapter, a sleeve (Sealtight, 840 μm, F247, Mikrolab Aarhus A/S, Denmark) was glued (UV adhesive) onto the filling tube, Fig. 2. The end of the tube was cut in a slanted manner in order to pass the nozzle and minimize residual sample at the end of the tube. Before first use of the filling tube, it was inserted through the dissolution syringe valve bore and through the inner tube, all the way to the sample vial. When the tube reached the bottom of the empty vial, it was retracted such that the end of the tube just passed the nozzle of the inner tube (Fig. 2B). Thus no sample would contaminate the inner tube upon addition. A mark was put on the filling tube by the dissolution syringe valve bore, so the correct position would be easily found upon next use.

### 2.7. Addition of sample, DM and NM

#### 2.7.1. Addition of large samples

Approx 0.5 mL of sample was pulled into a 3 mL single use plastic syringe (carefully avoiding air bubbles) after which the filling tube was attached. The sample was then pushed through the filling tube in order to fill the dead volume (approx. 380 μL). An Eppendorf tube with sample was placed on the balance, tared, and sample (1.47 g) was drawn into the syringe. Air (few centimeters) was then drawn into the tube to prevent contamination of the FP inner wall. The syringe and filling tube were weighted before and after addition, to confirm correct addition of sample. The surface of the filling tube was thoroughly cleaned for potential impurities and inserted through the inner tube of the FP until the tube reached the bottom of the vial. The slanted tip made it possible for the filling tube to pass the nozzle of the inner tube. The filling tube was then retracted to the correct position, as indicated by the mark. The sample was carefully added by push of the syringe piston. After addition, air was drawn into the filling tube, and it could then be retracted from the FP without contaminating the inner tube.

38.0 g of DM was added to the dissolution syringe. The outlet of the syringe was plugged and the syringe put on the filling stand purge. The sample vial was carefully submerged into liquid nitrogen (vertical position to avoid splashing) and allowed to freeze (2 min). The FP was then flushed with helium for 2 min after which the system was pressure tested (40 psi for 2 min without losing pressure). When the FP tests were completed, the valve rotor was inserted and put into the closed position. The dissolution syringe was then connected to a part B, Fig. 1. Ca. 15.0 g of NM and 26.2 g of DM were added to the receiver of part B, a Medrad power

injector syringe was attached and the FP and receiver were ready to be inserted into the polarizer and QC module, respectively.

*2.7.2. Addition of small samples*

The filling tube was cleaned, dried and attached to a 1 mL syringe. Sample (40 μL) was placed in an Eppendorf tube, and drawn into the filling tube as a bolus, followed by ca. 10 cm air (Supplementary data Video 1). The filling tube was carefully inserted into the FP and pushed to the bottom of the vial. It was then retracted 0.5 cm. The syringe was removed, and helium was flushed through the filling tube (10 psi, 2 min) (Supplementary data Video 2). The filling tube was then removed from the FP. 13.3 g of DM and 138 μL NM were then added to the dissolution syringe. The FP was pressure tested as described for large samples. A short exit tube was attached (50 cm) and the FP was ready for being inserted into the polarizer. An empty 50 mL Falcon tube was used as a receiver for small samples.

*2.8. SPINlab QC (online measurements; large sample only)*

The QC module measures six parameters by methods that are non-contact with the product. The syringe valve is open for 10 s during the dissolution. The dissolution takes approx. 6 s. 5 s after the syringe valve closes, a part of the hyperpolarized sample is allowed to flow through a series of cavities by opening a valve in the bottom of the receiver. The QC parameters are measured in approx. 15 s, which means that the product (in the Medrad syringe) is released approx. 30 s after the dissolution is initiated. Pyruvate concentration is determined by absorbance at 360 nm, EPA concentration is determined by absorbance at 470 nm, pH is determined by ratio metric absorbance at 405 and 450 nm for a hydroxypyrene-1,3,6-trisulfonic acid (HPTS) dye in one of the cavities, polarization is measured by NMR and corrected for relaxation, temperature is measured by IR on the receiver and volume is a capacitance threshold sensor on the Medrad syringe. The QC module was calibrated prior to the experiments. Pyruvate concentration, EPA concentration and pH all required measurement of a dark, blank and several calibrants (GE Healthcare, USA) according to manufacturer's instructions. Polarization and flip angle calibration were performed by the use of a $^{13}C$ reference sample ($^{13}C_3$-glycerol doped to shorten $T_1$, QC daily check sample, GE Healthcare, USA) according to manufacturer's instructions. Temperature was calibrated by the use of a receiver filled with water of known temperature.

*2.9. Offline measurements*

pH: LAQUA pH/ION meter F-72 (HORIBA) with pH electrode DJ 113662-1385 (VWR) or Knick Portamess pH-meter 913 with pH electrode Hamilton mini electrode (KLC). Polarization: measured on a 400 MHz NMR (Agilent Technologies, USA). Acquisition parameters: 3° flip angle every 2 s, starting approx. 10 s post dissolution. The thermal signal was acquired by adding Omniscan (15 μL) to reduce $T_1$ to <1 s. 2000 averages with repetition delay 0.5 s, 3° flip angle. Software for analysis: MestReNova 10.0 and MATLAB R2015a, by which polarization and $T_1$ were calculated. PA concentration: For large samples the concentration was measured by quantitative NMR. Sample: sample from receiver (450 μL), [$^{13}$C]urea (15 μL, 400 mM), $D_2O$ (100 μL) and Omniscan (15 μL). Acquisition parameters: 90° flip angle, repetition delay 1.5 s. Software for analysis: TopSpin 3.2. For small samples the concentration was measured by absorbance on a BioTek EPOCH 2 microplate reader (Holm & Halby, Brøndby, Denmark) at wavelength 360 nm. Temperature was measured by the use of thermometers of type OMEGA HH804U Thermometer or Testo 110, AG Germany. EPA concentration: measured by absorbance at 465 nm (EPOCH plate reader with 10 mm cell). Output volumes were measured by weighing an empty Falcon tube before and after dissolution (Discovery Ohaus balance).

## 3. Results

*3.1. Large samples*

Eleven experiments were performed using four FP. The samples were polarized for 2.5 h on average to more than 90% of maximum polarization, followed by dissolution. The data from the QC module have been compared to offline measurements of the respective samples, Table 1. To secure a physiological acceptable pH, the NM in the receiver was adjusted accordingly to the amount of PA added (PA/NaOH ratio 1.6), which was in the range of 13.9–14.6 g. The target concentration in the case of large samples was 250 mM, which mimics a human dose.

*3.2. Small samples*

To demonstrate filling of small samples, seven experiments were performed, Table 2, using the same four FP as in the large sample study. The experiments were designed to mimic a target concentration, suitable for small animal dose (80 mM). Polarization measurements were made for four of these.

## 4. Discussion

The study shows that the new filling method of the FP can be performed in a reproducible manner, validated by QC parameters from the SPINlab and offline measurements. The method is robust with small relative standard deviations. We have demonstrated two extreme conditions; filling of large samples mimicking a human clinical dose, and small samples suited for small animal studies.

For the human dose, base is added to the receiver, in order for the radical to precipitate and be filtered off before entering the receiver. The acceptance criterion for residual EPA in the product is less than 3 μM [18]. The measured value is 1.2 ± 0.3 μM, well within specification, and demonstrating >99% removal. The mean

**Table 1**
Results from dissolutions compared to the respective off-line measurements (n = 11).

| | Average | Standard deviation | Relative STD (%) |
|---|---|---|---|
| PA/EPA added (g) | 1.47 | 0.02 | 1.4 |
| DM in syringe (g) | 38.0 | 0.1 | |
| DM in receiver (g) | 25.8 | 0.3 | 1.0 |
| NM in receiver (g) | 14.3 | 0.2 | 1.4 |
| PA/NaOH mol ratio | 1.6 | 0.002 | 0.1 |
| *Online results* | | | |
| Pyruvate conc. (mM) | 246 | 19 | 7.7 |
| pH | 7.71 | 0.17 | 2.2 |
| EPA conc. (μM) | 1.17 | 0.28 | 24 |
| Temperature (°C) | 32.0 | 1.3 | 4.0 |
| Volume (mL) | >40 mL | | |
| Polarization (%) | 34.2 | 2.9 (n = 3)[a] | 8.5 |
| *Offline results* | | | |
| Pyruvate conc. (mM) | 247 | | 8.3 |
| pH | 7.75 | 0.15 | 1.9 |
| EPA conc. (μM) | 0.68 | 0.21 | 31 |
| Volume (mL) (product in Medrad syringe) | 44.2 | 1.0 | 2.3 |
| Temperature (°C) | 31.7 | 0.5 | 1.6 |

[a] The NMR flip angle was incorrectly calibrated in the first experiments leading to saturation of the receiver and incorrect estimation of the polarization.

**Table 2**
Results from dissolutions with small sample filling (n = 7).

| | Average | Standard deviation | Relative STD (%) |
|---|---|---|---|
| PA/EPA added (mg)[a] | 40 | | |
| DM in syringe (g) | 13.4 | 0.2 | 1.6 |
| NaOH (10 M) syringe (g) | 0.138 | | |
| Pyruvate conc. (mM) | 70 | 7.4 | 11 |
| pH | 7.8 | 0.1 | 2 |
| EPA conc. (μM) | 70.5 | 7.5 | 11 |
| Product in receiver (g) | 5.3 | 0.6 | 12 |
| Temperature (°C) | 54 | 2.6 | 5 |
| Polarization (%) | 43.7 | 5.5 (n = 4) | 13 |
| $T_1$ | 53.8 | 2.0 (n = 4) | 4 |
| Recovery (%) | 82 | 12 | 15 |

[a] 40 mg was assumed to be added with no loss under the addition process.

value of the EPA concentration is five standard deviations below the acceptance criterion. The pyruvate concentration acceptance criteria are 220–280 mM [18], which is also achieved with three standard deviations margin. The acceptance criteria for pH are 6.7–8.2 [18]. The study was not perfectly centered in the range, which could be achieved by changing the volume of NM in the receiver. However, the range is about ten standard deviations in this study. pH is a critical safety parameter, demonstrating that filling and process performed very well and is robust. Since only approx. 44 mL are transferred to the Medrad syringe, recovery has been disregarded in the large sample case, since some of the sample is used in the QC and thereby trapped in the dead volume of the system. However, the volume transferred to the Medrad syringe is four standard deviations above the acceptance criterion. The FP's have been reused for demonstrational purposes and are not sterile, but we believe the approach could be translated into a low bioburden version by appropriate cleaning of the FP before filling. Sterility assurance can then be achieved by a validated, in-line sterile filter. The filling procedure should be compatible with normal pharmacy clean room environments.

For small samples, base is added to the dissolution syringe, which means that all the PA and EPA is transferred to the receiver upon dissolution, and recovery can thereby be estimated. Recovery is calculated from the product of pyruvate concentration and volume, and assume that the full 40 mg was deposited in the sample vial. Most of the 15–20% loss of sample is likely due to loss in the filling process. The pyruvate concentration in the receiver is highly linked to the performance of the fluid path, since the dead volume vary. The variability of 11% for the pyruvate concentration is acceptable for most animal studies. We have not systematically studied the minimal possible sample amount that can be deposited in the vial by our method, but we have tested volumes down to 10 mg. This could have significance for e.g. cell or perfused organ studies that only require dilute substrate concentrations. More important is the minimal volume that can be applied in the dissolution. We believe that the product volume of app 5 mL achieved in this study, is close to the minimum volume that can be reached without loss of polarization and reduced recovery. This is close to the same performance as e.g. the Hypersense optimized for small sample polarization. It would be reasonable to expect that the use of two-phase dissolution could reduce the effective dissolution volume even further as previously demonstrated [19].

The lower temperature of the solvent in the dissolution allows the use of all plastic components. Plastic components eliminates leaching of paramagnetic ions from e.g. stainless steel components and potential enhanced relaxation from these ions. The polyphenylsulfone that is used in the fluid path is a plastic with high toughness and impact strength, good long-term hydrolytic stability and chemical resistance. It withstands steam sterilization without any significant loss of properties. For other solvents than water, the chemical resistance at the given temperature and pressure conditions needs to be taken into consideration and tested.

The SPINlab corrects the polarization to the start of dissolution by assuming a $T_1$ of 65 s. This means that the measured polarization is corrected by a factor of approx. 1.5 in this study. The polarization for low dose is the actual measurement without any correction. However, the delay is only approx. 10 s from start of dissolution to measurement. The difference in polarization for the two situations is partly due to the higher magnetic field strength of the prototype polarizer (6.7 T vs 5.0 T), but also that some polarization loss is known to occur in the QC system.

The reusability of the FP's means reduced cost for research purposes, and no failed FP were observed within the ten times reuse that we arbitrarily defined as the maximum number of reuses on the SPINlab. The filling method has been tested extensively (>100 dissolutions) at Aarhus University Hospital, Skejby on the SPINlab, without failure of the fluid path during dissolution that have led to contamination of the polarizer. Failure in dissolution can happen due to e.g. moisture in the tubing that lead to blockage and prevention of flow. This happens at a low rate depending on operator skills. In our laboratory we use the fluid paths until failure since contamination of the polarizer is easier to clean. However, most failures occur during handling as fatigue of glue joints, typically after 20–50 uses. Wear and tear can also lead to failure in the pressure test and discard of the fluid path. More rarely the FP fails early in use due to defects in the plastic. The failures due to defects in the plastic appear to be unrelated to the filling method, but can lead to a burst inside the polarizer during dissolution depending on location of the defect. With the hundreds of dissolutions that we have performed with this method, there does not seem to be a higher frequency of fatal incidents than by single use.

## 5. Conclusion

The principle of the fluid path for dissolution-DNP enables independent control of solvent temperature and flow rate. The benefit is efficient dissolution at lower solvent temperature and use of all plastic components. The reproducibility of the dissolution process is high on all parameters relevant for clinical use. The fluid path can be used for any sample size from 10 μL to 1.1 mL, and produces a minimum product volume of approx. 5 mL up to the full volume of 44 mL for a patient.

## Acknowledgements

Rigshospitalet, Copenhagen, Denmark, is acknowledged for providing access to the SPINlab. Aarhus University Hospital, Skejby, Denmark, is acknowledged for testing the procedure and confirming reliability and performance. Furthermore, the authors wish to thank Danish National Research Foundation [grant number DNRF124] for financial support.

## Appendix A. Supplementary material

Supplementary data associated with this article can be found, in the online version, at http://dx.doi.org/10.1016/j.jmr.2016.09.015.

## References

[1] J.H. Ardenkjær-Larsen, B. Frindlund, A. Gram, G. Hansson, L. Hansson, M.H. Lerche, R. Servin, M. Thaning, K. Golman, Increase in signal-to-noise ratio of >10,000 times in liquid state NMR, PNAS 100 (18) (2003) 10158–10163.
[2] S. Kohler, Y. Yen, J. Wolber, A. Chen, M. Albers, R. Bok, V. Zhang, J. Tropp, S. Nelson, D. Vigneron, J. Kurhanewicz, R. Hurd, In vivo 13 carbon metabolic imaging at 3 T with hyperpolarized $^{13}$C-1-pyruvate, Magn. Reson. Med. 58 (2007) 65–69.

[3] H. Gutte, A.E. Hansen, H.H. Johannesen, A.E. Clemmensen, J.H. Ardenkjær-Larsen, C.H. Nielsen, K. Andreas, The use of dynamic nuclear polarization (13) C-pyruvate MRS in cancer, Am. J. Nucl. Med. Mol. Imaging 5 (2015) 548–560.
[4] K. Golman, R. in't Zandt, M. Lerche, R. Pehrson, J.H. Ardenkjaer-Larsen, Metabolic imaging by hyperpolarized $^{13}$C magnetic resonance imaging for in vivo tumor diagnosis, Cancer Res. 66 (22) (2006) 10855–10860.
[5] S. Meier, P.R. Jensen, J.Ø. Duus, Real-time detection of central carbon metabolism in living *Escherichia coli* and its response to perturbations, FEBS Lett. 585 (2011) 3133–3138.
[6] F.A. Gallagher, M.I. Kettunen, D.-E. Hu, P.R. Jensen, R. in't Zandt, M. Karlsson, A. Gisselsson, S.K. Nelson, T.H. Witney, S.E. Bohndiek, G. Hansson, T. Peitersen, M. H. Lerche, K.M. Brindle, Production of hyperpolarized [1,4-$^{13}$C2]malate from [1,4-$^{13}$C2]fumarate is a marker of cell necrosis and treatment response in tumors, PNAS 106 (47) (2009) 19801–19806.
[7] F.A. Gallagher, M.I. Kettunen, K.M. Brindle, Imaging pH with hyperpolarized $^{13}$C, NMR Biomed. 24 (2011) 1006–1015.
[8] C. von Morze, P.E. Larson, S. Hu, H.A. Yoshihara, R.A. Bok, A. Goga, J.H. Ardenkjær-Larsen, D.B. Vigneron, Investigating tumor perfusion and metabolism using multiple hyperpolarized $^{13}$C compounds: HP001, pyruvate and urea, Magn. Reson. Imaging 30 (2012) 305–311.
[9] K.W. Lipsø, P. Magnusson, J.H. Ardenkjær-Larsen, Hyperpolarized $^{13}$C MR angiography, Curr. Pharm. Des. 22 (2016) 90–95.
[10] J. Ardenkjaer-Larsen, S. Macholl, H. Jóhanneson, Dynamic nuclear polarization with trityls at 1.2 K, Appl. Magn. Reson. 34 (2008) 509–522.
[11] L. Lumata, S.J. Ratnakar, A. Jindal, M. Merritt, A. Comment, C. Malloy, A.D. Sherry, Z. Kovacs, BDPA: an efficient polarizing agent for fast dissolution dynamic nuclear polarization NMR spectroscopy, Chem. Eur. J. 17 (2011) 10825–10827.
[12] B.v.d. Brandt, E. Bunyatova, P. Hautle, J. Konter, DNP with the free radicals deuterated TEMPO and deuterated oxo-TEMPO, Nucl. Instrum. Meth. A 526 (2004) 53–55.
[13] S.J. Nelson, J. Kurhanewicz, D.B. Vigneron, P.E.Z. Larson, A.L. Harzstark, M. Ferrone, M. van Criekinge, J.W. Chang, R. Bok, I. Park, G. Reed, V.K. Weinberg, J. H. Ardenkjær-Larsen, A.P. Chen, R.E. Hurd, L.-I. Odegardstuen, F.J. Robb, J. Tropp, J.A. Murray, Metabolic imaging of patients with prostate cancer using hyperpolarized [1-$^{13}$C]pyruvate, Sci. Transl. Med. 5 (198) (2013) 1–11.
[14] A. Comment, J. Rentsch, F. Kurdzesau, S. Jannin, K. Uffmann, R. van Heeswijk, P. Hautle, J. Konter, B. van den Brandt, J. van der Klink, Producing over 100 ml of highly concentrated hyperpolarized solution by means of dissolution DNP, J. Magn. Reson. 194 (2008) 152–155.
[15] S. Bowen, J.H. Ardenkjaer-Larsen, Enhanced performance large volume dissolution-DNP, J. Magn. Reson. 240 (2014) 90–94.
[16] J.H. Ardenkjær-Larsen, A.M. Leach, N. Clarke, J. Urbahn, D. Anderson, T.W. Skloss, Dynamic nuclear polarization polarizer for sterile use intent, NMR Biomed. 24 (2011) 927–932.
[17] J. Jain, S. Dey, L. Muralidharan, A.M. Leach, J.H. Ardenkjær-Larsen, Jet impingement melting with vaporization: a numerical study, in: ASME Heat Transfer Summer Conference, Jacksonville, Florida, 2008.
[18] "Hyperpolarized [13C] Pyruvate Documentation Page," National Cancer Institute – the National Institute of Health, (Online), Available: <http://imaging.cancer.gov/programsandresources/cancer-tracer-synthesis-resources/hyperpolarized-C13-pyruvate-documentation> (accessed 28.06.2016).
[19] T. Harris, C. Bretschneider, L. Frydman, Dissolution DNP NMR with solvent mixtures: substrate concentration and radical extraction, J. Magn. Reson. 211 (2011) 96–100, http://dx.doi.org/10.1016/j.jmr.2011.04.001.